

Master's Degree course in Renewable Energy Engineering



**Politecnico  
di Torino**



**MARINE  
OFFSHORE  
RENEWABLE  
ENERGY LAB**

Master's Degree Thesis

## **Modeling the propulsion system of a full-electric motorboat**

### **Supervisors**

Prof. Giuliana MATTIAZZO

Dott. Oronzo DELL'EDERA

### **Candidate**

Stefano MUSARRA TUBI

MARCH 2023



## **Abstract**

Electrification is constantly gaining ground in the transport industry. Despite a lower diffusion pace, the maritime sector benefits from the momentum created by the automotive one. In situations where limitations regarding the required range autonomy do not hinder development, the electric boat market has been making significant progress. With an increased number of marinas installing charging facilities, recreational boating has experienced the rise of several competitive offers. In the meanwhile, vessels operating on short to medium journeys are already a commercially viable option for waterborne transport of passengers due to undeniable advantages in terms of comfort, efficiency, and environmental impact.

The present work develops a computationally efficient Simulink® model able to reproduce the propulsion system performances of a direct current electric motorboat equipped with a photovoltaic array as range extender. Firstly, relying on the availability of a few data sheet parameters, every relevant system component is described by means of a mathematical model able to capture its main dynamics and integrate it with those of the entire propulsion chain. Secondly, a case study on the feasibility of a taxi boat service in the Venetian lagoon is investigated. Finally, the obtained results are analysed and weighted through key performance parameters. The intended scope is to assess the practicability of a certain design or help adjust component specifications according to a particular boat function.



# Contents

<b>List of Figures</b>	5
<b>List of Tables</b>	7
<b>List of Symbols</b>	9
<b>1 Introduction</b>	15
<b>2 Literature review and adapted methodology</b>	19
<b>3 Theoretical introduction</b>	21
3.1 PV array and balance of plant . . . . .	21
3.2 Energy storage . . . . .	25
3.3 From boat resistance to propeller and motor load . . . . .	29
3.4 DC motor . . . . .	35
3.5 Proportional-integral controller . . . . .	38
3.6 Buck converter . . . . .	39
3.7 Buck-Boost converter . . . . .	40
<b>4 Model description</b>	41
4.1 System overview . . . . .	41
4.2 System components and Simulink® implementation . . . . .	43
<b>5 Main assumptions and limitations</b>	75
<b>6 Numerical results</b>	79
6.1 Weather and random load generation . . . . .	79
6.2 Data to export . . . . .	81
6.3 Dynamic plots and performance weighting parameters . . . . .	82
<b>7 Conclusion</b>	93
<b>Bibliography</b>	98
<b>Appendix: MATLAB scripts</b>	99
<b>List of Acronyms</b>	113



# List of Figures

2.1	Methodology overview . . . . .	20
3.1	Single diode equivalent circuit model . . . . .	23
3.2	PV array curves under different irradiance and temperature conditions . . . . .	24
3.3	Battery discharge curve. Extracted parameters . . . . .	26
3.4	Battery discharge curve. Voltage as a function of depth of discharge . . . . .	28
3.5	Battery discharge curve. Voltage as a function of discharge time . . . . .	28
3.6	Resistance and propulsive power curve adopted in the simulation . . . . .	29
3.7	Propulsion chain: from resistance to brake power . . . . .	30
3.8	Propeller open water diagram . . . . .	32
3.9	Algorithm. Boat thrust coefficient as a function of advance ratio . . . . .	33
3.10	Open water diagram at $v_s = 5[m/s]$ . Matching of thrust coefficient . . . . .	34
3.11	Propeller load and relative parameters . . . . .	34
3.12	PMDC motor electrical circuit and torque representation . . . . .	35
3.13	Configuration of the control system for the DC motor . . . . .	36
3.14	Power in the propulsion chain as a function of boat velocity. . . . .	37
3.15	Schematic of a PI controller with anti-windup gain . . . . .	38
3.16	Simplified circuit of a buck converter . . . . .	39
3.17	Simplified circuit of a buck-boost converter . . . . .	40
4.1	Electrical and logical connections . . . . .	41
4.2	Simulink model template . . . . .	43
4.3	Day/Night pulse generator . . . . .	44
4.4	PV subsystem, 1 <sup>st</sup> level . . . . .	45
4.5	Random meteorological conditions on a summer day . . . . .	46
4.6	PV subsystem, 2 <sup>nd</sup> level . . . . .	47
4.7	PV subsystem, 3 <sup>rd</sup> level. PV Parameters . . . . .	48
4.8	PV subsystem, 3 <sup>rd</sup> level. PV module implicit equations . . . . .	49
4.9	Buck converter subsystem, 1 <sup>st</sup> and 2 <sup>nd</sup> level . . . . .	50
4.10	PV characteristic curve . . . . .	51
4.11	Buck converter subsystem, MPPT algorithm flowchart . . . . .	52
4.12	Buck converter subsystem, MPPT implementation . . . . .	53
4.13	Charge controller subsystem . . . . .	54
4.14	Minimum load (a) and maximum current (b) controller subsystems . . . . .	55
4.15	Simplified system circuit with focus on buck converter architecture . . . . .	56
4.16	Buck converter subsystem, equations . . . . .	57
4.17	Power distribution unit subsystem, 1 <sup>st</sup> and 2 <sup>nd</sup> level . . . . .	58
4.18	Battery bank subsystem, 1 <sup>st</sup> , 2 <sup>nd</sup> and 3 <sup>rd</sup> level . . . . .	59
4.19	Battery bank subsystem: equations for charge and discharge . . . . .	60

4.20	Buck converter 12V subsystem, 1 <sup>st</sup> level . . . . .	61
4.21	Buck converter 12V subsystem, 2 <sup>nd</sup> level . . . . .	62
4.22	Buck converter 12V, simplified electrical circuit . . . . .	63
4.23	Buck converter 12V subsystem, equations . . . . .	64
4.24	Buck converter 12V subsystem, PI controller . . . . .	65
4.25	DC motor subsystem, 1 <sup>st</sup> level . . . . .	66
4.26	DC motor subsystem, 2 <sup>nd</sup> level . . . . .	67
4.27	DC motor subsystem, speed (a) and torque (b) input under low SOC . . . . .	68
4.28	DC motor subsystem, speed and current PI controllers . . . . .	69
4.29	DC motor subsystem, equations . . . . .	70
4.30	Buck-Boost converter subsystem, 1 <sup>st</sup> and 2 <sup>nd</sup> level . . . . .	71
4.31	Buck-Boost converter subsystem, PI controller . . . . .	71
4.32	Buck-Boost converter coupled to electrical motor, simplified electrical circuit . . .	72
4.33	Buck-Boost converter subsystem, equations . . . . .	73
6.1	Load profiles . . . . .	80
6.2	Example of random load generation . . . . .	80
6.3	Calculation and data to export subsystem . . . . .	81
6.4	<i>Ad hoc day.</i> Velocity request . . . . .	82
6.5	<i>Ad hoc day.</i> Ambient conditions . . . . .	82
6.6	<i>Ad hoc day.</i> Power distribution . . . . .	83
6.7	<i>Ad hoc day.</i> Velocity load . . . . .	84
6.8	<i>Ad hoc day.</i> Load and motor rotational speed . . . . .	85
6.9	<i>Ad hoc day.</i> Load and motor torque . . . . .	85
6.10	<i>Ad hoc day.</i> Relevant currents . . . . .	86
6.11	<i>Ad hoc day.</i> Photoltaic (PV) power . . . . .	87
6.12	<i>Ad hoc day.</i> Wasted power and potential PV energy loss . . . . .	87
6.13	<i>Ad hoc day.</i> Relevant duty cycles . . . . .	88
6.14	<i>Ad hoc day.</i> Relevant voltages . . . . .	88
6.15	<i>Ad hoc day.</i> Motor power distribution . . . . .	89
6.16	<i>Ad hoc day.</i> DC motor shortcomings . . . . .	90
6.17	<i>Ad hoc day.</i> Estimated battery cycles . . . . .	90
6.18	<i>Ad hoc day.</i> Energy balance . . . . .	91
6.19	Energy balance in June . . . . .	92
6.20	Energy balance in January . . . . .	92



# List of Tables

2.1	Related works in literature . . . . .	19
3.1	PV module and array assumed data sheet . . . . .	22
3.2	PV module assumed data sheet. Extra parameters . . . . .	22
3.3	Single battery and battery bank data sheet . . . . .	26
3.4	Propeller data sheet . . . . .	30
3.5	DC motor data sheet . . . . .	37



# List of Symbols

Symbol	Description	Unit
$\alpha_I$	Short circuit current temperature coefficient	$[K^{-1}]$
$\beta_V$	Open circuit voltage temperature coefficient	$[K^{-1}]$
$\delta_0$	irradiance coefficient of open circuit voltage	$[-]$
$\Delta I$	Current variation	$[V]$
$\Delta I_L$	Maximum output current ripple	$[A]$
$\Delta I_{is}$	Input current ripple in favourable irradiance conditions	$[A]$
$\Delta I_{iw}$	Input current ripple in poor irradiance conditions	$[A]$
$\Delta I_{os}$	Output current ripple in favourable irradiance conditions	$[A]$
$\Delta I_{ow}$	Output current ripple in poor irradiance conditions	$[A]$
$\Delta P$	Power variation	$[W]$
$\Delta V$	Voltage variation	$[V]$
$\Delta V_{out}$	Maximum output voltage ripple	$[V]$
$\Delta V_{ow}$	Output voltage ripple in poor irradiance conditions	$[V]$
$\eta_H$	Hull efficiency	$[-]$
$\eta_o$	Open water efficiency	$[-]$
$\eta_R$	Relative rotative efficiency	$[-]$
$\eta_s$	Shaft efficiency	$[-]$
$\eta_{buck}$	Buck converter efficiency	$[-]$
$\eta_{el\_motor}$	Motor efficiency	$[-]$
$\eta_{el}$	Electrical efficiency of the whole motor system	$[-]$

$\eta_{gb}$	Gearbox efficiency	$[-]$
$\eta_{propulsive}$	Propulsive efficiency	$[-]$
$\eta_{tot}$	Total conversion efficiency of the propulsion chain	$[-]$
$\eta_{TRM}$	Transmission efficiency	$[-]$
$\lambda$	Coefficient related to the limited extractable energy from a battery	$[-]$
$\omega_c$	Current control bandwidth	$[Hz]$
$\omega_m$	Angular velocity of the motor shaft	$[rad/s]$
$\omega_s$	Speed control bandwidth	$[Hz]$
$\rho$	Salt water density	$[kg/m^3]$
$\tau$	Time constant	$[s]$
$A$	Exponential drop in voltage	$[V]$
$a$	Auxiliary parameter for PV modeling	$[V^{-1}]$
$B$	One third of exponential capacity	$[Ah]$
$B_m$	Viscous friction coefficient	$[Nm/(rad/s)]$
$BAR$	Blade area ratio	$[-]$
$C$	Capacitance	$[F]$
$D$	Duty cycle	$[-]$
$D_{mps}$	Typical duty cycle corresponding to MPP in favourable irradiance conditions	$[-]$
$D_{mpw}$	Typical duty cycle corresponding to MPP in poor irradiance conditions	$[-]$
$D_{prop}$	Propeller diameter	$[mm]$
$E_0$	Constant voltage	$[V]$
$E_a$	Back electromotive force	$[V]$
$E_{batt}$	Battery energy	$[KWh]$
$f_s$	Switching frequency	$[Hz]$
$I$	Current	$[A]$
$i_a$	Armature current	$[A]$
$I_{a\_rated}$	Rated armature current	$[A]$
$i_L$	Current flowing through the inductor	$[A]$
$I_s$	Module reverse saturation current	$[A]$

$i_{batt}$	Battery current	[A]
$I_{in}$	Input current	[A]
$I_{mp}$	Maximum power point current	[A]
$I_{out}$	Output current	[A]
$I_{ph}$	Module photo current	[A]
$I_{sc}$	Short circuit current	[A]
$it$	Extracted capacity	[Ah]
$J$	Advance ratio	[-]
$J_m$	Rotational inertia	[kg · m <sup>2</sup> ]
$K$	Polarization constant	[V/Ah]
$k_e$	Motor speed constant	[V/(rad/s)]
$K_i$	Integrall gain	[-]
$K_p$	Proportional gain	[-]
$k_p$	Number of propellers	[-]
$K_Q$	Propeller torque coefficient	[-]
$K_T$	Propeller thrust coefficient	[-]
$k_t$	Motor torque constant	[Nm/A]
$K_{ac}$	Anti-windup gain current controller	[A/V]
$K_{as}$	Anti-windup gain speed controller	[Nm <sup>-1</sup> s <sup>-1</sup> ]
$K_{aw}$	Anti windup gain	[-]
$K_{ic}$	Integral gain current controller	[V/A/s]
$K_{is}$	Integral gain speed controller	[Nm]
$K_{pc}$	Proportional gain current controller	[V/A]
$K_{ps}$	Proportional gain speed controller	[Nm · s]
$L$	Inductance	[H]
$L_a$	Armature inductance	[H]
$n_d$	Diode ideality factor	[-]
$N_s$	Number of cells	[-]
$N_{blades}$	Number of blades of propeller	[-]
$n_{max\_prop}$	Propeller rated speed	[rpm]
$N_{p\_strings}$	Number of parallel connected PV modules on a single row	[-]

$N_{par\_batt}$	Number of parallel connected batteries for each row	$[-]$
$n_{prop}$	Propeller rotational speed	$[rad/s]$
$N_{s\_module}$	Number of series connected PV modules on a single column	$[-]$
$N_{ser\_batt}$	Number of series connected battery sets connected in parallel	$[-]$
$P_{aux}$	Power requested from the auxiliary 12V loads	$[W]$
$P_{brake}$	Engine brake power	$[W]$
$P_{el}$	Electrical input power	$[W]$
$P_{mp}$	Maximum power	$[W]$
$P_{o\_w}$	Open water propeller power	$[W]$
$P_{propulsive}$	Propulsive power	$[W]$
$P_{prop}$	Propeller load (power)	$[W]$
$P_{rated}$	Rated motor power	$[W]$
$P_{thrust}$	Propeller thrust power	$[W]$
$Pitch_{prop}$	Propeller pitch	$[mm]$
$Pitch_{prop}/D_{prop}$	Propeller pitch/diameter ratio	$[-]$
$Q$	Capacity	$[Ah]$
$Q_{exp}$	Capacity at exponential voltage	$[Ah]$
$Q_{ext}$	Extracted capacity	$[Ah]$
$Q_{max}$	Maximum capacity at nominal discharge current	$[Ah]$
$Q_{nom}$	Capacity at nominal voltage	$[Ah]$
$Q_{prop}$	Propeller torque	$[Nm]$
$Q_{rated}$	Rated capacity	$[Ah]$
$R$	Boat resistance	$[N]$
$R$	Resistance	$[\Omega]$
$R_a$	Armature resistance	$[\Omega]$
$R_e$	Effective resistance	$[\Omega]$
$R_s$	Series resistance	$[\Omega]$
$R_{int}$	Internal resistance	$[\Omega]$
$R_{sh}$	Shunt resistance	$[\Omega]$

$T$	Thrust	$[N]$
$T$	Total switching period	$[s]$
$t$	Thrust deduction factor	$[-]$
$t$	Time	$[s]$
$T_e$	Torque generated by the electrical motor	$[Nm]$
$T_L$	Load torque	$[Nm]$
$T_{e\_rated}$	Rated torque generated from the motor	$[Nm]$
$t_{on}$	Time interval during which the switch is on	$[s]$
$T_{prop}$	Propeller thrust	$[N]$
$V$	Voltage	$[V]$
$V_a$	Armature voltage	$[V]$
$v_a$	Velocity of advance	$[m/s]$
$v_s$	Boat velocity	$[m/s]$
$V_{b\_oc}$	Open circuit battery voltage	$[V]$
$V_{batt}$	Battery voltage	$[V]$
$V_{exp}$	Exponential voltage	$[V]$
$V_{full}$	Fully charged voltage	$[V]$
$V_{in}$	Input voltage	$[V]$
$V_{mps}$	MPP voltage under Standard Testing Conditions (STC)	$[V]$
$V_{mp}$	Maximum power point voltage	$[V]$
$V_{nom}$	Nominal voltage	$[V]$
$V_{oc}$	Open circuit voltage	$[V]$
$V_{out}$	Output voltage	$[V]$
$w$	Wake factor	$[-]$





# Chapter 1

## Introduction

With more than 85% in volume of goods transported worldwide [1], maritime transport plays a strategic role in connecting countries across the oceans. Only in Europe, 77% of external trades and 35% of internal ones<sup>1</sup> are transported from ships, making seaborne activity a crucial link in the supply chain [2]. When it comes to passenger transport, the number of embarked and disembarked people in all European ports accounted for the record number of 420 million before pandemic, with Italy, Greece and Denmark in top three positions [3].

The indisputable economy and social growth contributions offered by the industry come at a cost for the environment. In fact, despite the relatively low  $CO_2$  emissions per weight carried and miles undertaken, maritime transport accounts at least for 3% of the global  $CO_2$  emissions [1, 2] and is cause of several other issues such as exhaust gases air pollution, water contamination due to waste discharges, oil spills and accumulation of marine debris. Additionally, freight and passenger transport produces underwater noise and favour the introduction of several non-indigenous species that pose a threat to marine creatures and their ecosystem [4].

Ocean transportation is forecasted to grow in the next decades, increasing the need for regulations and agreements on an international level. Among the different regulatory bodies, the International Maritime Organisation (IMO) plays a crucial part. Using 2008 data as reference, it deployed an *initial strategy* to cut Greenhouse Gases (GHG) emissions by a minimum of 50% by 2050. Legally-binding measures to reduce carbon intensity are currently adopted, such as the tightening of CII, EEDI or EEXI<sup>2</sup> requisites. Companies are obliged to comply with increasingly stringent short-term and mid-term requirements on energy efficiency and emission curtailment in order to create a more sustainable business in years to come [5]. Differently from the past, relying just on slow steaming<sup>3</sup> is not sufficient to meet new requirements. Firstly, it does not directly address the main goal of regulations, i.e. to undertake a path to sustainable growth by means of new technologies development. Secondly, it could put companies out of business when the adverse effects outweigh benefits [6]. To stay competitive, stakeholders are encouraged to develop new strategies. Response plans for existing ships usually consist in limitations on engine or shaft power, installation of energy saving devices, introduction of sustainable technologies as additional power sources, improvement of waste and heat recovery methods, weather routing<sup>4</sup> and so on [7].

---

<sup>1</sup>by value.

<sup>2</sup>CII: carbon intensity index, EEDI: energy efficiency design index, EEXI: energy efficiency existing ship index.

<sup>3</sup>The practice to reduce ship cruise speed in order to save on fuel costs.

<sup>4</sup>The technique to both spatially and temporally project the vessel route and eventually operate some changes to avoid harmful weather conditions.

New vessels have a greater flexibility and important modifications could still be done during design phases by, for instance, creating a longer and slimmer hull that can effectively reduce resistance and thus energy consumption. Besides the adoption of new alternative fuels, which will become more relevant in the next decades, ship electrification is an already affirmed key solution for decarbonisation [8]. Adopted in the design phase or as a retrofit option, an hybrid propulsion system<sup>5</sup> is usually crucial to comply with actual and possible future regulations and it ensures a higher degree of flexibility due to the integration with onboard electrical generation. Advantages such as reduction in operating costs, elimination of port manoeuvring emissions, availability of shore power when at berth and the possible introduction of sustainable technologies make hybridisation a valid option towards the creation of smarter propulsion systems.

The impact of electrification on the transport industry has not been overlooked by the nautical tourism. Although temporally shifted with respect to the automotive sector, recreational boating has found commercial opportunities in the use of electric boats for leisure activities and passenger transportation. The main advantages consist in [9]:

- A silent operation. Electric engines are less noisy than internal combustion ones at equivalent power. This condition provides extra comfort during navigation
- Reduced operating and maintenance costs. Electric motors are more efficient than those relying on fossil fuels, plus they are made of fewer mechanical parts which cut down maintenance cost. However, care must be taken in handling batteries to preserve their life and avoid a premature replacement.
- No local emissions of pollutants. Besides the benefits for marine ecosystems, it translates into the possibility to enter some restricted areas which are instead precluded to classic motorboats.
- The easier implementation of sustainable energy sources to the propulsion chain. It is the case of PV panels or hydro generators<sup>6</sup> used as range extender due to their capability to produce power onboard.

Similarly to what happens with bigger vessels, full-electric boats still suffer from limitations on range autonomy due to technological constraints on energy storage. However, conditions such as day cruising and passengers transportation on relatively short routes, makes it possible to select marine electric vehicles as competitive choices, especially when a reliable charging infrastructure is available. Relevant examples are offered by Swedish companies Candela and X Shore or the American Vision Marine Technologies<sup>7</sup>, which already provide several vessels for waterborne passenger transport or leisure activities both in Europe and USA. Together with many other companies all over the world they are corroborating the business, in collaboration with a large number of firms dedicated specifically to the power-train manufacture, such as the German Torquedo, the Finnish Oceanvolt, the Norwegian Evoy, the American Elco, the Chinese E-propulsion or the Dutch Bellmarine.

---

<sup>5</sup>A combination of conventional fossil fuel prime mover and electrical motors to fulfill vessel propulsion needs.

<sup>6</sup>Specifically for sailboats.

<sup>7</sup>Vision Marine Technologies is quoted in the stock exchange market.

Aiming at supporting the diffusion of electrical boating, the scope of the present work is to develop a model capable of simulating the operation of a full-electric propulsion system relying on shore power, batteries and photovoltaic panels. The model allows the user to test the performance of a selected design as a function of boat resistance and requested load profile, taking into account ambient conditions to accurately calculate the PV power production. Besides displaying simulation results, the model calculates and shows several performance indicators regarding energy management, whose purpose is to help the user converge towards a better propulsion system bulk design, to be used as reference starting point for possible subsequent optimizations.

Considering the necessity to simulate entire days or even months, the model could not contain detailed electrical reproduction of components that would carry a huge computational burden. The adopted methodology was therefore chosen as a compromise between accuracy and computational time. It makes use of generic mathematical models or average equations that capture the main dynamic of every relevant component and align it with those of the whole system to ensure physical truthfulness. MATLAB® Simulink® environment was chosen as simulating tool, as it suits well with a mathematical model and even provide some embedded equations for components that were used alongside literature sources as validating references. Provided data on ambient conditions and boat resistance, the model encompasses the whole propulsion chain from propeller to electrical input. A certain flexibility is permitted regarding the choice of propellers, PV panels, batteries and Direct Current (DC) motors, as long as data sheet and operating voltages constraints are respected, to allow a stable and physically accurate operation, especially with regards to energy converters and relative controls. Particular care is dedicated to the propeller thrust and boat resistance matching which sets the propulsive load to be sustained by the electric motor. Similarly, control logics are considered of utmost importance as they have to regulate power consumption to ensure an optimal energy management within safety limits.

To offer a clear explanation of its working logic, the model was described by means of a specific case study application. It deals with the design of the propulsion system for a small taxi boat operating in Venice lagoon, powered by a direct drive inboard DC motor, with batteries used as energy storage and PV panels as range extenders. A taxi boat operating routine is characterized by a large degree of load request uncertainty, which makes it a compelling test bench for the control systems of the energy converters installed onboard. All system components were modelled by means of data extrapolated from available data sheets, making sure to work with acceptable operating voltages conditions. With regards to the thesis structure, the work was divided as described below.

The next chapter contains an overview of several scientific articles that have dealt with a purpose similar to the one aimed at in the current work. Later in the chapter, the adopted mathematical approach is explained. Chapter 3 provides a theoretical introduction of the physical concepts at the base of the modeling. Components' working principles are portrayed in function of the role played within system dynamics. Some of them are taken for granted and thus not explicitly described. A comprehensive overview of the Simulink® model subsystems is then presented in Chapter 4. Care was given to break down and analyse every subsystem with a step by step approach, useful to highlight the role played by control logics. Chapter 5 is placed afterwards to further clarify assumptions and limitations of the adapted methodology with the intention to better orient its application to different case studies. Numerical results are shown and critically evaluated in chapter 6. Their visualization provides indeed a reliable option to confirm or recalibrate the system design. Conclusion are finally drawn in Chapter 7, where suggestions for future developments are also pointed out. The appendix contains the main MATLAB® script<sup>8</sup> at the base of the simulation, where all the calculations not previously shown can be found.

---

<sup>8</sup>and its related functions



## Chapter 2

# Literature review and adapted methodology

During the last decades, due to the technological advance in power electronics and electrical motors for the naval sector, many projects have studied the feasibility of hybrid or even fully electric propulsion system designs. Considering physical limitations on energy storage, the majority of case studies for small passenger boats were set in sites where relatively calm waters allowed to obtain a competitive range autonomy. Besides, photovoltaic panels were widely adopted as range extender or even as single energy source due to their capability to generate power onboard. Many examples can be found in literature, at different levels of system detail.

A list of relevant case studies are reported in Table 2.1. Its first rows focus on applications on relatively small boats, while the articles in the second section of the table pertains to bigger electric vessels, whose case studies were not mentioned due to excessive differences in power. Nonetheless, their electric propulsion system design does not differ so much from the one aimed at in the present work, making them a good resource to study the main components of a propulsion chain and their control systems. Additionally, many articles implement a Simulink® model to support the design, making them an important benchmark for the current system simulation. Every reference entry is flanked by a list of key points that summarize the relevant concepts covered in that paper.

Table 2.1. Related works in literature

Author	Case study	Key points	Prime mover	Li-ion batteries
Postiglione et al. [10]	Passenger catamaran	Focus on power electronics. Regenerative braking	$2 \cdot 12[kW]$ PMSM	$96[V]$ , $160[Ah]$
Spagnolo et al. [11]	Solar passenger catamaran	During sunny seasons, light water conditions. Yearly energy estimation	$2 \cdot 8[kW]$ PMSM	$499[V]$ , $180[Ah]$
Al Mehedi et al. [12, 13]	River passenger boat	Component sizing. Cost-effective design. Detailed Simulink® modeling	$5[kW]$ PMDC	$48[V]$ , $18.5[kWh]$
Obaid et al. [14]	General hybrid boat	PV and fuel cell integration. Battery management system based on fuzzy logic	$2[kW]$ AC	$24[V]$
Swe [15]	River cruising boat	Sizing of power supply systems. Numerical results	$4.7[kW]$ PMSM	$48[V]$ , $1000[Ah]$
Bigorra [16]	Leisure boat	Complete overview and sizing of components. Focus on hardtop design	$30[kW]$ PMSM	$375[V]$ , $30[kWh]$
Chao et al. [17]	River cruising boat	Focus on integration and control of distributed PV system. Direct utilization of solar energy	Not specified	$320[V]$ , $60[kWh]$
Spagnolo et al. [18]	Lake passenger boat	Power management system. Energy storage calculations	$2 \cdot 40[kW]$ BLDC	$486[V]$ , $414[Ah]$

Author	Key points
Alexander [19]	Power distribution model. Control scheme and design optimisation. Economical analysis through cost functions. Simulink® modeling
Kim et al. [20]	Qualitative and quantitative comprehensive design procedures for all electric ship propulsion system. Simulink® modeling
Breines [21]	Dynamic simulation of battery powered vessel. High power and voltage involved. Focus on energy management and operation modes. Simulink® modeling
Freire et al. [22]	Relatively low power applications. Details on propulsion chain component performances and dynamic modeling
Bassam et al. [23]	Insights on fuel cell integration. Real ship data. Cost analysis. Simple mathematical ship simulator implemented in Simulink®
Zalani et al. [24]	Optimal design to improve electrical machine performance of a plug-in electric boat
Narendra et al. [25]	Description of photovoltaic and electrical motor coupling by means of converters, drives and control algorithms

Once considered the market trends and the increasing number of case studies dedicated to recreational boating and passenger transport, what clearly arise is the need of a simulation tool that allow to assess boat performances in a specific site and for a desired mission. The here developed model of an all electric propulsion system can be an important ally in that direction, supporting the sector growth in the first conceptual design phases of the projects.

As outlined in the introduction, in order to simulate months or even years, it is not possible to maintain the same accuracy that a design at circuit level would offer. The current model should be seen as a tool to evaluate performances and consequently gain insights and suggestions for resizing the main system components. The latter are modelled via mathematical relationships that substitute the actual electric connections, yet still provide information on the most relevant mechanical and electrical quantities. The objective is similar to other case studies in literature, however its novelty lies in the possibility to simulate the whole propulsion chain, from propeller to energy storage, relying on data sheet informations and boat resistance, while providing not only final energy balances results but also dynamic evolutions of the system variables.

The methodology adopted is summarized in Figure 2.1.

Sources	Simulink® implementation	Validation of single component model	Tuning of control parameters	Overall model physical assessment
Books, papers and online resources are the theoretical foundations of the mathematical modeling. They provide reliable and computationally efficient equations for the components involved in the simulation with the scope to analyse voltage and current variations throughout the whole domain.	Equations and generic model relationships are converted into a Simulink® environment, meaning that mathematical relationships are translated into blocks diagrams linked by a signal network. MATLAB® workspace acts as source and sink for system's inputs and outputs.	Every component model is tested with ad-hoc generated inputs. Validation is performed through comparison with existing Simulink® models or literature references. Care is given to respect data sheet compliances, physical limits and energy conservation.	Control logic must be tailored to the case study under examination. Controller parameters are tuned to ensure relatively fast and accurate results, while numerical issues are solved through mathematical artifacts that ensure system stability without compromising its dynamics.	Once set the temporal and spatial domain, the simulation is launched. Verification of model results is carried out through both numeric and visual inspections. Design performances are critically evaluated to provide insights on the feasibility of a certain configuration for the assigned boat mission.

Figure 2.1. Methodology overview

## Chapter 3

# Theoretical introduction

*Before having a look at the model description presented in Chapter 4 it is useful to introduce the working principle of several fundamental components involved in the simulation. Mathematical modelling equations flank a theoretical description, with an obvious focus on the current application.*

### 3.1 PV array and balance of plant

PV cells are electronic devices able to generate DC electricity when exposed to light. This phenomenon gets the name of photovoltaic effect [26]. The interconnection of several cells forms a PV module (panel) with specific voltage and current characteristics. Usually, in order to fit photovoltaic generation to a specific application, solar panels are linked into a series-parallel configuration, becoming a PV array. Despite the latter is already a generative unit, other components are crucial to create a proper PV subsystem. They are referred to under the term Balance Of System (BOS). Most relevant ones for the present application are [27]:

- Mounting structure. Needed to support the panels and eventually guide them towards the Sun. As to the present case, no tracking algorithm was considered. Due to the unpredictable routes assigned to the boat, panels are assumed horizontally fixed to the hard top.
- DC-DC converter. Needed to adapt the varying PV voltage to that of the other system components. Its operation is dictated by a charge controller via a Pulse Width Modulation (PWM) signal. It is further discussed in section 3.6.
- Inverter. It performs DC to Alternate Current (AC) electricity conversion. It is needed to provide power to AC loads onboard. However, all the loads involved in the case study under consideration require DC current, thus, it was not implemented in the model.
- Storage. Based on batteries. Extra energy can be stored and provided as an alternative source when PV cannot entirely sustain the load request. It is described in section 3.2.
- Charge controller. It regulates power production. A fundamental task consists in the ability to disconnect PV generation to prevent battery overcharge or to shut it off during the night, when a reverse flow of power could occur. As to the present system, charge controller will act on the DC-DC converter through power electronics to ensure maximum power tracking or load following while preserving battery integrity. Its working logic is further described in section 4.2.3.

- Wiring, fuses, relays and other functional or safety equipment. They are not dealt with in the present mathematical model, but would have to be accurately calibrated to the specific real world application.

A boat can be considered as a stand alone system while sailing since it has to rely solely on the power produced on board. However, in port, shore power acts as further power source, connecting the system to the grid.

Table 3.1. PV module and array assumed data sheet

		Module	Array (12 ÷ 14[m <sup>2</sup> ])
Open circuit voltage	$V_{oc}[V]$	38.00	114
Short circuit current	$I_{sc}[A]$	8.85	26.55
Maximum power point voltage	$V_{mp}[V]$	30.88	92.64
Maximum power point current	$I_{mp}[A]$	8.29	24.87
Maximum power	$P_{mp}[W]$	256	2304

Table 3.2. PV module assumed data sheet. Extra parameters

Voltage temperature coefficient	$\beta_V[K^{-1}]$	-0.36%
Current temperature coefficient	$\alpha_I[K^{-1}]$	0.05%
Number of cells	$N_s[-]$	60
Diode ideality factor	$n_d[-]$	1.26

Tables 3.1 and 3.2 contain the data sheet fundamental parameters utilized in the present model. They are provided at STC:

- Irradiance: 1 [ $\frac{kW}{m^2}$ ]
- Module temperature<sup>1</sup>: 25[°C]
- Air mass: 1.5

Each module connected in series increase the array voltage but has no effect on current. On the contrary, connecting new modules in parallel increases current but does not alter voltage. The module-array relation is clarified in eq. 3.1 and 3.2. The PV array of the present case study is composed of 9 modules, arranged in 3 rows ( $N_{s\_module}$ ) and 3 columns ( $N_{p\_strings}$ ).

$$V_{array} = V_{module} \cdot N_{s\_module} \quad (3.1)$$

$$I_{array} = I_{module} \cdot N_{p\_strings} \quad (3.2)$$

---

<sup>1</sup>Cells temperature can significantly differ from the ambient one. Calculating its value would require a deeper analysis considering that panels are cooled by air flow when the boat is in movement. Being that not the scope of the present work, module temperature is always assumed equal to the surrounding ambient one plus 15[°C], accepting the magnitude of the error originated from the choice.



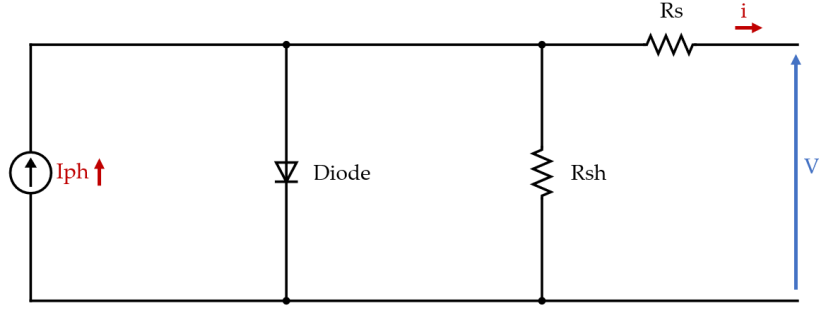


Figure 3.1. Single diode equivalent circuit model

The performance model implemented in the current work was provided by [28]. It makes use of the single diode mathematical model, whose equivalent circuit is depicted in Figure 3.1 and defined by the current-voltage relation described implicitly in eq. 3.3. The reader is referred to [28] and Appendix 7 to find out more about the parameters involved in the calculation.

$$I = I_{ph} - I_s \cdot \left( e^{\frac{V + I \cdot R_s}{a}} - 1 \right) - \frac{V + I \cdot R_s}{R_{sh}} \quad (3.3)$$

Where:

- $I[A]$ : module current
- $I_{ph}[A]$ : module photo current
- $I_s[A]$ : module reverse saturation current
- $V[V]$ : module voltage
- $R_s[\Omega]$ : series resistance
- $a = \frac{\delta_0}{V_{oc}}[V^{-1}]$ : auxiliary parameter
- $\delta_0[-]$ : irradiance coefficient of  $V_{oc}$
- $V_{oc}[V]$ : open circuit voltage
- $R_{sh}[\Omega]$ : shunt resistance

The single diode model is considered accurate enough for the scope of this work as it does not require an excessive computational effort, allows to introduce the dependence on temperature and irradiance and is able, with the exception of partial shading conditions<sup>2</sup>, to reproduce PV characteristic curves that are easy to implement in a Simulink® model [29].

---

<sup>2</sup>Partial shading is considered out of the scope of this work. It is computationally demanding to consider shading while the boat is travelling in between Venice canals.

The selected performance model relies on semi-empirical expressions that, being theoretically well-founded, allow to correctly estimate the array behaviour in function of irradiance and temperature, which are in fact the main ambient conditions affecting PV performance. The possibility to use only data sheet parameters as input data is a great strength of the model. Another plus is its ability to calculate key points by means of both explicit and implicit formulations [28]. As it will be seen in section 4.2.2, the performance model will be used to calculate PV ideal power at different ambient conditions, while also providing the open circuit voltage and short circuit current references to the subsystem where the voltage and current implicit calculation takes place. PV array actual operating point will instead be determined by the buck converter configuration, as a consequence of the control logic imposed to it<sup>3</sup>. To assess the mathematical model accuracy, its output was tested under varying ambient conditions, compared to the one of a *PV array* block<sup>4</sup> in Simulink® and considered acceptable as there was a relative error lower than 1[%] for each point of the curve. Figure 3.2 contains current and power curves as a function of voltage provided either a fixed temperature<sup>5</sup> of 25[°C] or a fixed irradiance of 1000[W/m<sup>2</sup>].

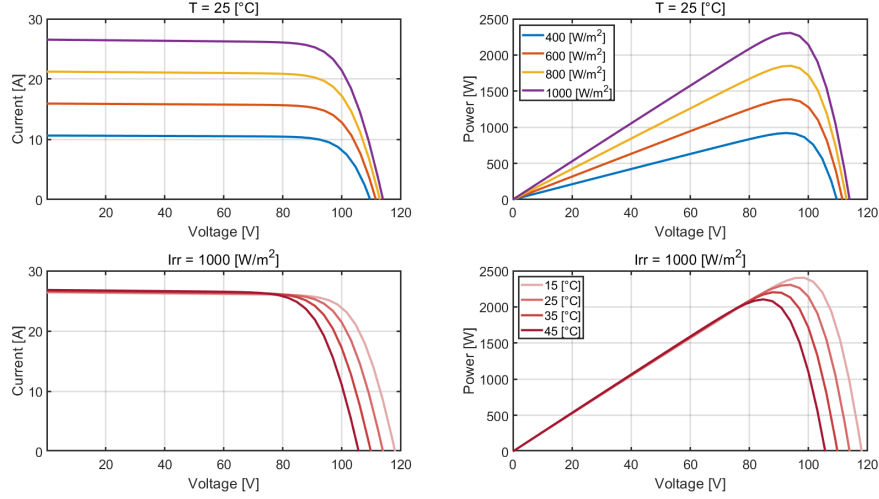


Figure 3.2. PV array curves under different irradiance and temperature conditions

The open circuit voltage  $V_{oc}$  coincides with the abscissa intersection of the Voltage-Current (V-I) curve, while the short circuit current  $I_{sc}$  coincides with the ordinate one. The maximum power point is easily recognisable from the power curves at the right, with  $V_{mp}$  and  $I_{mp}$  being the corresponding values voltage and current values. One may note that:

- Irradiance has an important influence on  $I_{sc}$ , and a smaller one on  $V_{oc}$ , so that  $V_{mp}$  does not vary significantly.
- Temperature has a relatively neglectable effect on  $I_{sc}$ , but the same is not true for  $V_{oc}$ . One may note how  $V_{mp}$  values are shifted to the left.

<sup>3</sup>The PV array will not power a traditional resistive load. Its terminals will be connected to a buck converter, which links the array to a DC bus where batteries, motor and additional auxiliary loads are connected in parallel.

<sup>4</sup>With the same data sheet parameters

<sup>5</sup>As already stated on page 22 ambient temperature is assumed equal to the module one.

## 3.2 Energy storage

Considering the intention to propel a relatively small motorboat via DC motors and the desire to integrate PV panels as range extender, lithium batteries<sup>6</sup> are probably the best technology to opt for. In fact, besides their compatibility with direct current, they can provide reliable energy, offer a good degree of design flexibility and avoid local emissions. Furthermore, they maintain operation silent and require little to no maintenance. An alternative option could be that of using a fuel cell. However, technologies are at a different level of maturity, with batteries being currently the more compact, safe, efficient and economically attractive option for small vehicles and short travels [30]. Drawbacks such as relatively low energy capacity have to be taken into account when considering the types of routes to be taken. Indeed, a back up power device such as a DC generator is required to ensure a safe navigation in case of undesired situations, such as power shortages due to erroneous estimations. The need for disposal and subsequent end-of-life replacement of batteries should also be considered, but pertain to an economical analysis which is not included in current work.

Despite power electronics can compensate even broad voltage difference, the choice of the battery bank voltage is crucial for the interconnection with other system components. Considering the present case study, PV panels always work at a voltage higher than the battery one, so that a buck converter can always be controlled with acceptable duty cycles. The same is true for the buck converter which links the battery bank with the 12[V] auxiliary loads. As to the motor, it will be seen in section 3.4 that its DC drive requires a constant voltage input. Therefore, a buck-boost converter is placed to ensure a voltage of 56[V] to the motor drive terminal, whatever the value of the battery voltage and thus the DC bus. Regarding the design of battery capacity, its value is not as pivotal as the voltage one. A high capacity value may reduce waste of solar energy and increase velocity-range performances. However, batteries are heavy and costly, and a large battery bank would increase boat displacement and thus water resistance, reduces space available on board, require larger charging times and a bigger initial expense. Accurate technical and economic analysis have to take place to obtain an optimum that suits boat's mission.

Table 3.3 shows the main data sheet parameters of the reference battery chosen for the simulation: the existing U27-24XP model from the U-Charge XP series from Valence Lithion [31]. It was chosen as reference battery between those already implemented in the *Battery (Table-Based)* block in Simulink® to allow an easier comparison between the present and the already established *generic battery model* [32]. The latter is indeed the reference performance model adopted in the current simulation. Its fundamental equations are shown later in this section.

When multiple batteries are linked together, voltage and capacity sums up according to eq. 3.4 and 3.5.

$$V_{batt} = V_{single\_batt} \cdot N_{ser\_batt} \quad (3.4)$$

$$Q_{batt} = Q_{single\_batt} \cdot N_{par\_batt} \quad (3.5)$$

The adopted battery bank layout consists in a total of eight batteries: two sets of four units connected in parallel. The resulting parameters can be found in Table 3.3.

---

<sup>6</sup>Lithium battery type has been preferred to others due to their well-established superior capacity in terms of power and energy density, allowing the best size, weight and efficiency compromise in the class.

Table 3.3. Single battery and battery bank data sheet

Lithium iron phosphate ( $LiFePO_4$ ) chemistry		Single battery	Battery bank
Nominal Voltage	$V_{nom}[V]$	25.6	51.2
Capacity@ C/5, 25°C	$Q_{rated}[Ah]$	71.84	287.36
Energy	$E_{batt}[KWh]$	1.84	14.72
Internal resistance	$R_{int}[\Omega]$	1.389e-2	6.945e-3

Please note that the internal resistance is assumed constant. The one of the whole battery bank is calculated according to eq. 3.6.

$$R_{int} = R_{int\_single\_batt} \cdot \frac{N_{ser\_batt}}{N_{par\_batt}} \quad (3.6)$$

Data sheet values are not sufficient to recreate an accurate enough battery performance model. Usually, manufacturers provide also discharge profiles at different C-rates<sup>7</sup>. Data relating to the nominal discharge rate can be utilized to extract useful parameters which are then fed to the mathematical model. An example of discharge curve and relative parameters is shown in Figure 3.3. The appendix contains all the formulations that are not shown in this section.



Figure 3.3. Battery discharge curve. Extracted parameters

<sup>7</sup>The battery C rating is related to the charge or discharge current and provides an estimation of speed at which a battery gets charged or discharged. A discharge C-rate of 1C means that a fully charged battery is totally discharged in the time span of 1 hour, while a 0.2C rate is expected to discharge it in 5 hours.

MATLAB<sup>®</sup> *generic battery model* [32], which was adopted in this work, intrinsically assumes that:

- The internal resistance does not vary with the current flowing through it, as already stated.
- The charge characteristic curve is equal to the discharge one. Parameter are indeed extracted only from the latter curve.
- Battery memory effect and self-discharge are not considered.
- No Peukert's law is not applied, i.e. battery capacity is considered constant whatever the charge or discharge current amplitude.

The model implemented in the present simulation further simplifies the battery behaviour because no temperature or aging effect are considered even though they could potentially be an extension of the current formulation, as suggested by [32]. Hypothesis such as these find a motivation when looking at the whole picture. It would not be rational to dedicate a lot of computational effort to the modelling of a specific component when the others involved do not pertain to the same level of accuracy. Similarly, modelling all the components with a higher degree of precision would not reach the main scope of the work, i.e. a fast and accurate enough performance simulation that can lead to the bulk design of an all electric boat propulsion system.

Eq. 3.7 and 3.8 shows the charge and discharge formulations implemented in the Simulink<sup>®</sup> subsystems of section 4.2.5.

$$\text{Discharge}(i^* > 0) \quad V_{batt} = E_0 - K \cdot \frac{Q}{Q - it} \cdot i^* - K \cdot \frac{Q}{Q - it} \cdot it + A \cdot \exp(-B \cdot it) - R_{int} \cdot i_{batt} \quad (3.7)$$

$$\text{Charge}(i^* < 0) \quad V_{batt} = E_0 - K \cdot \frac{Q}{it + 0.1 \cdot Q} \cdot i^* - K \cdot \frac{Q}{Q - it} \cdot it + A \cdot \exp(-B \cdot it) - R_{int} \cdot i_{batt} \quad (3.8)$$

Where:

- $V_{batt}[V]$ : battery voltage
- $E_0[V]$ : constant voltage
- $A[V]$ : exponential drop in voltage
- $B[Ah^{-1}]$ : one third of exponential capacity
- $K[V/Ah]$ : polarization constant
- $Q[Ah]$ : maximum battery capacity
- $it[Ah]$ : extracted capacity
- $i_{batt}[A]$ : current flowing through the battery
- $R_{int}[\Omega]$ : battery internal resistance

An important distinction is to be made between battery closed circuit and open circuit voltage. The latter can be considered as ideal, because it reflects battery voltage only when there is no current flow (open circuit) and thus no internal impedance, which is instead the cause of a voltage drop when current flows through it. Their relation can be found in eq. 3.9. The current  $i_{batt}$  is considered positive when the battery is discharging.

$$V_{batt} = V_{b\_oc} - R_{int} \cdot i_{batt} \quad (3.9)$$

Finally, Figures 3.4 and 3.5 contains the battery bank discharge curves at different current amplitudes. The blue curve at 50[A] roughly corresponds to the battery bank nominal C-rate ( $0.2C$ ). Lower voltages and shorter duration are experienced at higher current. The reverse is also true. Ideally, one should maintain the current withdrawal close to nominal conditions during operation, but it is not easily achievable with a motorboat that follows no fixed route or timetables. On the other hand a proper night charge can be carried trough. Currents will be limited to a value close to  $0.1C$  to achieve a compromise between charging time and battery life preservation.

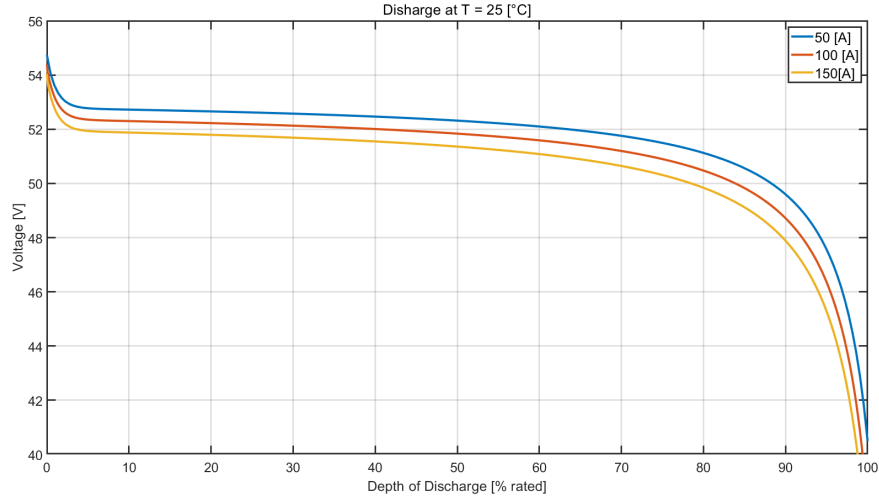


Figure 3.4. Battery discharge curve. Voltage as a function of depth of discharge

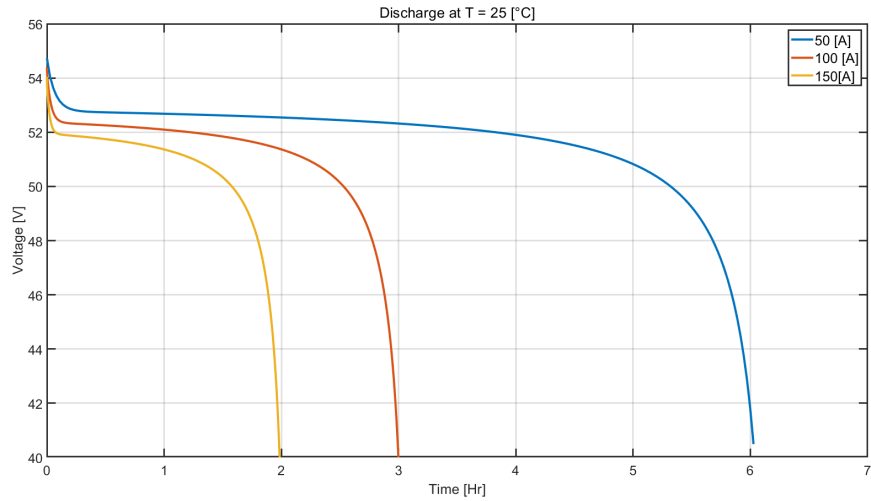


Figure 3.5. Battery discharge curve. Voltage as a function of discharge time

### 3.3 From boat resistance to propeller and motor load

A propulsion system has to provide mobility to a boat in within a range of design and off-design conditions. In order to accomplish the task, information on boat resistance  $R$  under different ambient conditions have to combined with the expected behaviour of the propulsor, so that the propulsion system can provide the right amount of thrust to overcome resistance and safely control the boat. As to the scope of the present model, it is expected to already posses boat resistance curves that can used as input to the simulation. What instead can be optimised are the propulsion chain components, such as propeller, gearbox and prime mover. Resistance varies according to speed, size and geometry of the boat, together with external factors such as sea state, water depth and fouling [33]. As to the following, only the design resistance curve is passed to the model to facilitate the reading of results. Boat resistance at different velocities is shown in Figure 3.6, together with the resultant propulsive power needed, i.e. the product of resistance and speed. The curve is provided by a research group of Politecnico di Torino and pertains to the resistance of a passenger boat prototype, of modest dimensions, with a displacement of 1.5 tons. It refers to light sea conditions. A maximum speed of 5 [m/s] is chosen since the limit speed in the Venetian lagoon is set to 20 [km/h].

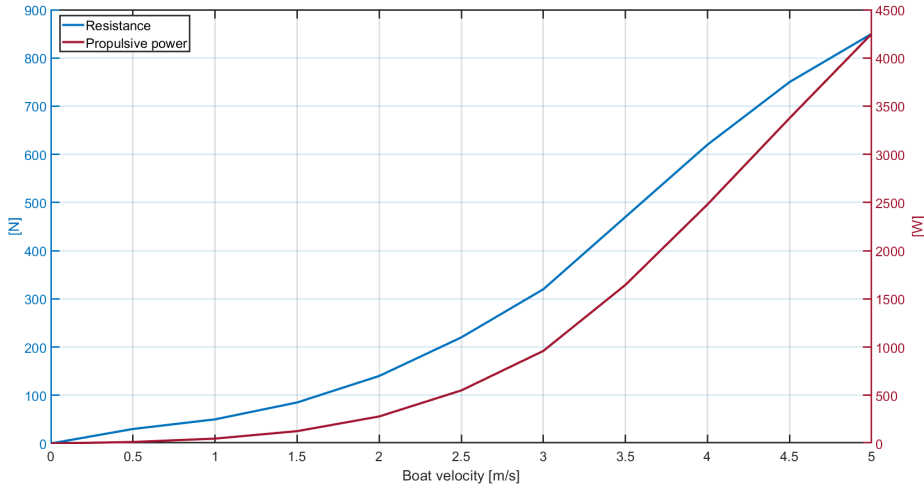


Figure 3.6. Resistance and propulsive power curve adopted in the simulation

Please note that the propulsion plant will often operate under off-design conditions which will change the slope and shape of the resistance curve. Some examples are:

- Change of boat displacement due to a weight distribution other than design one. For instance, adding more batteries or increasing the number of people onboard increase the total weight.
- Rougher or lighter sea state conditions
- Very low water depth
- Accumulation of hull fouling

The accuracy level of resistance curves determines how close the model can simulate a real world application.

Once obtained the boat resistance, the propulsion chain has to be traced backwards so that the input power can be derived. A useful scheme for the propulsion chain is presented in Figure 3.7. It follows the design rules described in [33]. Powers from ship demand to electric supply are represented, linked by efficiencies. The latter can be grouped in the product of two efficiency representing key passages: electrical power converted into mechanical one to drive the propeller which in turn faces other losses before delivering an effective power to the hull.

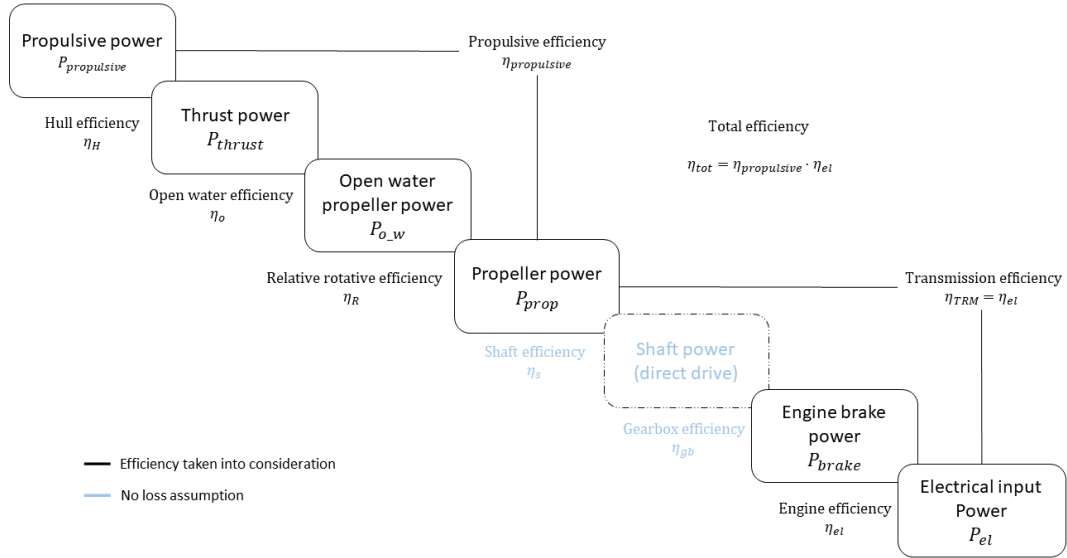


Figure 3.7. Propulsion chain: from resistance to brake power

A screw type, fixed pitch, general purpose propeller from Torqueedo [34] was selected. It is compatible with the Cruise 10.0 or 12.0 motor models from the same brand, whose power rating is in the range assumed for the electric engine in section 3.4. The selected propeller is a good compromise between a low to medium speed request and a sufficient torque capability, which is a peculiarity of five blades propellers. Its data sheet parameters are shown in Table 3.4

Table 3.4. Propeller data sheet

Number of blades	$N_{blades}[-]$	5
Diameter	$D_{prop}[mm]$	320
Pitch	$Pitch_{prop}[mm]$	330
Pitch/Diameter ratio	$Pitch_{prop}/D_{prop}[-]$	1.03125
Rated speed	$n_{max\_prop}[rpm]$	1400
Blade area ratio (assumed)	$BAR[-]$	0.75



Propellers have to overcome resistance by delivering thrust. A part of it is lost due to added resistance<sup>8</sup>, which is taken into account by the thrust deduction factor  $t$ . Additionally, due to the creation of a boundary layer at the water-hull interaction, there is a difference between the actual boat speed  $v_s$  and that of water at the propulsor location (velocity of advance  $v_a$ ). This reduction is taken into account by the wake factor  $w$ , with  $v_a = (1 - w) \cdot v_s$ . The two terms were assumed according to usual guide rules suggested by [33]:  $t = 0.15$  and  $w = 0.20$ .

The hull efficiency  $\eta_H$ , defined as the ratio between the effective propulsive power and the thrust power delivered by the propeller, can be calculated as a function of the two parameters:

$$\eta_H = \frac{1 - t}{1 - w} \quad (3.10)$$

In case of boats pushed by a single screw propeller, hull efficiency can usually assume values higher than unity. This happens as the beneficial effect of a slower water velocity at propeller inlet usually overcompensates the extra thrust required to overcome added resistance caused by the propeller interaction with the flow. As to the propeller itself, it receives mechanical power in terms of torque and rotation and outputs a thrust force at a certain boat speed. Conversion losses are covered by the open water efficiency  $\eta_o$ <sup>9</sup>, which is usually measured in test tunnels with an uniform velocity field. Its estimation will be seen in the following subsection.

$$\eta_o = \frac{T_{prop} \cdot v_a}{2\pi \cdot Q_{prop} \cdot n_{prop}} \quad (3.11)$$

Where:

- $T_{prop}[N]$ : propeller thrust
- $v_a[m/s]$ : velocity of advance
- $Q_{prop}[Nm]$ : propeller torque
- $n_{prop}[rad/s]$ : propeller rotational speed

When propellers are mounted on a boat, the open water efficiency is further multiplied by the relative rotative efficiency  $\eta_R$  (assumed equal to 0.99), which instead takes into account the flow distortion caused by the hull. The efficiencies mentioned so far are all embraced under the propulsive efficiency:  $\eta_{propulsive} = \eta_H \cdot \eta_o \cdot \eta_R$ .

Proceeding towards the start of the propulsion chain, the rotational power is transmitted to the propeller by the same shaft put into rotation by the inboard electric motor. This configuration is called direct drive. It brings several advantages compared to geared drives when efficiency and weight distribution are key aspects in the design phase. As described in section 3.4, this configuration requires the installed motor to provide a sufficient amount of torque at relatively low rotational speeds<sup>10</sup>. When the latter is not achievable, a traditional gearbox is usually installed and the input shaft is put into rotation by a higher rpm motor. Moreover, installing a gearbox can increase power density, thus reducing the total space requested from the motor system. Shaft losses, which usually occur due to friction in shaft bearings, have been neglected in the simulation ( $\eta_s = 1$ ). Due to the direct drive configuration, shaft power is equal to the usable power output of the engine, i.e. the brake power. Therefore no gearbox transmission losses can occur ( $\eta_{gb} = 1$ ).

---

<sup>8</sup>Resistance curves are usually calculated when the propeller is not attached to the hull.

<sup>9</sup>It is called open water as this is the name of the open water tanks where propellers are usually tested.

<sup>10</sup>Generally lower than 1500 rpm.

This lead to the conclusion that transmission losses ( $\eta_{TRM}$ ) considered from the model only account for the conversion of electric power into mechanical one operated from the motor.

$$\eta_{TRM} = \eta_{el} = \frac{2\pi \cdot Q_{prop} \cdot n_{prop}}{V \cdot I} \quad (3.12)$$

Where  $V \cdot I$  represents the power drawn from the motor system, which is composed by the motor, its drive and a buck-boost converter controlling its input voltage.

### 3.3.1 Propeller and motor matching

The performance of a propeller can be described by water advance velocity  $v_a$  at the propeller inlet, thrust  $T_{prop}$  and torque  $Q_{prop}$ . Those physical quantities are made non-dimensional by means of the water density  $\rho$ , the propeller angular speed  $n_{prop}$  and diameter  $D_{prop}$ . In particular, the three non-dimensional parameters are:

$$\text{The advance ratio } J = \frac{v_a}{n_{prop} \cdot D_{prop}} \quad (3.13)$$

$$\text{The thrust coefficient } K_T = \frac{T_{prop}}{\rho \cdot n_{prop}^2 \cdot D_{prop}^4} \quad (3.14)$$

$$\text{The torque coefficient } K_Q = \frac{Q_{prop}}{\rho \cdot n_{prop}^2 \cdot D_{prop}^5} \quad (3.15)$$

Regarding propeller capability to converting the rotational input into a thrust force, is can be expressed by the open water efficiency  $\eta_o$ , computed as a function of the above parameters [33].

$$\eta_o = \frac{K_T \cdot J}{2\pi \cdot K_Q} \quad (3.16)$$

The performance of a propeller are usually enclosed in an open water diagram, where  $\eta_o$ ,  $K_T$  and  $K_Q$  are represented as a function of  $J$ . A typical diagram is shown in Figure 3.8. Propeller diameter and water velocity of advance are considered fixed, so that an increasing advance ratio corresponds to a decreasing propeller tip speed.  $K_Q$  is multiplied by ten for better readability.

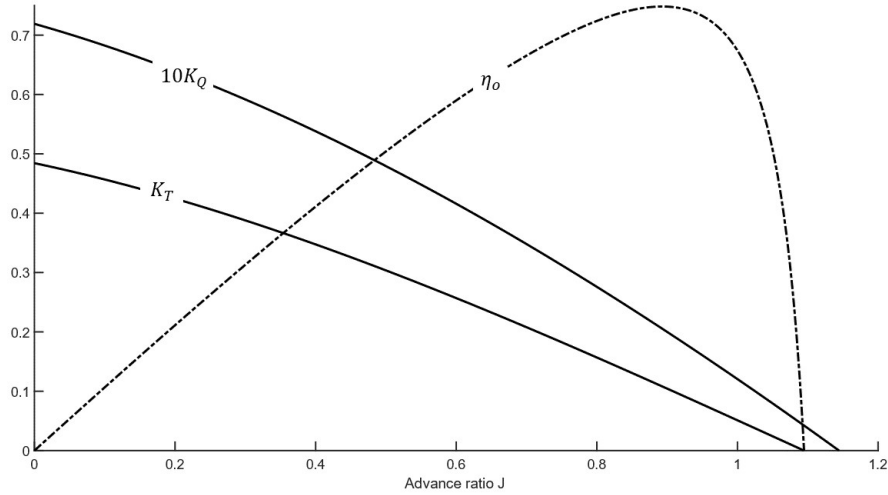


Figure 3.8. Propeller open water diagram

Open water diagrams become useful when designing a propeller from specific boat characteristics or when the intention is to calculate operating points in a pre-existing design. MATLAB<sup>®</sup> script *propcalc*, created by doctor E.A.E. Duchateau from TU Delft University, is a tool able to calculate the Wageningen B-Series polynomials from the polynomial fits provided by [35]. It was chosen for the present simulation as it can output the propeller open water diagram parameters when fed with info on advance ratio, number of blades, blade area ratio<sup>11</sup>, pitch/diameter ratio and Reynolds number<sup>12</sup>. When considering a particular ship, propeller design consists in finding the optimal propeller geometry and speed when efficiency is the criterion to prioritize<sup>13</sup>. As to the current work, a reverse path is followed: the goal is to find the operating points of a specific propeller when matched with a certain boat resistance. Therefore, *propcalc* was used to obtain propeller open water diagrams at different boat velocities, utilizing as input data in Table 3.4. An example of curve derivation for the case under consideration is presented in the following algorithm (Figure 3.9), considering just a specific design condition:  $v_s = 5[m/s]$ . Equations and respective derivation can be found in [33], while their implementation is contained in the MATLAB<sup>®</sup> script in the appendix.

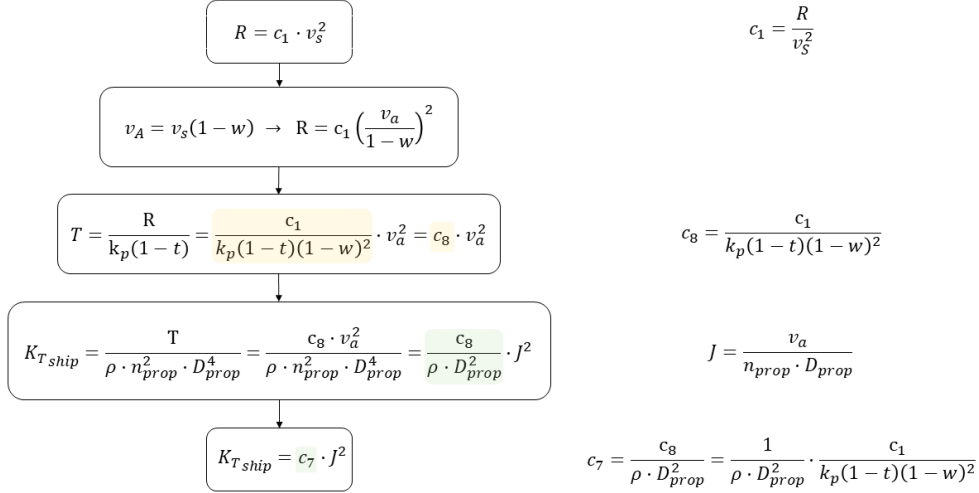


Figure 3.9. Algorithm. Boat thrust coefficient as a function of advance ratio

Note that constants  $c_1, c_8$  and  $c_7$  are not fixed but vary accordingly to boat velocity, resistance and propeller properties. To find the propeller characteristics able to sustain a desired boat velocity, the thrust coefficient required from the boat has to match that of the propeller. As the propeller geometry is fixed, the only free parameters able to change is the propeller rotational speed.

<sup>11</sup>It is the ratio of the blades projected area (not considering the hub) over the area swept by the same blades (propeller disk/circle) when the propeller is rotating.

<sup>12</sup>It was seen to have a neglectable effect on propeller characteristics

<sup>13</sup>Limits on attainable diameter and tip speed are to be considered to maintain physical restrictions.

Figure 3.10 contains the visualization of the matching on the open water diagram, from where torque and propeller load  $P_{prop}$  can also be calculated.

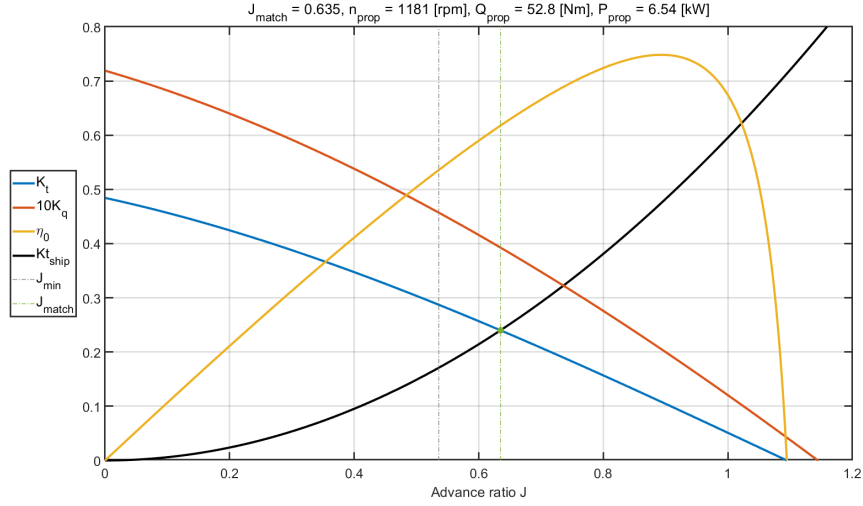


Figure 3.10. Open water diagram at  $v_s = 5[m/s]$ . Matching of thrust coefficient

Repeating the process for all the desired operating conditions allow to define the propeller load. Results are shown in Figure 3.11.

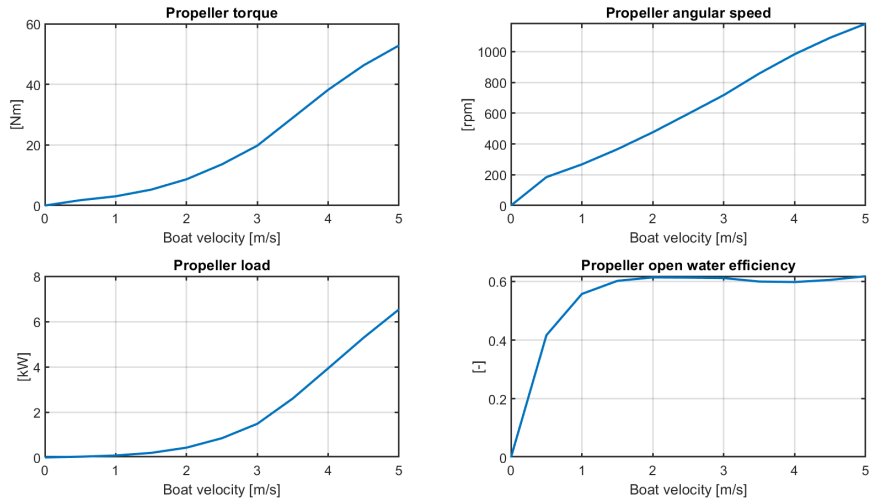


Figure 3.11. Propeller load and relative parameters

Due to the direct drive configurations and the above mentioned assumption, propeller load coincides with brake power. Thus, it is straightforward to link brake power and power input through the electrical efficiency  $\eta_{el}$ .

### 3.4 DC motor

Once crossed backwards the propulsion chain, brake power in terms of torque and rotational speed was computed. Those quantities are delivered from the electric motor. Traditional induction or brushed DC motors have been replaced by more efficient solutions. Indeed, the majority of motors dedicated to the recreational marine sector are either Permanent Magnet Synchronous Motor (PMSM) or Brushless Direct Current Motor (BLDC) machines. The former is an AC synchronous motor with permanent magnets on its rotor whose magnetic field rotate at synchronous speed with the stator one. The latter has an almost identical construction, but is electronically commutated<sup>14</sup> by means of a DC current supply. Both motors perform efficiently, provide good flexibility and a silent operation. The commutation of BLDC machines still poses some limits, such as torque ripples, but on the other hand makes use of a relatively simpler control logic. The higher efficiency, power density and torque offered by PMSM motor comes instead at a higher cost and a more complex regulation [36, 37]. The bigger assumption made throughout the whole model consists in modelling an advanced BLDC or PMSM motor by means of a brushed DC model whose parameters are partly assumed. It was done due to the undeniable model simplicity and the easiness in speed control, which can be performed by means of solely voltage regulation<sup>15</sup>. A traditional electrical equivalent circuit was indeed implemented in the simulation. It is shown in Figure 3.12. Despite describing the operation of a brushed PMDC motor, it still relies on the same drive principle: rotational speed can be controlled by modulating the input voltage, while torque request can be satisfied by varying the draw of current. Therefore, it suits well with the level of detail and computational burden aimed at in the present work. Current and speed controller are of the Proportional Integral (PI) type, whose description can be found in section 3.5. The reference theory for the following formulations can be instead found in [38, 39].

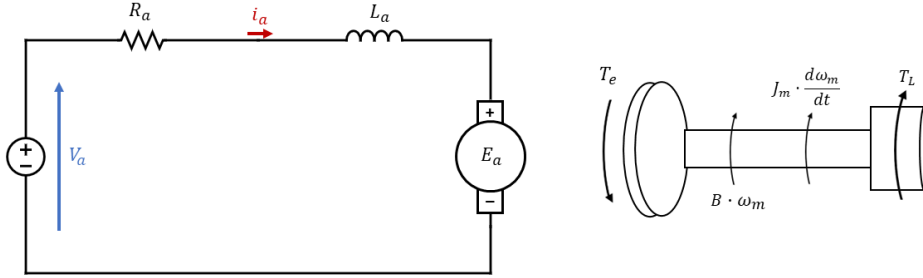


Figure 3.12. PMDC motor electrical circuit and torque representation

As to the electrical (eq. 3.17) and mechanical (eq. 3.17) modelling:

$$V_a = R_a \cdot i_a + L_a \cdot \frac{di_a}{dt} + E_a \quad (3.17)$$

$$T_e = J_m \frac{d\omega_m}{dt} + B_m \cdot \omega_m + T_L \quad (3.18)$$

<sup>14</sup>In contrast to traditional brushed motors which makes use of mechanical brushes for commutation

<sup>15</sup>Permanent Magnet Direct Current (PMDC) motors rotational speed is directly proportional to the applied armature voltage.

Where:

- $V_a[V]$ : armature voltage
- $R_a[\Omega]$ : armature resistance
- $i_a[A]$ : armature current
- $L_a[H]$ : armature inductance
- $E_a[V]$ : back Electro-Motive Force (EMF)
- $T_e[Nm]$ : torque generated by the electrical motor
- $B_m[Nm/(rad/s)]$ : viscous friction coefficient
- $\omega_m[rad/s]$ : angular velocity of the motor shaft
- $J_m[kg \cdot m^2]$ : rotational inertia
- $T_L[Nm]$ : load torque

Rotational inertia and friction causes the torque needed from the motor to be higher than the one requested from the propeller, as expressed in eq. 3.18. As to the rotational speed, it has to be equal to the propeller one, since they are linked by the same shaft. Besides, being constant the magnetic flux created by permanent magnets, the induced voltage in the conductors ( $E_a$ ) is directly proportional to the angular velocity of the motor  $\omega_m$ .

Motor electrical and mechanical systems are coupled. Torque is proportional to current, while back EMF to rotational speed. Equations 3.19 establish the electro-mechanical coupling. Note that the numerical values of the two proportionality constants are the same, so that  $k_t = k_e$  [38].

$$\begin{cases} T_e = k_t \cdot i_a \\ E_a = k_e \cdot \omega_m \end{cases} \quad (3.19)$$

The scheme in Figure 3.13 reports the controller configuration able to regulate the DC motor power. It mainly consists of two cascade feedback controllers which guarantee the system output to be as close as possible to the input reference. Control parameters have to be properly tuned to become able to reject disturbances in a stable way. A more accurate description can be found in sections 3.5 and 4.2.7. As noticeable, no position control is taken into account as it usually is not so relevant for an inboard marine engine.

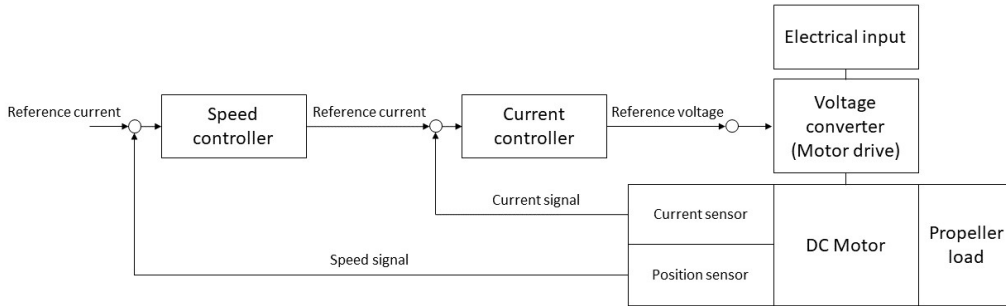


Figure 3.13. Configuration of the control system for the DC motor

Regarding the choice of motor parameters, unfortunately, it is not always possible to obtain an exhaustive list of data sheet parameters. Table 3.5 contains some data provided by the manufacturer. Torqueedo Cruise 12.0 model [40] was utilized as reference, even though it refers to an outboard geared motor. It was done since the brand provides the propulsive power output at rated conditions, and thus the overall propulsion chain efficiency, which is a really useful parameter to help assuming those that are not directly provided. Derived values are instead extrapolated, assuming the relationship showed in the equations below. A good design would require to check if both propeller and motor operating conditions do not exceed the rated ones.

Table 3.5. DC motor data sheet

Provided			Derived		
Rated input power	$P_{rated}[W]$	12000	Rated armature current	$I_{a\_rated}[A]$	250
Propulsive power	$P_{propulsive}[W]$	6720	Rated torque	$T_{e\_rated}[A]$	78.6
Nominal voltage	$V_{nom}[V]$	48	Armature resistance	$R_a[\Omega]$	7.68e-3
Maximum propeller speed	$n_{max\_prop}[rpm]$	1400	Armature inductance	$L_a[H]$	1.7e-3
Overall efficiency	$\eta_{tot}[-]$	0.56	Rotational inertia	$J_m[kg \cdot m^2]$	0.025
Motor efficiency	$\eta_{el\_motor}[-]$	0.96	Friction coefficient	$B_m[Nm/(rad/s)]$	0.01
			Motor constant	$k_t[Nm/A]$	0.302

As to power rating, a slightly oversized motor was chosen to allow the boat to cope with harsher sea states even in off-design conditions.

$$I_{a\_rated} = P_{rated}/V_{nom} \quad (3.20)$$

$$T_{e\_rated} = P_{rated} \cdot \eta_{el\_motor} / n_{max\_prop} \quad (3.21)$$

$$R_a = V_{nom} / I_{a\_rated} \cdot (1 - \eta_{el\_motor}) \quad (3.22)$$

$$k_t = T_{e\_rated} / I_{a\_rated} \quad (3.23)$$

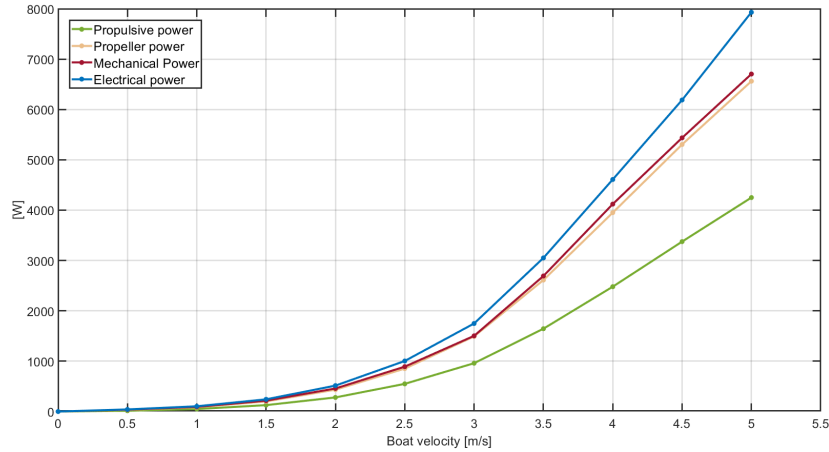


Figure 3.14. Power in the propulsion chain as a function of boat velocity.

As shown, the mechanical output power delivered from the motor is slightly higher than the propeller load due to the friction and inertial torque it experiences.

### 3.5 Proportional-integral controller

A PI controller typical scheme is shown in Figure 3.15. It is a closed loop controller with the capability to adjust control inputs<sup>16</sup> in function of feedbacks on the output signal. It combines the properties of proportional and integral controllers to obtain a good compromise in response speed and precision. In particular:

- Proportional controllers, whose output is proportional to the error by a gain coefficient ( $K_p$ ), usually provide a quick response. However, a wrong choice of gain values can cause instability plus they are not capable to completely eliminate the error. In fact, there is always a steady state error which the controller cannot nullify.
- Integral controllers, whose output is the integral of the error multiplied by a gain value ( $K_i$ ), are instead able to eliminate the error but suffer from errors build up in the integral term which slow down its convergence.

There are applications in which the controller output has to be constrained in between certain values. Nevertheless, saturating the output value does not hinder the integrating action. In case of sustained errors the integral term can accumulate a considerable value which makes it really hard for the controller to respond in an efficient way to the subsequent changes in error. This behaviour gets the name of *integral windup*. Recovering would require several errors of the opposite sign. To avoid a similar drawback, the magnitude of the integral block has to be kept at a reasonable value. An established method consists in calculating the difference between controller and limiter output, multiply it by a gain ( $K_{aw}$ ), and subtracting the result from the error computation. The anti-windup gain is usually set as the inverse of the proportional gain [38].

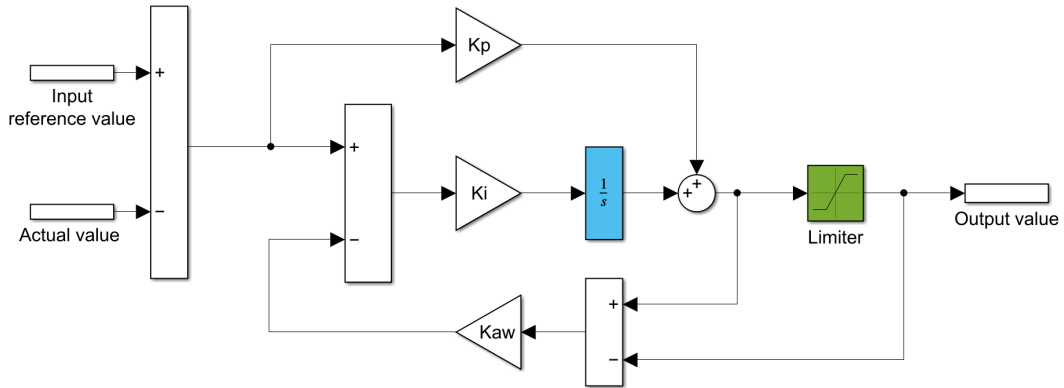


Figure 3.15. Schematic of a PI controller with anti-windup gain

PI controllers are largely used in DC motor drive system to control position, speed and current signals. They also find an application in the duty cycle regulations of DC-DC converters. As to the former, controller gains can be set in relation to some physical values such as the switching frequency of the motor and its armature parameters. Regarding the latter, tuning is usually necessary to avoid instability in the way the output responds to the change in error. Both cases are later analysed in Chapter 4.

<sup>16</sup>The absolute error between the input reference value and the actual signal value



### 3.6 Buck converter

A buck converter is DC-DC converter able to step down the input voltage to a desired output by means of the action of a switch. A switching element such as a transistor is usually implemented. For instance, a MOSFET or an IGBT. The switch allows to alternatively charges an inductor which is used as storage element. It accumulates energy during the on state, when input current flows through, and releases it back when the switch is turned off to ensure continuous flow of current to the load. A capacitor in parallel helps maintaining a constant output current while smoothening voltage ripples. Thus, the controller makes it possible to obtain a specific lower voltage value on the load terminals by varying the switching time intervals and so the amount of time the input source is effectively connected to the circuit. PWM technique is typically implemented to chop the input power as a function of its duty cycle  $D$ . Considering an ideal circuit, eq. 3.24 describes the effect on voltage value when the converter is operating in continuous conduction mode. Due to energy conservation the output current has to increase proportionally to the decrease of voltage. Therefore, if the voltage is halved the current increases by a factor two.

$$V_{out} = V_{in} \cdot D \quad \rightarrow \quad I_{out} = \frac{I_{in}}{D} \quad (3.24)$$

System 3.25 describes voltage and current average behaviour during both the on and off intervals of the switching period [41], obtained by applying Kirchhoff laws to the circuit in Figure 3.16.

$$\begin{cases} t \in (0, t_{on}] \\ L \frac{di_L}{dt} = V_{in} - V_{out} \\ C \frac{dV_{out}}{dt} = i_L - \frac{V_{out}}{R} \end{cases} \quad \begin{cases} t \in (t_{on}, T] \\ L \frac{di_L}{dt} = -V_{out} \\ C \frac{dV_{out}}{dt} = i_L - \frac{V_{out}}{R} \end{cases} \quad \rightarrow \quad \begin{cases} t \in [0, T] \\ L \frac{di_L}{dt} = -V_{out} + V_{in} \cdot D \\ C \frac{dV_{out}}{dt} = i_L - \frac{V_{out}}{R} \end{cases} \quad (3.25)$$

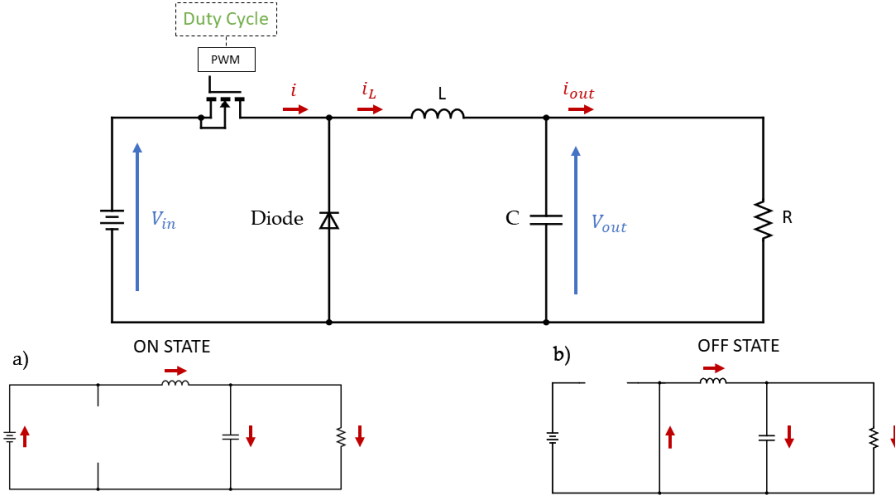


Figure 3.16. Simplified circuit of a buck converter

As to the current simulation, duty cycle control will play a crucial role in conditioning the operating points of the PV array or regulating the output voltage of the 12V grid.

### 3.7 Buck-Boost converter

A buck-boost converter operates with the same circuital components of a buck converter. Their layout makes it possible to output a voltage either higher or lower than the source one. The disposition shown in Figure 3.17 is of the inverting typology, meaning that the output voltage presents an opposite polarity with respect to the input one. Whenever a specific application would need it, it is possible to create a non-inverting converter by modifying the electrical circuit, introducing extra components (a diode and a switch) and adapting the control logic. Considerations on efficiency can be found in [42]. When no losses are considered, eq. 3.26 describes the effect on the output voltage value when the converter is operating in continuous conduction mode. Due to energy conservation, input and output power has to be equal. Therefore, the current increase or decrease is inversely proportional to the voltage variation.

$$|V_{out}| = V_{in} \cdot \frac{D}{1-D} \quad \rightarrow \quad |I_{out}| = I_{in} \cdot \frac{1-D}{D} \quad (3.26)$$

System 3.27 describes voltage and current average behaviour during both the on and off intervals of the switching period [41, 43], obtained by applying Kirchhoff laws to the circuit in Figure 3.17.

$$\left\{ \begin{array}{l} t \in (0, t_{on}] \\ L \frac{di_L}{dt} = V_{in} \\ C \frac{dV_{out}}{dt} = -\frac{V_{out}}{R} \end{array} \right. \quad \left\{ \begin{array}{l} t \in (t_{on}, T] \\ L \frac{di_L}{dt} = -V_{out} \\ C_o \frac{dV_{out}}{dt} = i_L - \frac{V_{out}}{R} \end{array} \right. \quad \rightarrow \quad \left\{ \begin{array}{l} t \in [0, T] \\ L \frac{di_L}{dt} = V_{in} \cdot D - V_{out} \cdot (1-D) \\ C \frac{dV_{out}}{dt} = i_L \cdot (1-D) - \frac{V_{out}}{R} \end{array} \right. \quad (3.27)$$

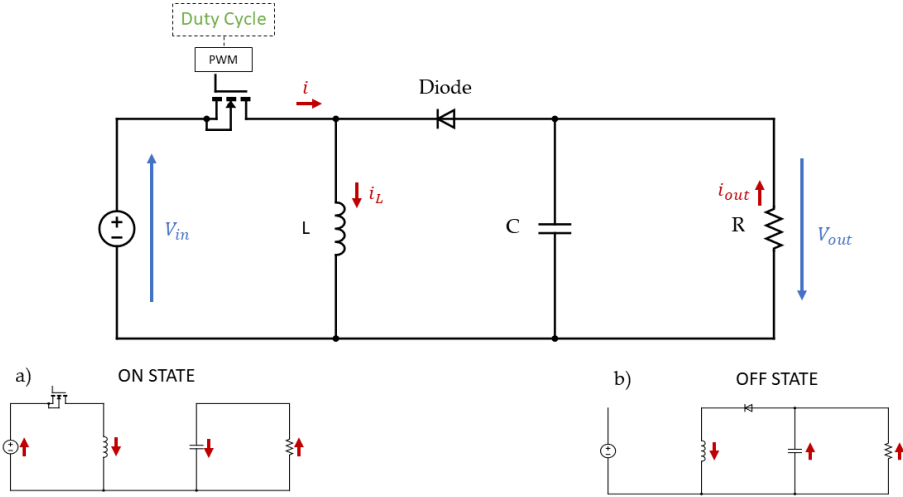


Figure 3.17. Simplified circuit of a buck-boost converter

As to the present case study, the converter characteristics makes it a suitable option for the link between motor drive and battery: a constant input voltage can indeed be fed to the motor drive for a broad range of DC bus voltages.

## Chapter 4

# Model description

*System architecture is analysed at different levels, together with a focus on the electrical and control parameters that define connections between different components.*

### 4.1 System overview

As a starting point, Figure 4.1 reveals the system blocks, highlighting the main flows of power together with necessary control links to assure a proper energy management. The system working voltages added to the scheme provide a clearer suggestion of the conversion steps faced by electrical power. They are the reference ones implemented in the case study under consideration.

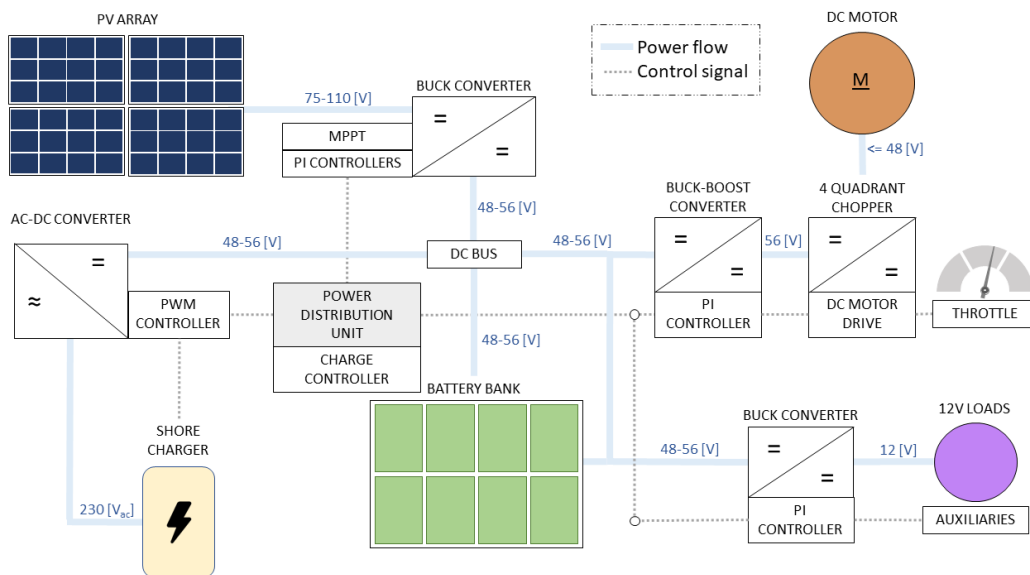


Figure 4.1. Electrical and logical connections

Regarding power generation, the model receives electricity provided either by the photovoltaic array installed on the boat hard top or by the charging station located at the berth (shore charger). The incoming PV power is used either to feed the electric loads, directly, or to charge the battery bank. On the other hand, shore power just accomplishes the latter. Loads are represented by the boat engine (DC motor), providing propulsion, and the auxiliary systems (12V loads) needed to allow a safe navigation and a satisfying customer experience. Due to the necessity of dealing with different voltage values in accordance with the behaviour of single system components, it is crucial to rely on power electronics. It plays a vital role in ensuring a correct system operation. Indeed, it would not be possible to operate efficiently and safely without the aid of control units. One may note the presence of several voltage converters coupled with the relative control system, which all refers to the charge controller. The latter can be considered as the system brain as far as power management is concerned. It acts with the following logic when the boat is in operation.

- PV power < Load demand  
PV panels operate at their Maximum Power Point (MPP). This energy is directly used to provide part of the load demand, while the missing is requested to the battery bank. Care must be given so that the discharge rate of the battery does not exceed the manufacturer specifications. As it will be seen in Section 4.2, low State of Charge (SOC) values determine some limits in the power that can be extracted from the battery.
- PV power > Load demand and  $SOC < 99.5\%$   
PV panels operate at their MPP. Part of the PV power is used to feed the electrical load, while the remaining part is stored in the battery for future use. Whenever charging currents overcome the 30 [A] threshold, the charge controller operates on the buck converter duty cycle to limit PV power production.
- PV power > Load demand and  $SOC = 99.5\%$   
Batteries cannot store any extra energy. PV panels are forced to operate away from the MPP to exactly follow the load demand. Despite part of the potential PV power is lost, it does not produce excessive heat, removing the need for extra energy dissipation. If no power is requested, PV panels are disconnected from the system.

Obviously, there are moments during which no PV production is available. In that case, batteries act as the only energy source. Whenever the latter are heavily discharged, loads are disconnected from the system to avoid damage and reduction of cycle lifetime, as it will be seen in section 4.2.7. It is important to mention the strict division between two times of the day:

- *Day*: The boat is available for operation only from 07:00 to 22:00 of every day
- *Night*: During night-time batteries are charged up from the charging station at the dock. Shore power starts flowing at 22:00 and may continue, to the utmost, until 07:00 in the morning. It is stopped if SOC reaches a value of 99.5 [%]. As to the charging current, it is constant and equal to 10 [%] of the battery bank rated capacity. It allows to easily simulate the charging process saving computational time. If the intention was to accurately model the battery behaviour, one would give priority to other charging methods closer to a real life application, such as those described in [44–46].

All the components in the scheme above are considered in the Simulink® model, with the exception of the shore power converter and its PWM controller, mentioned here but kept out of the following discussion. In particular, although DC alternatives are gaining ground, most of the charging stations actually available at ports offer just an AC plug. Thus, shore power has to



### 4.2.1 Day and night charge subsystem

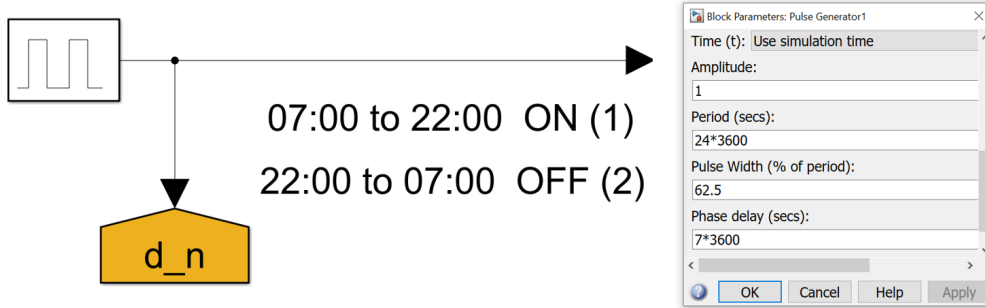


Figure 4.3. Day/Night pulse generator

The pulse generator shown in Figure 4.3 is set to switch between the two phases of the day:

- During operation, from 07:00 to 22:00,  $d_n = 1$ . The boat is not connected to the dock and the only power source available is the PV array.
- During the night charge, from 22:00 to 07:00,  $d_n = 0$ . The boat is connected to the dock and batteries are charged with shore power, while everything else, be it source or load, is shut down. The latter means that even though PV panels could produce energy before 7:00 or after 22:00, it would not be used to charge batteries.

The control signal  $d_n$  plays a fundamental role in the system, substituting actual gesture of handling the electrical cable to connect or disconnect the boat from the charging station.. If the boat covered a predetermined route in between docks equipped with a shore charger,  $d_n$  could have been set differently, to allow battery charging even during a temporary stop.

### 4.2.2 PV array subsystem

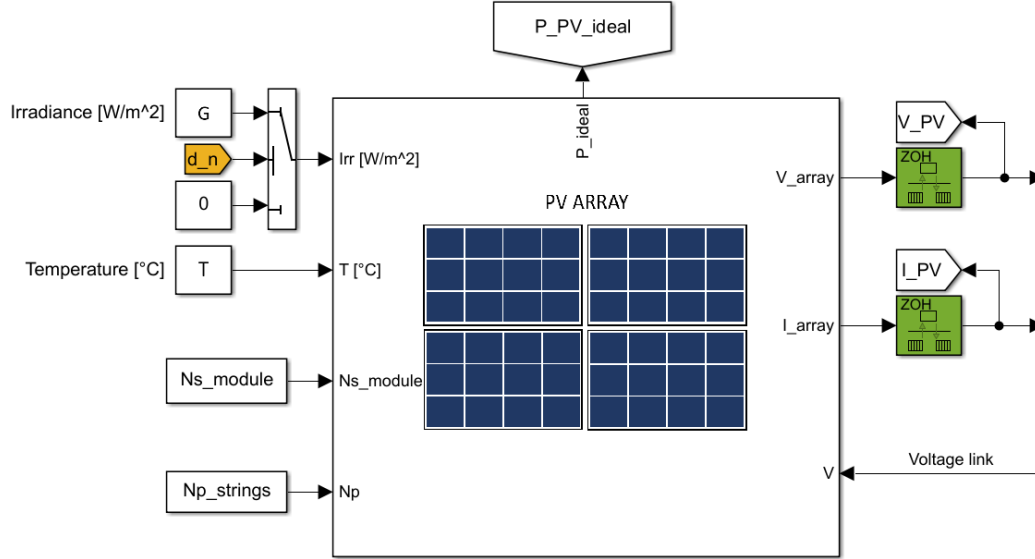


Figure 4.4. PV subsystem, 1<sup>st</sup> level

Inputs of the subsystem shown in Figure 4.4:

- *Irradiance* [ $\text{W/m}^2$ ]: fundamental ambient condition with the most relevant impact on the array power production. Data are passed to the system from MATLAB® by using a *from workspace* block. It uses interpolated hourly data of a typical meteorological year for the period that needs to be simulated. One may note how, if  $d\_n = 0$ , then the irradiance value passed to the system equals a null value, which means that the PV panels are switched off during the night charge.
- *Temperature* [ $^{\circ}\text{C}$ ]: it affects PV yield in a significant way. It is passed to the block in the same fashion of irradiance values.
- *Ns\_module* [-]: it is the number of rows in the array layout. Multiplying this constant by the voltage of a single panel produces the actual one of the PV array.
- *Np\_strings* [-]: it is the number of columns in the PV array layout. Representing parallel strings, it is directly related to the total current that flows across the array. Multiplying this constant by the current flowing through a single panel produces the actual one of the PV array.
- *V* [ $\text{V}$ ]: as it will be shown when analysing the buck converter circuit equations, it represent the voltage at which the array operates. One may note a certain redundancy, since the array voltage is also one of the block output. This signal is called *Voltage link*, in order to emphasize the mutual connection and the continuous data exchange between PV array and buck converter.

Outputs of the subsystem shown in Figure 4.4:

- $P\_PV\_ideal$  [W]: it is the product of the Maximum Power Point Tracking (MPPT) voltage and current, in the ideal case. It is a useful reference to measure the accuracy of the MPPT controller.
- $V\_array$  [°C]: it represent the actual PV array voltage. However, the signal value is fed to a rate transition block before entering the buck converter. Specifically, the green block is a Zero Order Hold (ZOH). It holds its input for a specified sample period. It is needed to input discrete data to the MPPT algorithm so that it has time to adjust the duty cycle and calculate the relative voltage at which the panels are forced to operate. If the ZOH block was not present, the MPPT would work with constantly changing data, making it impossible to find the optimum voltage. Being the model sensible to the chosen sample time, it is crucial to accurately tune its value<sup>2</sup>. Indeed, an excessively high or low value would led the system to operate away from the MPP, be unstable or request a lot of time.
- $I\_array$  [A]: it represent the actual PV array current. What has been said regarding to the previous output also applies to this one. It is needed that the two ZOH blocks delay the signals of an equal time span.

An example of the ambient conditions fed to the block for a period of two days is reported in Figure 4.5

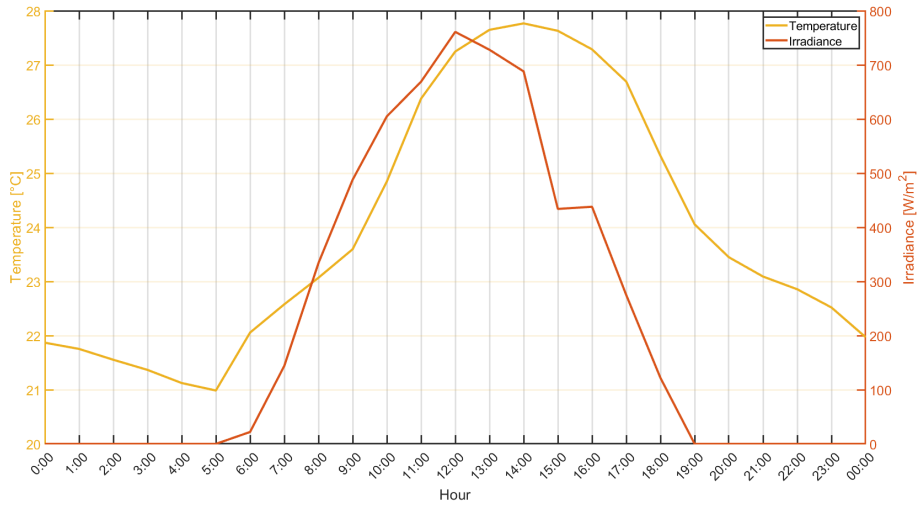


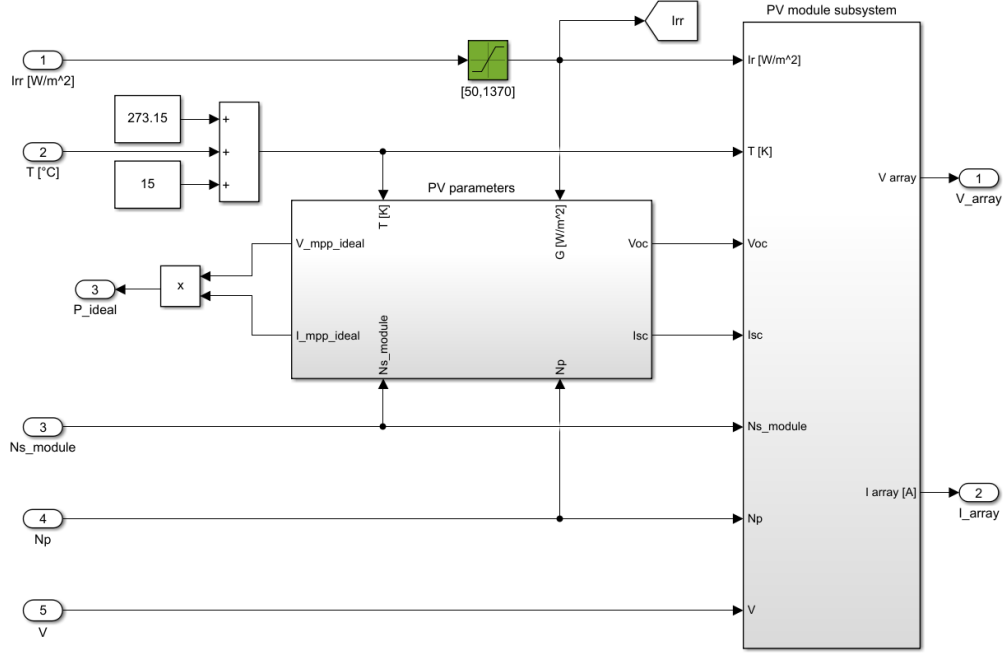
Figure 4.5. Random meteorological conditions on a summer day

As to the present case study, irradiance and temperature hourly data derive from the typical meteorological year for the site in consideration (Venice, Italy). They were obtained by means of PVGIS online tool [48, 49]. Since the boat does not travel along without fixed routes, it is not trivial to assign a proper horizon to better calculate the radiative component striking on the panels. It may, perhaps, be correct to utilize as surrounding landscape the one where it spends most of the time, i.e. the harbour.

---

<sup>2</sup>As it influences the maximum time step adopted from the variable step solver.



Figure 4.6. PV subsystem, 2<sup>nd</sup> level

By looking at Figure 4.6, one may easily follow the routes to other subsystems. In particular, the irradiance signal passes through a saturation block. The latter outputs only values from 50 to 1370  $[W/m^2]$ . The upper limit, i.e. the solar constant, was chosen to avoid using unrealistic or wrong irradiance values. It is however to clarify that the maximum normal surface irradiance usually does not overcome 1000  $[W/m^2]$  due to atmosphere attenuation. As to the lower limit, it was selected purely for computational reasons as the model becomes unstable when null values of irradiance are fed to these blocks (e.g. divisions by zero). However, the minimum irradiance necessary to activate the panels production is set from MATLAB®, and equal to 80  $[W/m^2]$  for the specific case. Thus, a value of 50  $[W/m^2]$  will still be seen as null from a numerical perspective. As to the temperature signal in Celsius degrees, it is converted to Kelvin for consistency reasons inside the equations, while 15  $[°C]$  are added to take into account that module cell temperatures are usually higher those of the surrounding air. This assumption is further motivated in Chapter 5.

It is crucial to understand that, the explicit equations for  $V_{mp}$  and  $I_{mp}$  provided by [28] are utilized to calculate the ideal power deliverable from the array. Additionally, explicit calculation of  $V_{oc}$  and  $I_{sc}$  are fed as reference inputs for the implicit module described in Figure 4.8, which calculates the operating point based on the effective resistance seen from the panels<sup>3</sup>.

<sup>3</sup>A buck converter, coupled with an MPPT adjusts its duty cycle and so the effective resistance  $R_e$  seen from the PV array, which, at the end of the day, is what physically defines the value of its operating voltage:  $V = R_e \cdot I$ .

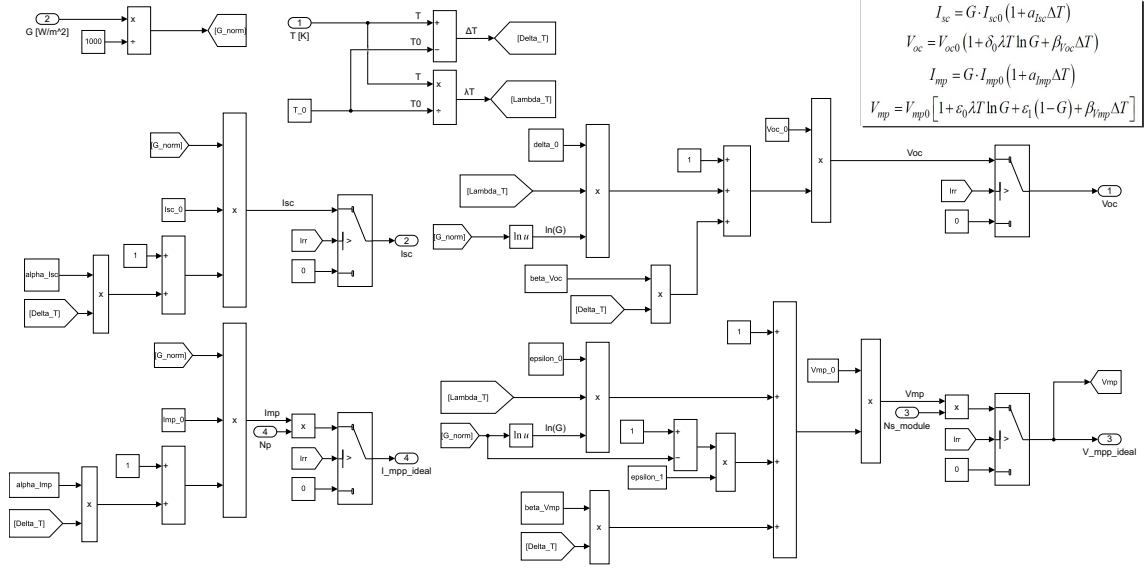
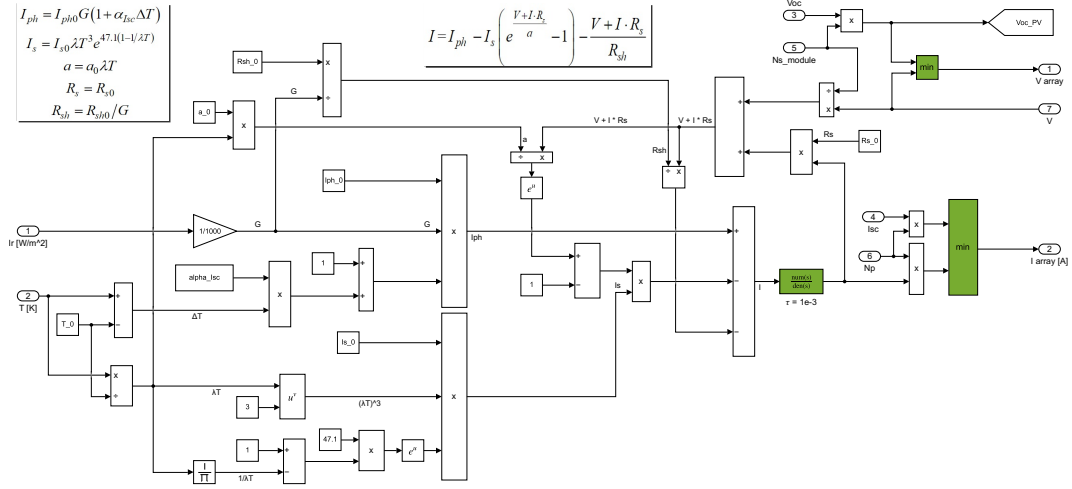

 Figure 4.7. PV subsystem, 3<sup>rd</sup> level. PV Parameters

Figure 4.7 contains a Simulink<sup>®</sup> implementation of the performance model equations developed by [28]. As already described, it is a useful theoretical method that fits well with the level of accuracy that the present work is intended to obtain. In fact, relying just on data sheet information it allows to obtain the explicit irradiance–temperature dependence of the following fundamental parameters:

- Open circuit voltage  $V_{oc}$
- Short circuit current  $I_{sc}$
- Maximum power point voltage  $V_{mp}$
- Maximum power point current  $I_{mp}$

The MPP voltage and current values are then multiplied by, respectively, the number of series modules and that of parallel strings to obtain the actual values for the whole array, which are in fact used to calculate the ideal PV power production. It is to note that these four parameters represents the subsystem output only if the irradiance value striking on the PV panels in that time of the simulation is higher than the minimum one necessary to activate it. If this is not true, a null value is passed as output.


 Figure 4.8. PV subsystem, 3<sup>rd</sup> level. PV module implicit equations

Finally, Figure 4.8 shows the equations needed for the implicit calculation of the voltage and current relation for a PV panel. It requires an iterative solving method but allows to obtain every working point on the V-I curve, being therefore useful when linking a PV array with a buck converter that control its point of operation. Calculations use of the implicit V-I relationship for a single diode PV model, with formulas provided by [28] and the schematic approach suggested in [50].

One may note some important blocks that have been coloured in green. The two *min* ones are needed to prevent the PV subsystem to output a non-realistic current or voltage value. As it can be seen, they makes it impossible for the system to output voltages higher than  $V_{oc}$  or currents bigger than  $I_{sc}$ . Finally, it is to note again that the current value, which is the system output, is needed also as input to solve the equation. Thus, a circular dependence arises between some blocks of the subsystem, creating an algebraic loop [51]. In case of continuous signals, inserting a memory block, which uses a discrete sample time, would cause the solver to largely increase the number of steps it takes to simulate the model. Instead, a good solution is that to insert a Transfer Functions (TF) with a relatively small time constant, with the scope of slightly delaying the signal without compromising the system dynamic [52]:

$$TF = \frac{1}{\tau + 1} = \frac{1}{1e - 3s + 1} \quad (4.1)$$

Where  $\tau$  is the time constant [s].

As to the block under consideration, it was chosen a  $\tau = 0.001[s]$ . In the following, one may note the usage of several other transfer function blocks to obtain the same result. However, the time constant value can differ because it is optimized for the specific case.

### 4.2.3 MPPT, charge controller and buck converter subsystem

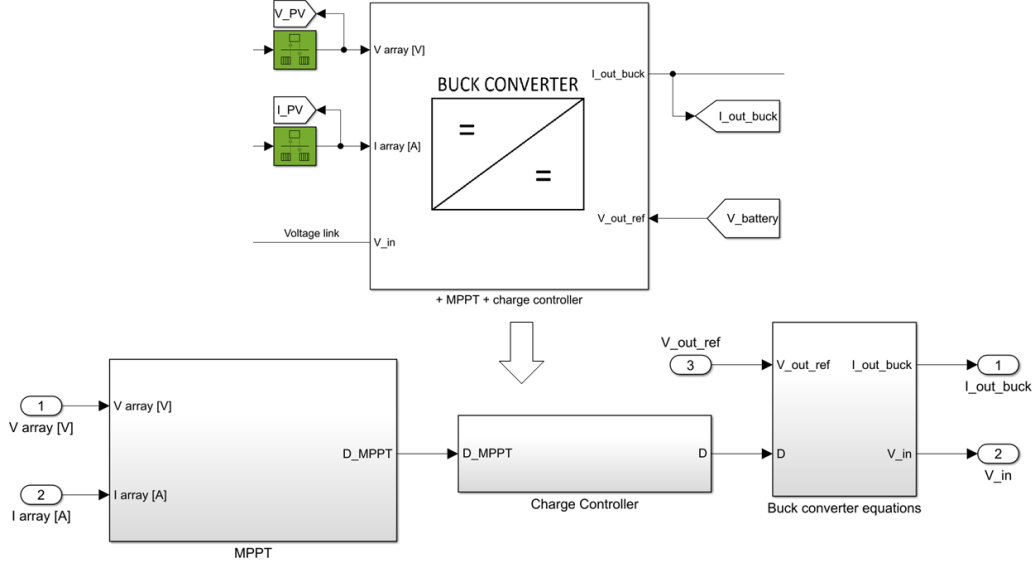


Figure 4.9. Buck converter subsystem, 1<sup>st</sup> and 2<sup>nd</sup> level

Figure 4.9 shows how the buck converter subsystem is internally composed. The MPPT, once received the array voltage and current inputs, calculates the duty cycle that would allow the panels to operate at their maximum power point. Then, the signal is passed to the charge controller which, with the help of other useful data info (i.e. Battery SOC and current), outputs a duty cycle value that fits the actual working condition. Regarding the duty cycle role in the buck converter - PV interaction, it useful to rely on the following general equation:

$$V_{out} = V_{in} \cdot D \quad \rightarrow \quad V_{in} = V_{out}/D \quad (\text{ref. eq. 3.24})$$

In the case under exam  $V_{in}$  represents the PV voltage, while  $V_{out}$  the battery one, and so the DC bus. As it has been said, the converter has to deal with varying input and output voltages: the PV array one is constantly adjusted by controlling the duty cycle in order to reach MPP or adapt to the charge controller commands, while the battery bank one changes when current flows through the batteries. The converter basically changes the effective resistance seen from the panels and brings their operating point to the desired one. A good perspective can be found in the reverse formulation in eq. 3.24. Starting from the physical connection with the battery voltage ( $V_{out}$ ), the duty cycle value ( $D$ ) allows to determine the PV panels voltage.

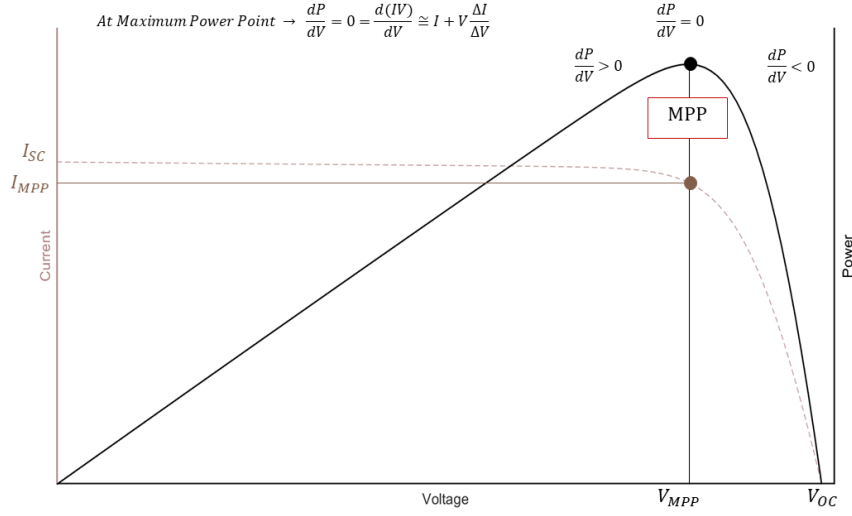


Figure 4.10. PV characteristic curve

An example of the MPPT operation is intuitable by looking at the characteristic curve in Figure 4.10, assuming a constant output voltage.

It is clear the intent of a MPP tracker: understanding the position of the actual operating point and adjusting the duty cycle to bring it towards the MPP for that specific irradiance and temperature condition. The curve can be split in two regions:

- The one at the left of the MPP, where  $dP/dV > 0$ . Here an increase in the PV voltage causes an increment in the power produced. Thus, if the operating point is situated along that curve, the duty cycle should lower its value, allowing the PV voltage to rise.
- The one at the right of the MPP, where  $dP/dV < 0$ . Here an increase in the PV voltage causes a decrement in the power produced. Thus, if the operating point is situated along that curve, the duty cycle value should increase, allowing the PV voltage to lower.

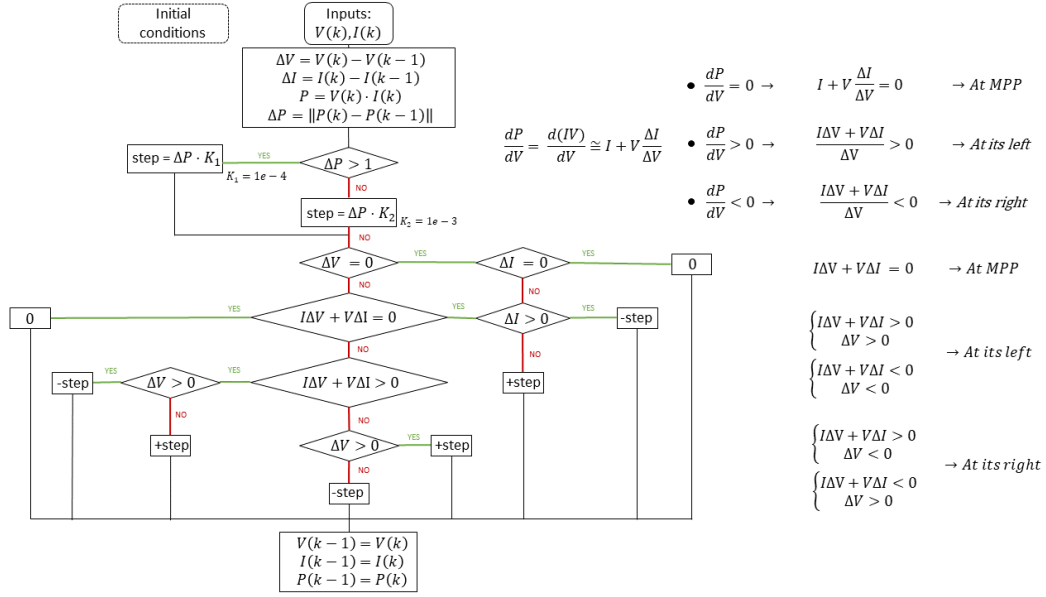


Figure 4.11. Buck converter subsystem, MPPT algorithm flowchart

Figure 4.11 reveals the algorithm implemented in the MPPT subsystem. It is based on the variable step incremental conductance technique but provides a lighter computational burden, as discussed in [53]. This is done by remodelling the equations in order to eliminate any division calculations, substituting them with relational operators.

The present algorithm, which has been adapted to a buck converter, slightly modifies the original code by introducing two different scaling factors ( $K_1$  and  $K_2$ ) in the step calculation. It is a matter of accuracy. In fact, introducing a second factor allows to better tune the algorithm response to the possible changes in power. Thus, despite the added complexity, it boosts productivity as it facilitates to find a better compromise between precision and convergence speed, which is not always attainable by using a single scaling factor. The splitting dis-equation:  $\Delta P > 1$  was chosen to reasonably divide the step length in accordance with the entity of  $\Delta P$ , so that small changes do not produce excessively small duty cycle variations and vice versa. By looking at the dis-equations on the right side of the flowchart in Figure 4.11 it is possible to comprehend the sign attributed to the duty cycle step: it is always opposed to the desired  $\Delta V$  direction.

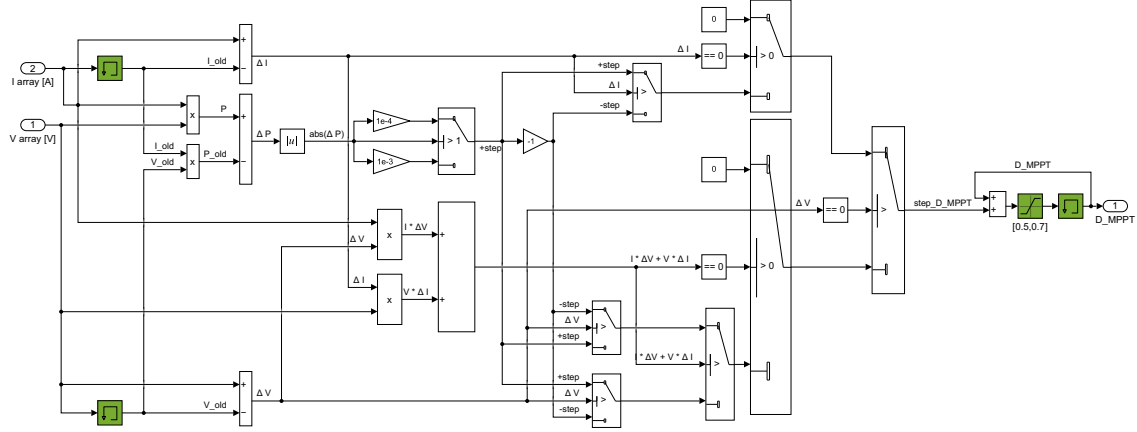


Figure 4.12. Buck converter subsystem, MPPT implementation

Figure 4.12 shows the subsystem in which the algorithm is implemented through Simulink® blocks. It is noticeable that the memory green block allows to store the value at step  $k - 1$ , which is then used to compute the  $\Delta$  values for current, voltage and power. As to the decision passages in the flowchart, they are reproduced with switch blocks adopting the same logic seen in the flowchart. The last switch corresponds to the end of the MPPT algorithm. Its output, `step_D_MPPT`, represents the variation in duty cycle expected to produce an PV voltage closer to the MPP one, which is in fact added to the last recorder duty cycle value. Before being sent to the charge controller, the signal enters a saturation block which limit its value to feasible boundaries.

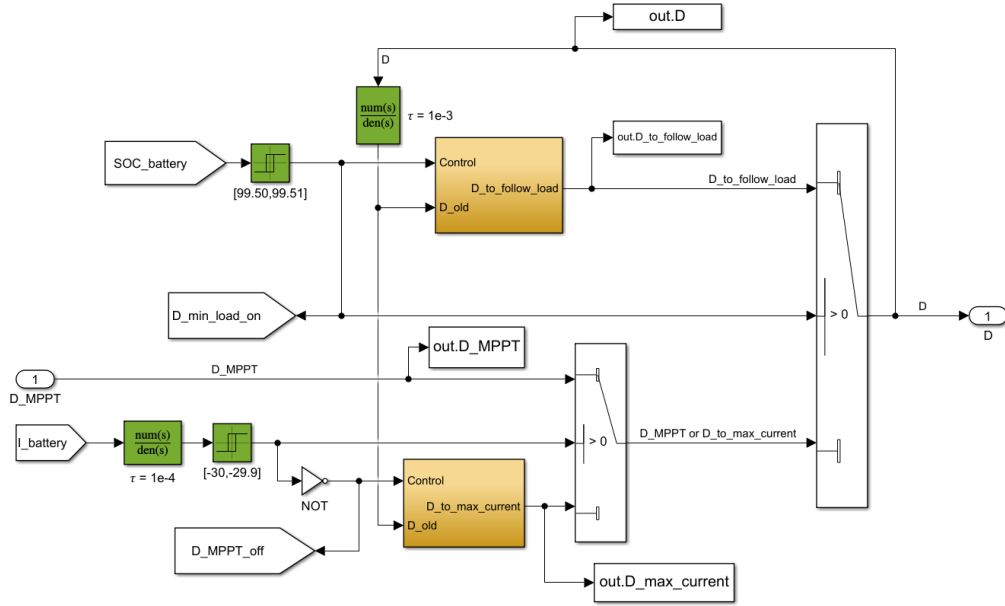


Figure 4.13. Charge controller subsystem

Figure 4.13 shows the expanded charge controller subsystem. It acts as an interface between PV panels and battery, with the scope to protect the latter, minimize heat loss due to energy dispersion and optimize the system working conditions. It can output one of the duty cycle values coming out from three different tracker, all related to a specific intention, which are nothing but the working mode already listed in Section 4.1. In particular:

- If the battery is completely charged ( $\text{SOC} = 99.5 \text{ [\%]}$ ):  
the relay block linked to the battery state of charge outputs a true logic signal that allows the actual duty cycle to be that of the *minimum load* controller. It forces the PV panels to operate away from their MPP and follow load needs. It stops being fed to the PWM generator once the battery starts discharging as the current requested from the electrical loads becomes higher than the maximum one provided by the PV array.
- If the battery is not completely charged ( $\text{SOC} = 99.5 \text{ [\%]}$ ) and the current entering the battery is lower than 30 [A]:  
the MPPT output duty cycle is passed to the PWM generator and the batteries are charged up with the highest power transfer possible.
- If the battery is not completely charged ( $\text{SOC} = 99.5 \text{ [\%]}$ ) and the current entering the battery becomes higher than 30 [A]:  
operating at the MPP would cause the charging current to overcome its threshold value. The controller adjust its duty cycle in order to obtain a constant current equal to 30 [A]. It stops working if even at MPP the PV panels can not provide the 30 [A] charging current.

Duty cycle values are stored in the workspace. As to the two boolean *Goto* tags shown (`D_min_load_on` and `D_MPPT_off`), they are linked to the data extrapolation subsystem in Figure 6.3. Finally, two transfer function blocks allows to brake algebraic loops in the same fashion it was explained on page 49.



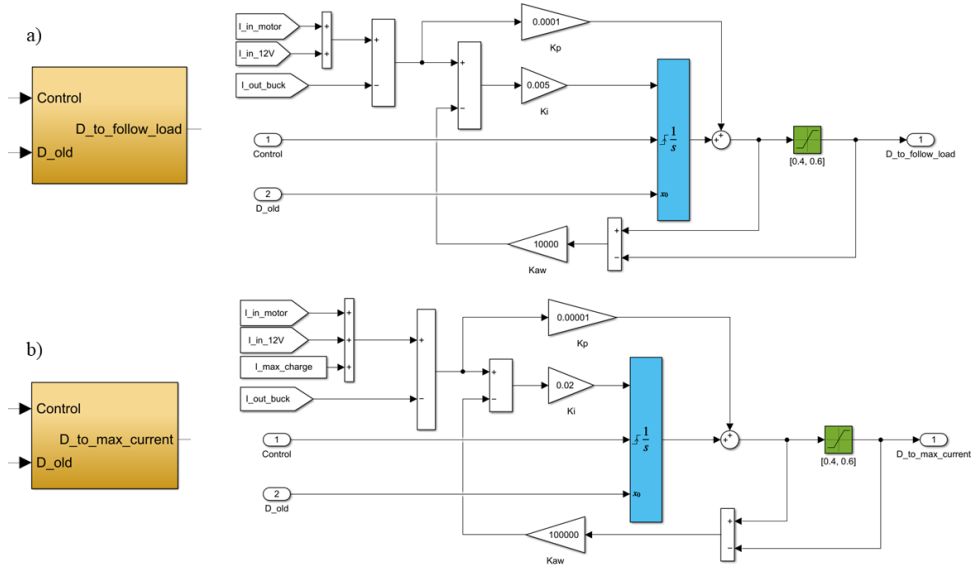


Figure 4.14. Minimum load (a) and maximum current (b) controller subsystems

The two PI controllers at the service of the charge controller are expanded in Figure 4.14. They are shown close to each other to allow an easier comparison. Except for the difference in the gain values, which is due to parameter optimization, attention must be given to the reference current they are designed to obtain. Whenever the case, the first controller adjusts the duty cycle in order to minimize the difference between the current coming out from the buck converter and the one requested from the loads, hence the name: *D\_to\_follow\_load*. As to the second controller, during those periods in which PV panels are able to cover load demand and provide a power so large to charge the battery with an excessively high current, it moves their operating point so that the current entering the battery bank does not overcome the limit threshold. It is done by introducing a fictitious load demand (*I\_max\_charge*), equal to the desired charging current.

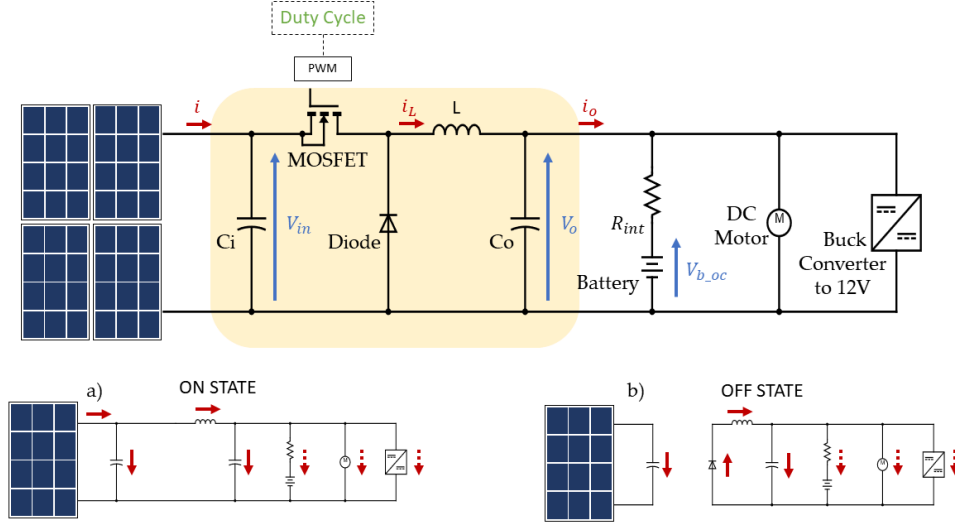


Figure 4.15. Simplified system circuit with focus on buck converter architecture

A simplified circuit for the buck converter is shown in Figure 4.15. The input voltage coming from PV panels is brought down to that of the DC bus, which connects in parallel the battery bank, the DC motor drive and the buck converter related to the 12V grid. A filter capacitor  $C_i$  reduces voltage ripples on the input side of the converter. Despite an extra diode right after the PV panels is useful to prevent undesirables reverse current flows, it was not inserted due to the simplicity intent of the circuit in consideration. A good initial estimation for the design parameters (inductance  $L$  and capacitances  $C_i$  and  $C_o$ ) of a buck converter that has to deal with a varying input and output can be found in [54]:

$$L = \frac{2 \cdot V_{mps} \cdot D_{mps} \cdot (1 - D_{mpw})}{\Delta I_{ow} \cdot f_s} \quad (4.2)$$

$$C_i = \frac{\Delta I_{is}}{\Delta I_{iw} \cdot f_s} \quad C_o = \frac{\Delta I_{os}}{32 \cdot \Delta V_{ow} \cdot f_s} \quad (4.3)$$

Where:

- $V_{mps}[V]$  MPP voltage under STC
- $D_{mps}[-]$ : typical duty cycle corresponding to MPP in favourable irradiance conditions
- $D_{mpw}[-]$ : typical duty cycle corresponding to MPP in poor irradiance conditions
- $\Delta I_{iw}[A]$ : input current ripple in poor irradiance conditions
- $\Delta I_{ow}[A]$ : output current ripple in poor irradiance conditions
- $f_s[Hz]$ : switching frequency
- $\Delta I_{is}[A]$ : input current ripple in favourable irradiance conditions
- $\Delta I_{os}[A]$ : output current ripple in favourable irradiance conditions
- $\Delta V_{ow}[V]$ : output voltage ripple in poor irradiance conditions

$$\begin{cases} t \in (0, t_{on}] \\ C_i \frac{dV_{in}}{dt} = i - i_L \\ L \frac{di_L}{dt} = V_{in} - V_o \\ C_o \frac{dV_o}{dt} = i_L - i_o \end{cases} \rightarrow \begin{cases} t \in (t_{on}, T] \\ C_i \frac{dV_{in}}{dt} = i \\ L \frac{di_L}{dt} = -V_o \\ C_o \frac{dV_o}{dt} = i_L - i_o \end{cases} \rightarrow \begin{cases} t \in [0, T] \\ C_i \frac{dV_{in}}{dt} = i - D \cdot i_L \\ L \frac{di_L}{dt} = -V_o + D \cdot V_{in} \\ C_o \frac{dV_o}{dt} = i_L - i_o \end{cases} \quad (4.4)$$

$$V_o = V_{batt} = V_{b\_oc} - R_{int} \cdot i_{batt} \quad (\text{ref eq. 3.9})$$

Introducing characteristic equations for the circuit components and applying Kirchhoff's laws it is possible to obtain the state equations of the buck converter average model, in the same fashion it was done for a PV boost converter linkage in [55]. Each system describes the behaviour during on and off time intervals of the switching device, while the overall average equations (4.4) are obtained by adding the two systems with duty cycle as weight factor. As to the output voltage, equation ref eq. 3.9 shows that it is equal to the battery one, which is in fact the algebraic sum of the battery open circuit voltage plus the internal resistance  $R_{int}$  times the current flowing through the battery. Currents are considered positive when discharging the battery bank.

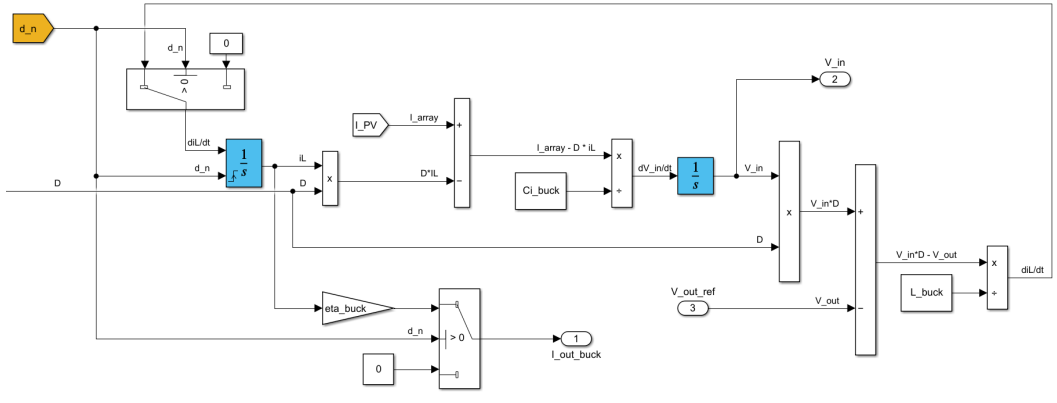


Figure 4.16. Buck converter subsystem, equations

The buck converter subsystem is finally reported in Figure 4.16. It implements the system of averaged equations. However, both the battery bank open circuit voltage and the current flowing through can be calculated, thus, the third equation in the system can be avoided by directly utilizing the DC bus voltage. Indeed, battery bank, DC motor and buck converter share the same terminals.

In the ideal average model, the output current is equal to the one passing through the inductor in the time interval. One may note that during the operating part of the day the converter efficiency is taken into account by reducing the actual output current fed to the rest of the circuit. Care must be given to the switch block in the top-left position. It filters the derivative signal for the current, assigning a null value during night charge. It avoids useless computations from 22:00 to 07:00 that would slow down the simulation. In addition, the current integrator is reset at every change in  $d_n$ , to output a null initial current at every day-night shift.

#### 4.2.4 Power distribution unit subsystem

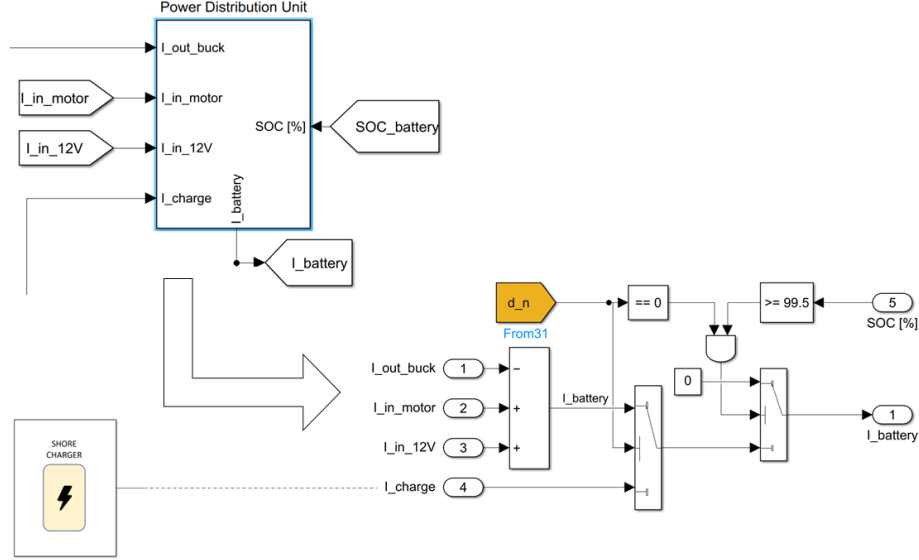


Figure 4.17. Power distribution unit subsystem, 1<sup>st</sup> and 2<sup>nd</sup> level

The Power Distribution Unit (PDU), which has to be considered in strict relation with the charge controller, handles the current entering or exiting the battery bank.

- During the operating day, when the load request is higher than the PV capacity, it simply prioritizes the use of power coming from panels through the buck converter, asking the battery to compensate for the rest. In the opposite situation, it charges the battery with any photovoltaic excess power, if allowed from the charge controller.
- During the night, it feeds the battery solely with the current coming from the charging station at the dock, until it is completely charged or the working day has newly begun. Please note that, as previously mentioned,  $I_{charge}$  coming out of the shore charger subsystem is just a constant value referring to a DC current.

### 4.2.5 Battery bank subsystem

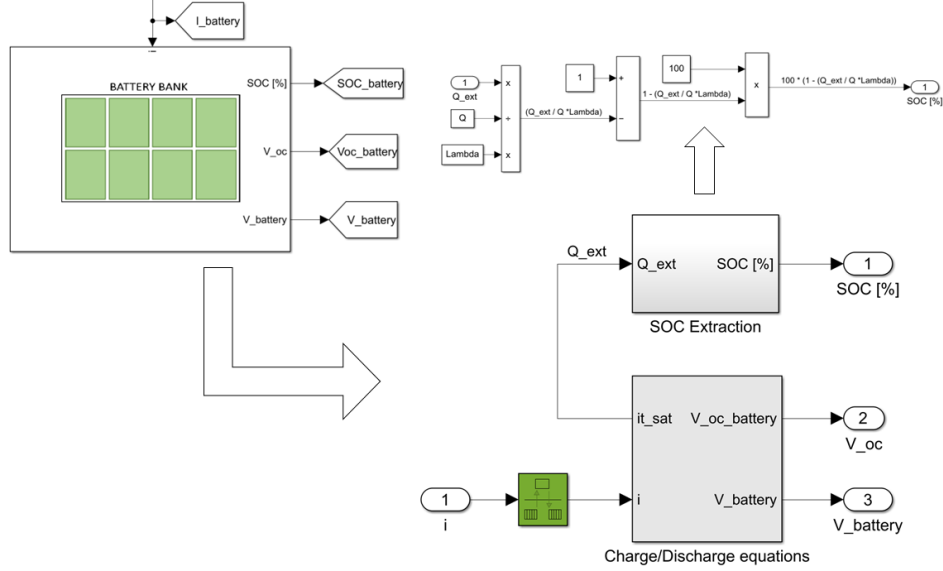


Figure 4.18. Battery bank subsystem, 1<sup>st</sup>, 2<sup>nd</sup> and 3<sup>rd</sup> level

Figure 4.18 reveals the inner battery bank subsystem layout. The second level contains a subsystem where all the charge and discharge parameters are fed to the equations in order to calculate the battery voltage and capacity. A Rate Transition Block is placed at the current input to properly handle data transfer. As to the second subsystem, which is expanded in the top-right of the figure, it allows to calculate the battery state of charge from the extracted capacity. It is based on the ampere-hour measurement method, which simply calculates the integral of the current leaving or entering the battery in the specified period [56]. Despite being considered difficult to implement in a real life situation due to the accuracy requested to the sensors, it suits well a mathematical model such as the one adopted in the present case, which relies on the following equation:

$$\text{SOC} = 100 \cdot \left( 1 - \frac{Q_{\text{ext}}}{Q'} \right) = 100 \cdot \left( 1 - \frac{Q_{\text{ext}}}{Q} \cdot \lambda \right) \quad (4.5)$$

Where  $Q'$  is calculated by dividing the maximum battery capacity  $Q$  by a coefficient  $\lambda$  related to the limited extractable energy. In the case under consideration  $\lambda$  was extrapolated from the MATLAB® inner function for the *generic battery model* block by creating a lithium battery with the same parameters as the one used in the model [32].



### 4.2.6 Buck converter to auxiliary loads subsystem

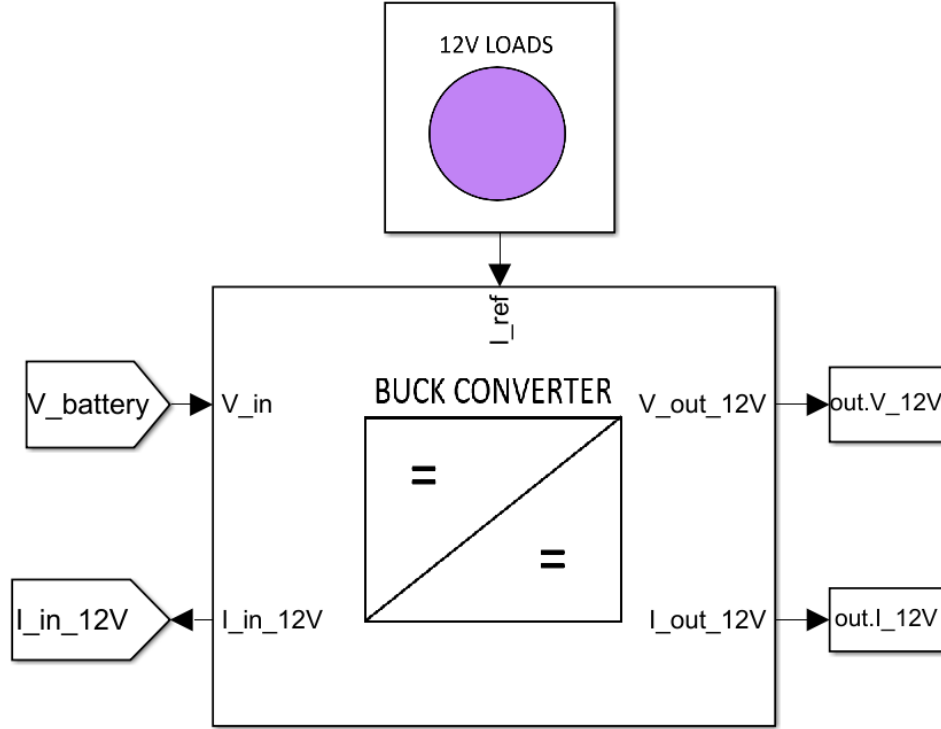


Figure 4.20. Buck converter 12V subsystem, 1<sup>st</sup> level

The model is designed to consider also the power request from electric loads operating at a voltage different from the DC bus one. In the current configuration, 12[V] loads such as navigation lights and monitors, bilge pumps, electric toilets, VHF and radio systems, cabin lights, electrical chargers, air conditioners where assumed to be present onboard. The electric power needed to sustain the loads is determined by the current drawn input of the block in figure ( $I_{ref}$ ). It is considered to be constant but can also be a time-series object if data on load usage are provided. Transferring energy to the 12V loads requires to step down the battery terminal voltage. This is accomplished through the conversion operated by the subsystem in Figure 4.20. The latter receives as input the battery voltage and the current requested from auxiliary devices, and outputs the following:

- $V_{out\_12V}$ : which represents the voltage at grid terminals, it is constantly kept around 12[V] by the PI controller.
- $I_{out\_12V}$ : which represents the output current transferred to the loads. It is kept close to the reference input current ( $I_{ref}$ )
- $I_{in\_12V}$ : it is the input current requested from the DC bus net of conversion efficiency.

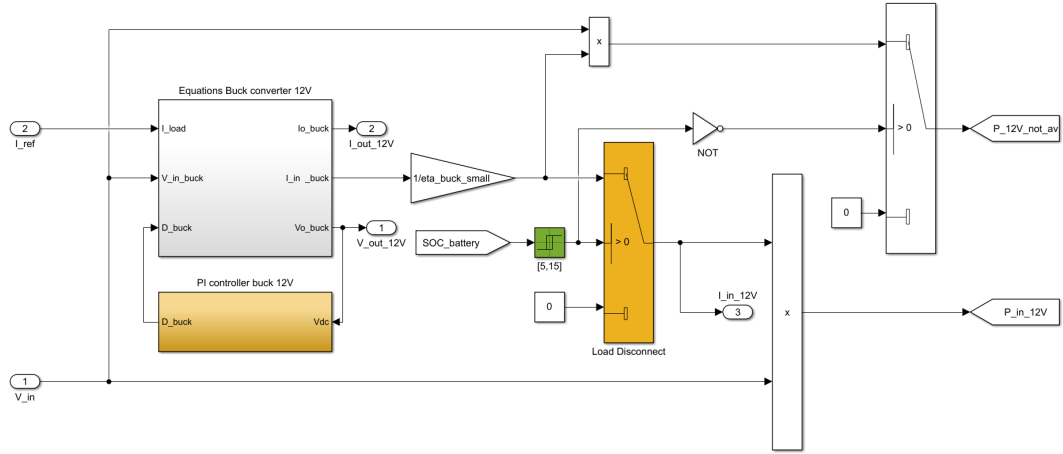


Figure 4.21. Buck converter 12V subsystem, 2<sup>nd</sup> level

Figure 4.21 shows the second subsystem level. Here, input voltages and reference currents are fed to the actual subsystem containing the circuit equations. One can note how the PI controller is constantly monitoring the output voltage of the converter and adjusting it by means of duty cycle control. During the operating day, a relay block allows the switch to disconnect the load when battery falls below 5[%] charge, and activate it again when brought back at least to 15[%] of its capacity<sup>4</sup>. This is done to prevent an useless charge-discharge cycles around the lower SOC threshold. If the relay is on, the input current requested to the DC bus is equal to the ideal one coming out from the mathematical equations for the conversion state divided by the presumed efficiency of the buck converter. If the load is not disconnected the latter is multiplied by the input voltage to obtain the power requested from the buck converter. On the other hand, the switch on the top-right corner of the figure outputs the power ideally requested from the loads which is not provided due to their forced disconnection.

<sup>4</sup>Please note that during the day only the PV array is connected to the battery. The latter means that if no extra power is coming from the panels the battery will not be charged until the boat is brought to the deck and connected to the shore charger.



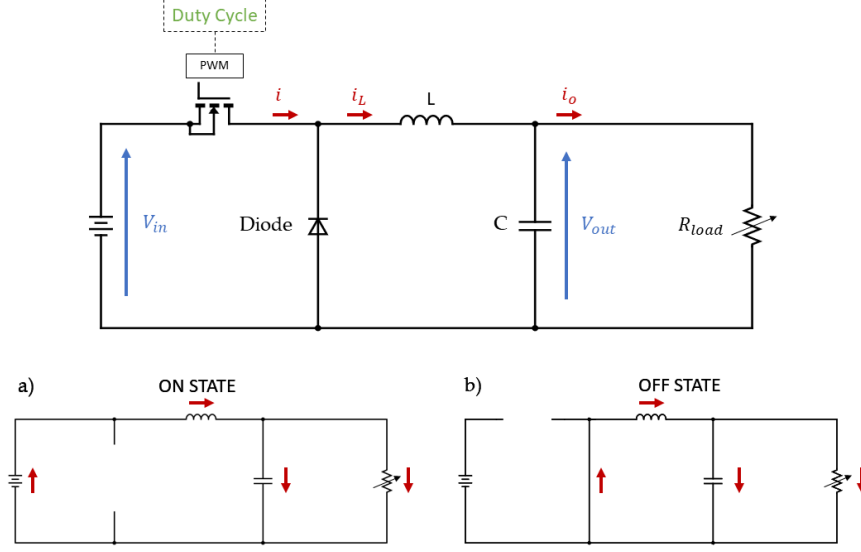


Figure 4.22. Buck converter 12V, simplified electrical circuit

A simplified electrical scheme is reported in Figure 4.22. It is similar to the main buck converter one, with the difference that here auxiliary loads are modelled by means of a variable resistor able to represent the variability in current demand of the 12V grid. However, for simplicity, the output voltage-load resistance ratio was substituted with the requested current, as shown in eq. 4.9. Thanks to this, it is possible to intuitively model the load demand by just adjusting the current reference passed as input to the subsystem.

As to the inductor and capacitor dimensioning, the following design rules were followed [59]:

$$L = \frac{V_{out} \cdot (V_{in} - V_{out})}{\Delta I_L \cdot f_s \cdot V_{in}} \quad (4.6)$$

$$C = \frac{\Delta I_L}{8 \cdot f_s \cdot \Delta V_{out}} \quad (4.7)$$

Where:

- $V_{out}[V]$ : output voltage
- $V_{in}[V]$ : usual input voltage. It varies between the minimum and maximum battery one.
- $\Delta I_L[A]$ : maximum output current ripple
- $f_s[Hz]$ : switching frequency
- $\Delta V_{out}[V]$ : maximum output voltage ripple

$$\begin{cases} t \in (0, t_{on}] \\ L \frac{di_L}{dt} = V_{in} - V_{out} \\ C \frac{dV_o}{dt} = i_L - \frac{V_{out}}{R_{load}} \end{cases} \begin{cases} t \in (t_{on}, T] \\ L \frac{di_L}{dt} = -V_{out} \\ C \frac{dV_o}{dt} = i_L - \frac{V_{out}}{R_{load}} \end{cases} \rightarrow \begin{cases} t \in [0, T] \\ L \frac{di_L}{dt} = -V_{out} + V_{in} \cdot D \\ C \frac{dV_o}{dt} = i_L - \frac{V_{out}}{R_{load}} \end{cases} \quad (4.8)$$

$$\frac{V_o}{R_{load}} = i_o \quad (4.9)$$

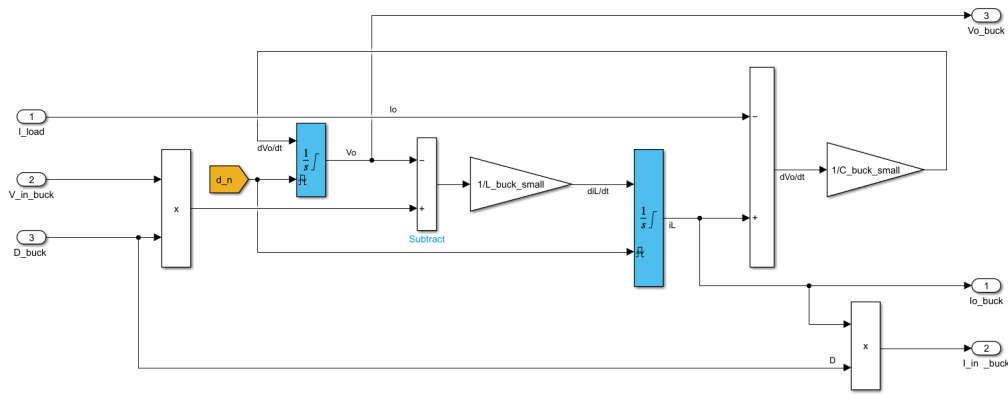


Figure 4.23. Buck converter 12V subsystem, equations

In system 4.8 the average model is calculated from the combination of Kirchhoff's laws with characteristics equations for the inductive and the capacitive elements, in the same manner it was done in 3.25. Its straightforward Simulink<sup>®</sup> implementation is depicted in Figure 4.23. A `d_n` flag is placed as reset signal of the voltage and current integrators to output null values during the night, where all the loads are effectively disconnected from the circuit.

Remembering eq. 3.24, where the overall average and ideal buck converter input-output voltage relation was shown, it is straightforward to assign an input current value equal to that shown in eq. 4.10 to ensure energy conservation. Note that the average current flowing through the inductor equals the output one.

$$i_{in} = i_L \cdot D = i_{out} \cdot D \quad (4.10)$$

Efficiency is indeed taken into account outside the ideal equations subsystem.

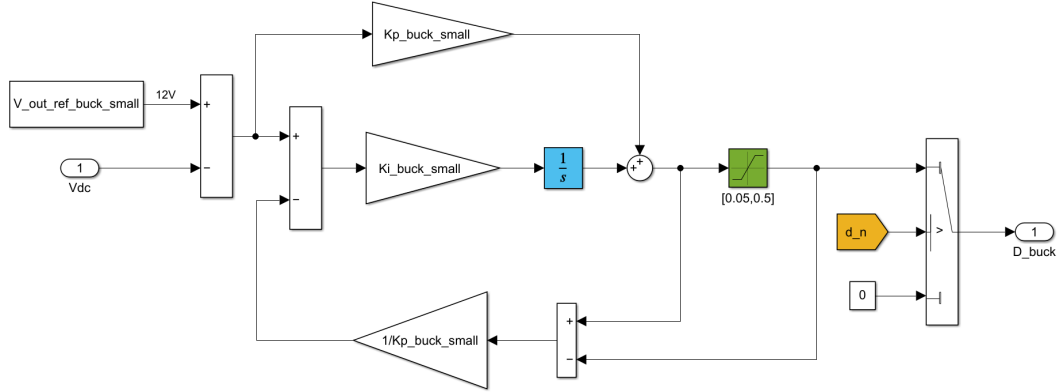


Figure 4.24. Buck converter 12V subsystem, PI controller

Finally, by looking at the Simulink® blocks in Figure 4.24, it is possible to understand how the duty cycle signal is generated. It is the result of a PI controller which constantly compares the output voltage of the buck converter with the reference value set at 12[V] and tries to minimize the error difference between the two by varying the duty cycle. One may note a saturation block, which limits any unfeasible values and a switch at the right of the model, which outputs null duty cycle values when the boat is not operating.

### 4.2.7 DC motor subsystem

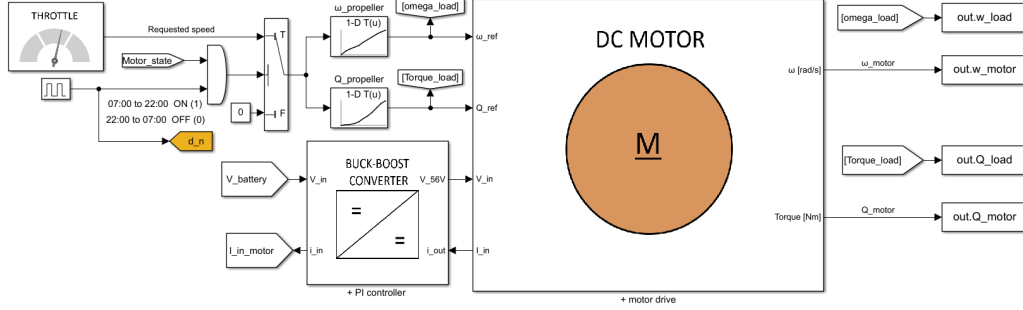


Figure 4.25. DC motor subsystem, 1<sup>st</sup> level

Figure 4.25 clarifies the role played by the motor subsystem in the Simulink® model. It begins with the principal model input: the requested velocity of advance on the water surface. Mimicking the physical action of a skipper willing to travel at a certain number of knots, the throttle subsystem outputs some pre-determined velocity profiles, in  $[m/s]$ . They are fed to the model in the same fashion it is done with ambient conditions, i.e. through *from workspace* block carrying time series objects. Then, they pass through a switch block whose role is to output null values whenever the boat is connected to the charging station or the engine is switched off. The latter condition will be analysed when expanding the DC motor subsystem. The output signal is then transformed into propeller requirements. It is done by utilizing two lookup table blocks which contains the propeller-load relation analysed in SECTION X. Thus, the velocity signal becomes a couple of reference values, one for the angular speed and another for the torque of the propeller. To sum up, by knowing the boat resistance curve is possible to transform the speed request into two reference values for the propeller working conditions that are known to generate the desired effect, i.e. the boat travelling at a particular speed. It is to note that, as the motor and the propeller are in a direct drive configuration, they share the same shaft and so the same rotational speed.

A buck-boost converter is placed in between the DC bus and the engine to stabilize the system operation. Whatever the DC bus voltage, the motor drive input is brought to a constant value of 56 [V]. The buck-boost typology was selected in order to allow the use of batteries with a voltage range exceeding the motor drive input and thus requiring a step down in voltage. Despite an additional converter lowers the overall efficiency, it is fundamental for reliability reasons.

As to the outputs, the current input needed from the motor drive becomes the reference output for the buck-boost converter, while the resulting angular speed and torque are used to assess the correct motor behaviour. In particular, the shaft rotational speed has to be exactly equal to the propeller one, while the output torque is slightly higher due to viscous friction and rotational inertia.

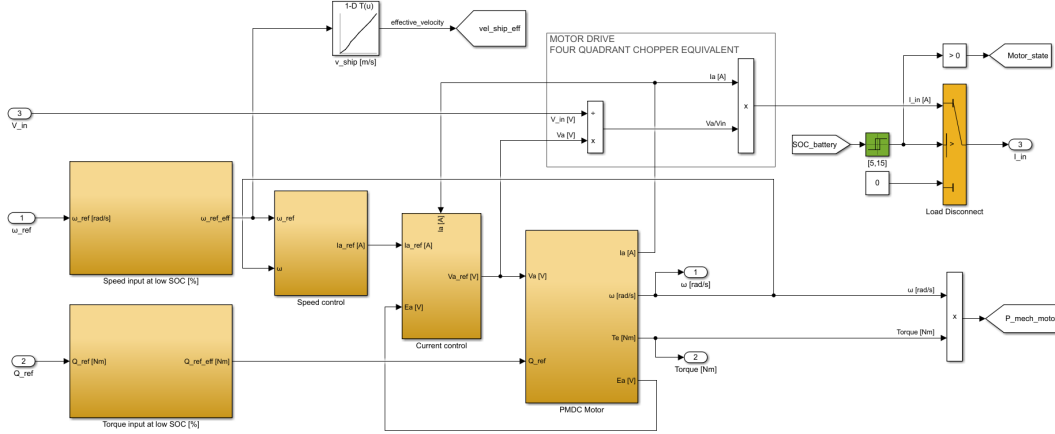
Figure 4.26. DC motor subsystem, 2<sup>nd</sup> level

Figure 4.26 shows the internal disposition of the DC motor subsystem. Proceeding from left to right the first subsystems encountered consist in an additional control logic intended to prevent unexpected and fast battery discharging. It is in fact known that the amount of power needed to propel a boat is roughly proportional to the cube of velocity, which means that driving fast require a certain energy cost that needs to be thoroughly considered. Thus, if the battery SOC reaches certain pre-defined levels, the controller limits the boat attainable velocity. Despite it may take longer to reach the desired destination, it is done as safety measure to avoid running out of propulsive energy. However, if an emergency situation would require full speed at low capacity values, that would still be made possible. So, this should be an user-deactivable additional feature. Once calculated the effective rotational load parameters, the angular velocity signal gets halved. The first branch enters a lookup table and is transformed back to a velocity signal which reproduces the effective sailing speed. The second branch is instead fed to a closed-loop controller cascade: a speed controller compares  $\omega_{motor}$  with  $\omega_{ref}$  and outputs a reference armature current. The latter is likewise fed to a current controller which similarly tries to maintain the effective armature current  $I_a$  close to  $I_{ref}$  and finally outputs the reference armature voltage. The latter is sent to both the motor drive and the PMDC motor subsystem, where the system equations are finally solved.

Regarding motor control, rotational speed can be adjusted through voltage regulation while torque is directly proportional to current, as already seen in CHAPTER X. As to the motor drive, it is a DC-DC converter able to convert a fixed input DC voltage (56 [V]) into a different, variable, one. It exploits a four-quadrant chopper which steps down the voltage to the desired reference value by independently commanding four switching devices. It can operate with all the possible current and voltage polarities. In this context, it is to mention that, besides allowing a forward and reverse motoring<sup>5</sup>, it could be utilized to allow hydro-generation whenever the propeller could rotate as a consequence of an external force, as in the case of the wind in a sailboat. However, as the present case study deals with a motorboat, the four-quadrant chopper circuit description is considered out of scope.

<sup>5</sup>From a load perspective, forward or reverse motoring do not differ, as the only difference is the current direction in the motor imposed by the circuit configuration.

The following shows the average equations used to easily simulate the four quadrant chopper ideal behaviour [38] without the need of a pulse generator:

$$V_{out} = (2D - 1) \cdot V_{in} \quad (4.11)$$

$$i_{in} = (2D - 1) \cdot i_{out} \quad \rightarrow i_{in} = V_{out}/V_{in} \cdot i_{out} \quad (4.12)$$

Where  $D$  is the duty cycle of the PWM signal. Eq. 4.12 is indeed implemented inside the Simulink® model in Figure 4.26. The resulting motor drive input current is asked to the system only if the battery SOC is higher than 5 [%]. Otherwise, a load disconnection is forced and kept until an SOC = 15 [%] is reached back. It is the same logic already seen in section 4.2.6. One may finally note how the load disconnection automatically triggers the *Motor\_state* flag, which causes the shut down of the motor and avoid unnecessary computations.

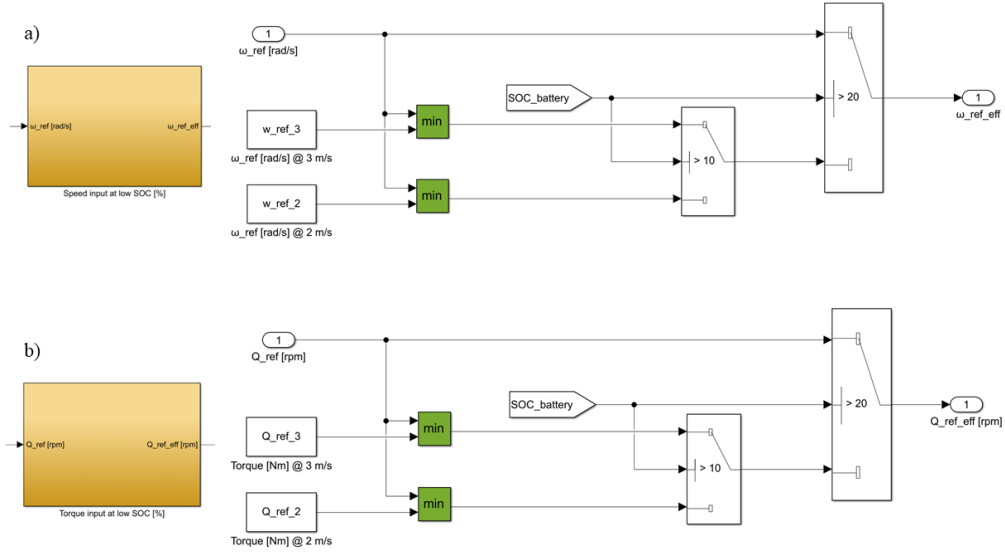


Figure 4.27. DC motor subsystem, speed (a) and torque (b) input under low SOC

The aforementioned power limitation control subsystems are shown in Figure 4.27. Depending on the battery residual charge, different shaft angular speed and propeller torque references may become the output of the switch blocks at the right of the figure. In particular:

- if SOC [%]  $\in (10, 20]$  the limit threshold on the boat attainable velocity is set to 3[m/s]. Thus the relative reference parameters are fed to the system whenever the originally requested speed is higher than 3[m/s].
- if SOC [%]  $\leq 10$  the limit threshold on the boat maximum attainable velocity is further lowered and set to 2[m/s].

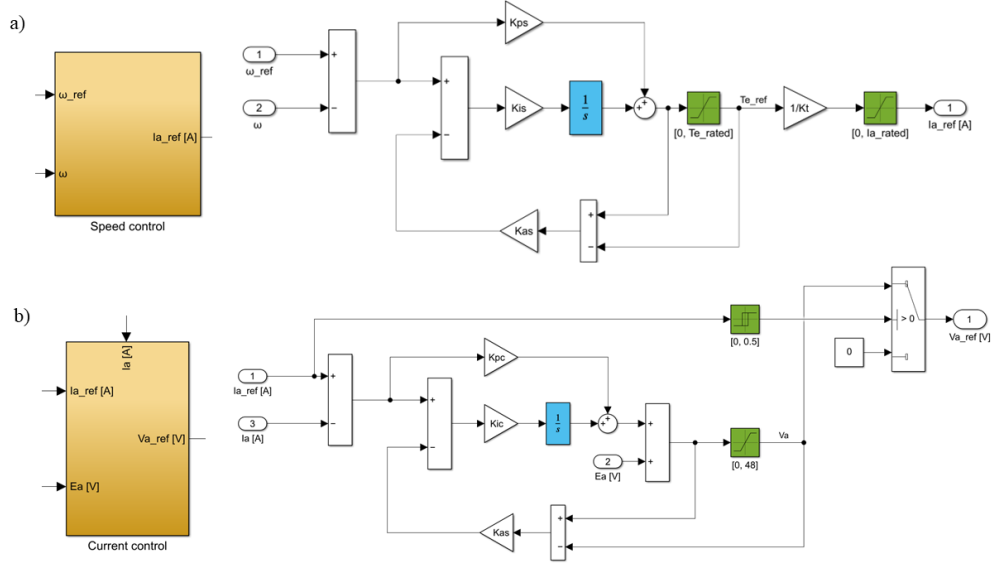


Figure 4.28. DC motor subsystem, speed and current PI controllers

The system architecture of the two PI cascade controllers relative to speed and current is depicted in Figure 4.28. A correct choice of gain constants is crucial for the stable operation of a PI controller. In the case under consideration, gains are determined by bandwidths  $\omega^6$ . Since the response time of the armature current is faster than the one of the motor rotational speed, they react differently to a sudden change in voltage. In this context, the frequency of the inner controller should be around one order of magnitude higher than the outer controller one<sup>7</sup>. As to the present case, the following equations have been used to determine the PI controller gains [38], assuming a chopper switching frequency of 1[KHz].

- $\omega_c = 50[\text{Hz}]$ : current control bandwidth
- $\omega_s = 5[\text{Hz}]$ : speed control bandwidth
- $K_{pc} = L_a \cdot \omega_c [\text{V/A}]$ : proportional gain current controller
- $K_{ic} = R_a \cdot \omega_c [\text{V/A/s}]$ : integral gain current controller
- $K_{ac} = K_{pc}^{-1} [\text{A/V}]$ : anti-windup gain current controller
- $K_{ps} = J \cdot 5 [\text{Nm} \cdot \text{s}]$ : proportional gain speed controller
- $K_{is} = J \cdot \omega_s [\text{Nm}]$ : integral gain speed controller
- $K_{as} = K_{ps}^{-1} [\text{Nm}^{-1} \text{s}^{-1}]$ : anti-windup gain speed controller

<sup>6</sup>More info on the concept of bandwidth in control system can be found in [38].

<sup>7</sup>In other words, to prevent current control from interfering with speed control, the latter bandwidth has to be at least five times narrower than the current control bandwidth [38].

All the saturation blocks in figure allows to obtain meaningful output values for torque, current and voltage. As to the latter, null value is passed through the switch whenever current reference points are so small to be caused just by system instability towards zero speed request, i.e. when the motor is not working.

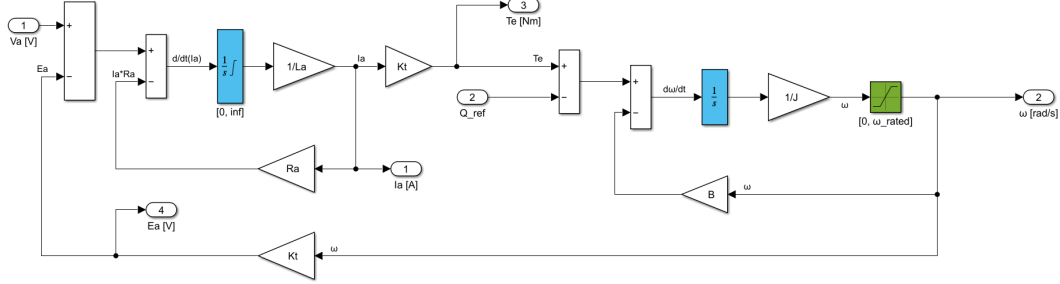


Figure 4.29. DC motor subsystem, equations

The DC motor electro-mechanical linkage shown on Figure 4.29 is based on the following system, which is the result of what is dealt with in section 3.4:

$$\begin{cases} J_m \frac{d\omega_m}{dt} = T_e - B_m \omega_m + T_L \\ L_a \frac{di_a}{dt} = V_a - R_a i_a - E_a \end{cases} \quad (4.13)$$

Where:

- $J_m [kg \cdot m^2]$ : rotational inertia
- $\omega_m [rad/s]$ : angular velocity of the motor shaft
- $T_e [Nm]$ : electric motor output torque
- $B_m [Nm/(rad/s)]$ : viscous friction coefficient
- $T_L [Nm]$ : load torque
- $L_a [H]$ : armature inductance
- $V_a [V]$ : armature voltage
- $i_a [A]$ : armature current
- $R_a [\Omega] = \frac{V_{a\_rated}}{I_{a\_rated}} \cdot (1 - \eta_{motor})$  armature resistance
- $E_a [V]$ : back electromotive force

Equations in system 4.13 are linked by the motor constant  $K_t [Nm/A]$  shown in section 3.4.

- $T_e = k_t \cdot i_a$  (ref. eq. 3.19)
- $E_a = k_t \cdot \omega_m$  (ref. eq. 3.19)

Finally, one may note how the integration output of the current derivative is limited to a non-negative value, while the rotor angular speed entity cannot overcome the rated value to respect data sheet constraints.



### 4.2.8 Buck-Boost converter subsystem

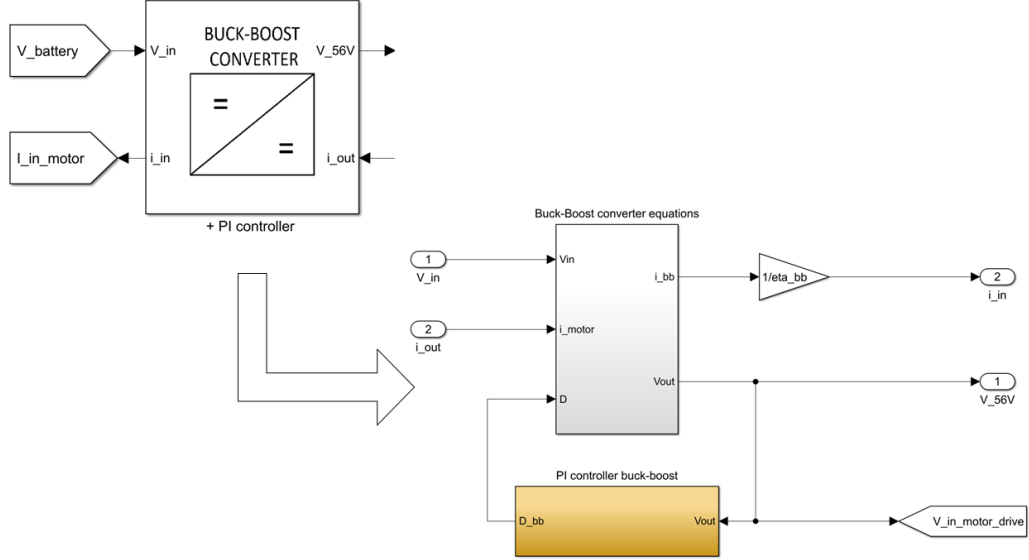


Figure 4.30. Buck-Boost converter subsystem, 1<sup>st</sup> and 2<sup>nd</sup> level

The buck-boost converter subsystem is further expanded in Figure 4.30. Considering that the equations solved in the inner subsystem are ideal, the requested input current is further divided by the converter efficiency so that losses are taken into account,. As to the output voltage, it becomes the input of the motor drive and it is kept constant by a PI controllers which constantly adjust the PWM duty cycle to fulfill the 56[V] voltage requirement.

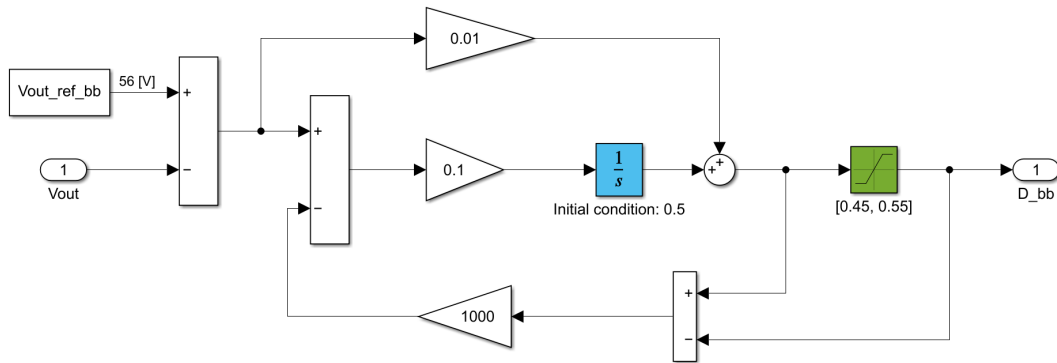


Figure 4.31. Buck-Boost converter subsystem, PI controller

Figure 4.31 contains the scheme of a classic PI controller, which was already discussed in this section. Gain constants and saturation limits are obviously to be optimized for the case study into consideration.

A buck-boost converter circuit scheme is presented in Figure 4.32. It is an inverting DC-DC converter, therefore it outputs a voltage with reverse polarity (negative).

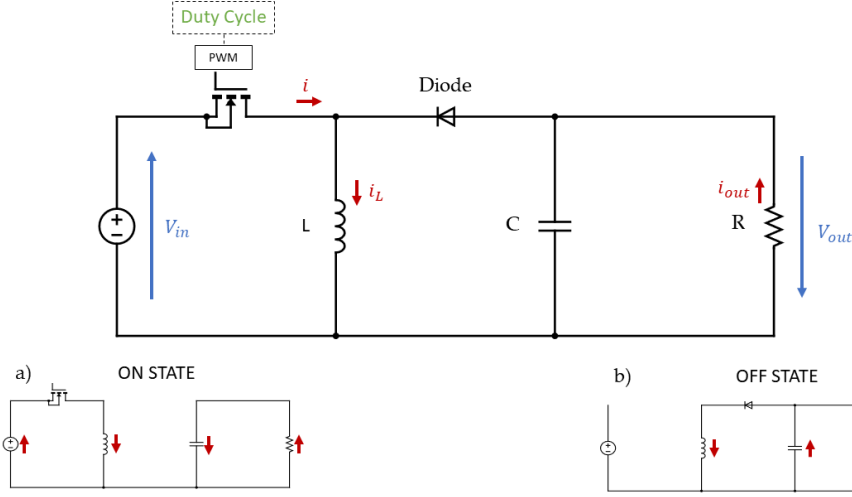


Figure 4.32. Buck-Boost converter coupled to electrical motor, simplified electrical circuit

The ideal generalized equation linking input and output voltages is [60]:

$$|V_{out}| = V_{in} \cdot \frac{D}{1 - D} \quad (\text{ref. eq. 3.26})$$

Thus,  $D = 0.5$  ideally produces no effect, while higher duty cycle values rise the output voltage and vice versa. As to the converter design, inductance ( $L$ ) and capacitance ( $C$ ) values were selected according to [61, 62]:

$$L = \frac{V_{in} \cdot D}{f_s \cdot \Delta I_{out}} \quad (4.14)$$

$$C = \frac{V_{out} \cdot D}{f_s \cdot \Delta V_{out}} \quad (4.15)$$

Where:

- $V_{in}[V]$ : usual input voltage. It varies between the minimum and maximum battery one
- $D[-]$ : duty cycle relative to the chosen usual input voltage
- $V_{out}[V]$ : output voltage, set to 56[V]
- $\Delta I_{out}[A]$ : maximum output current ripple
- $f_s[Hz]$ : switching frequency
- $\Delta V_{out}[V]$ : output voltage ripple

Its average model equations, adapted from [41, 43], can be found below:

$$\begin{cases} t \in (0, t_{on}] \\ L \frac{di_L}{dt} = V_{in} \\ C \frac{dV_{out}}{dt} = -i_{out} \end{cases} \quad \begin{cases} t \in (t_{on}, T] \\ L \frac{di_L}{dt} = -V_{out} \\ C_o \frac{dV_{out}}{dt} = i_L - i_{out} \end{cases} \rightarrow \begin{cases} t \in [0, T] \\ L \frac{di_L}{dt} = V_{in} \cdot D - V_{out} \cdot (1 - D) \\ C \frac{dV_{out}}{dt} = i_L \cdot (1 - D) - i_{out} \end{cases} \quad (4.16)$$

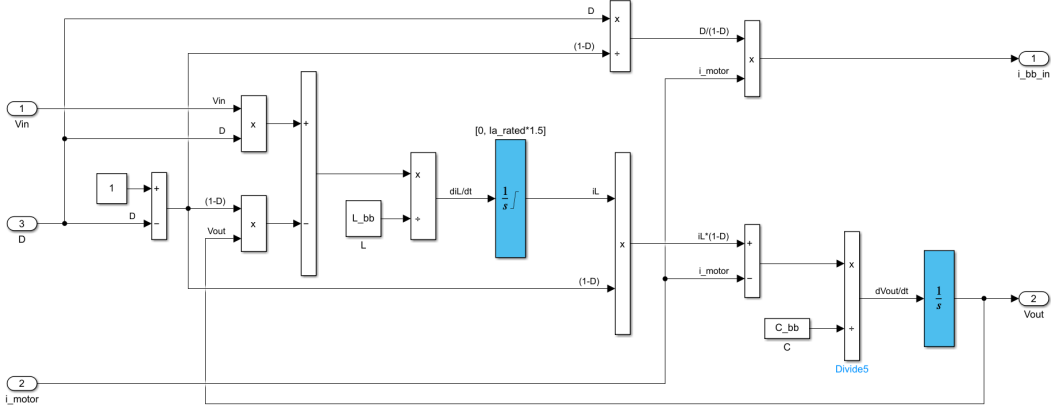


Figure 4.33. Buck-Boost converter subsystem, equations

Figure 4.33 shows the Simulink® implementation of the buck-boost converter equations. The current integrator block output is constrained for convergence reasons. The input current is calculated in a similar fashion it is done for the buck converter, with the difference that the multiplying factor to ensure energy conservation is  $\frac{D}{1-D}$ , according to eq. 3.26.



## Chapter 5

# Main assumptions and limitations

The model allows to simulate even several weeks of operation without requiring a huge computational effort. It is made possible by simplifying the modelling of every component and aligning it to the same degree of detail of the others. Generally, an effective measure to increase the modelling accuracy would be that to consider varying efficiency depending on components working operations. However, the majority of data are directly extrapolated from data sheets, which are usually incomplete with regards to the simulation scope and thus pose the necessity to assume some model parameters. Simplifications and assumptions necessary lead to limitations and discrepancies in term of accuracy and adhesion to reality. An overview of the potential deviations with regards to a real world system are listed below, some of them have already been mentioned in the precedent chapters.

- Back-up generator. Undoubtedly, a proper propulsion system design would rely on a back-up power source, usually diesel powered, brought onboard to ensure an additional reserve of energy in case of battery fault or discharge. However, no emergency generators were included in the simulation as it was considered not significant for the purpose of the model. Energy shortcomings, covered by the back-up generator in a real life application, are utilized in Chapter 7 to better ponder design performances.
- PV array. Both rigid or flexible panels can be installed on the boat hard top. They are supposed to be installed on a flat surface and thus able to capture the horizontal component of irradiance. The occupied area was specified to be in between  $12 \div 14[m^2]$  depending on the selected cell type and efficiency<sup>1</sup>. No shading effects are considered. This choice may produce a significant error if the majority of boat trips take place in between Venice canals. Moreover, PV surface temperatures are assumed equal to the ambient one plus  $15[^\circ C]$  to obtain a trade-off between two extremes and facilitate calculations. The assumption is exaggerated during the first and last hours of the day, when the PV cells temperature cannot differ so much from the ambient one, but, on the other hand, it may result weak during the hottest hours due to the important radiative contribution. This last case is however partially compensated when considering that panels are cooled by air when the boat is in movement. If necessary, more precise calculations on cell temperatures could be done according to what is proposed in [63].

---

<sup>1</sup>Monocrystalline cell perform the best. They are followed by multi-crystalline and thin-film types. Differences in terms of price, durability and mechanical properties exist [27].

- Voltage conversion devices. Buck and buck-boost DC-DC converters have been modelled by means of ideal average equations for equivalent Single Ended Primary Inductor Converter (SEPIC) topologies. Different types of converters exist, with both isolated or non-isolated circuit types. They cover different potential application depending on the power transfer, efficiency and safety needed. However, PWM through duty cycle control is a broadly adopted switching regulation methodology that brings them together. As a consequence, the current work modelling makes use of ideal average equations function based on duty cycle inputs. Energy conservation is granted, while losses are taken into account by considering constant efficiencies, irrespectively from power transfers. As to the PI controllers, Simulink® already offers a tuning tool to dimension gain parameters. When not applicable, a trial and error method was followed.
- Batteries. Despite the possibility to implement aging effects on the Simulink® *generic battery model*, they were not taken into account to lighten the computational burden. Additionally, considering temperatures effects in a meaningful way requires a precise description of the battery bank ambient conditions, which would still be affected by a considerable guessing error, neutralizing all the effort taken in that direction.
- Charging station. Although most charging columns installed in ports provide AC power as output, shore power was considered as a DC input to the model, assuming that conversion has already occurred.
- Motor system. Guessing the motor operating points<sup>2</sup> out of the rated condition provided by manufacturers hides several challenges. Additionally, the physical constructions of the common used BLDC or PMSM motors would require a suitable mathematical model, heavier to simulate with respect to the equivalent one utilized. For this reason, as clarified in section 3.4, the prime mover is supposed to be a PMDC motor whose characteristics are partially extracted from data sheet and partially derived by assumptions, with the scope to create an operating curve that maintain physical consistency and thus performance reliability. As to the motor drive, no switching losses are considered. The voltage conditioning efficiency is in fact virtually absorbed by the buck-boost converter upstream so that the result from the combination of converter, motor drive and actual DC motor losses results in an overall transmission efficiency from the electrical motor system to the mechanical output fed to the shaft.
- Propeller. Open water diagrams are calculated thanks to the *propcalc* tool mentioned in section 3.3.1, fed with partially estimated parameters, such as the blade aspect ratio. It is to note how the simulated screw propeller performances were those of a fixed pitch type. Some new designs rely on controllable pitch propellers to ensure higher propulsive efficiencies and better manoeuvrability.
- Motor-propeller mechanical link. A direct drive configuration for the inboard motor was assumed as it is an already established option for moderate power, higher efficiency boats. A gearbox can however be added to the system by modifying the torque and rotational speed signals according to the design gear ratio.
- Auxiliary loads. Their current request is considered constant throughout the day, as if the load variations were spread across the whole operating period, with no variations. It can obviously be done differently according to the case under consideration.

---

<sup>2</sup>in terms of torque, rotational speed, efficiency and thus power.

Regarding the operating routine, boats may usually find a charging station in between one route and another. They do not need to rely solely on the capability of PV panels to charge the battery bank but could be connected to shore power during stops and pauses. This possibility is however not shown to be more conservative with regards to the utilizable power. As to the Simulink® model visualization, charge controller subsystems were scattered throughout the whole domain while in reality they are usually placed in power distribution or control boxes. Finally, a consideration of paramount importance is to be done towards the choice of the operating voltages. In fact, the stability of the system is dependent from a proper integration of energy converters and energy utilizers. Once chosen the rated voltage and power of the prime mover, i.e. the electric motor, other system components need to be linked accordingly, respecting voltage and current restrictions in terms of safety and physical feasibility. In the case study, a 48[V] motor was selected since it usually offers a good compromise for leisure boat propulsion systems below 20[kW], as it can be seen by looking at the commercialized models. Different operating voltages can obviously be simulated, as long as practicability is concerned, i.e. the mutual relationship between PV panels, batteries, motor and DC-DC converters is properly designed and ensures system stability<sup>3</sup>.

Besides the aforementioned assumptions, important model limitations concern the weight and volume of the system constituent elements, which are not analysed but, together with budget constraints, set crucial boundaries to the design optimisation procedure. Adding weight increases boat displacement and thus water resistance, while the volume occupied by the propulsion system has to respect the actual space dedicated onboard. As to economical considerations, they are to be considered out of the scope of the present thesis.

---

<sup>3</sup>To make an example, once found data sheet information, one could opt to model a system where a 96[V] motor is linked to 150[V] solar panels, 24[V] batteries and 24[V] auxiliary loads as long as converters are correctly designed.





## Chapter 6

# Numerical results

*Results concerning the model application to the Venetian lagoon case study are here reported. The chapter is divided in several sections whose scope is to:*

- *explain how the unpredictable load request of a taxi boat was simulated*
- *show how relevant informations are extracted from the Simulink® model*
- *visualize model dynamics in the time span of a single day and observe key results able to weight system performances when the simulation is carried out on a larger time span*

### 6.1 Weather and random load generation

Ambient conditions values are needed to correctly assess PV production. They consist in temperature and horizontal irradiance data for the site where the taxi boat operates. Relying on databases such as the PVGIS online tool [49], it is possible to obtain a hourly resolution for the aforementioned ambient conditions, making it possible to simulate precise moments of a specific year, or even better utilize data from a typical meteorological year to estimate the array expected performances on the desired time interval. Data are stored in a spreadsheet file which is called directly from MATLAB® workspace before running the model. A function stores the values in *time series objects* which are then fed to the PV subsystem through *from workspace* blocks.

With regards to the specific case study, a MATLAB® function was created<sup>1</sup> to address the issue of non predictable and varying routes. It works by generating casual load profiles during the boat operating time. In particular, looking at usual travel durations across Venetian lagoon, a total of eight possible types of velocity duty were created, considering relatively slow or fast trips lasting 15, 30, 45 or 60 minutes. They are portrayed in Figure 6.1. A probability of occurrence is assigned to each of them. The same approach is followed with regards to pause intervals of the same amount of time. In this way random loads and pauses successions are obtained. Moreover, by multiplying pause durations by a certain coefficient (*pause\_weight*) it is possible to reproduce monthly differences in the expected number of trips undertaken by the boat. Obviously, the most disparate measures can be taken to introduce load variability in agreement with the real boat mission and site of operation.

---

<sup>1</sup>The function was named: *load\_and\_weather*. Its script can be found in the appendix.

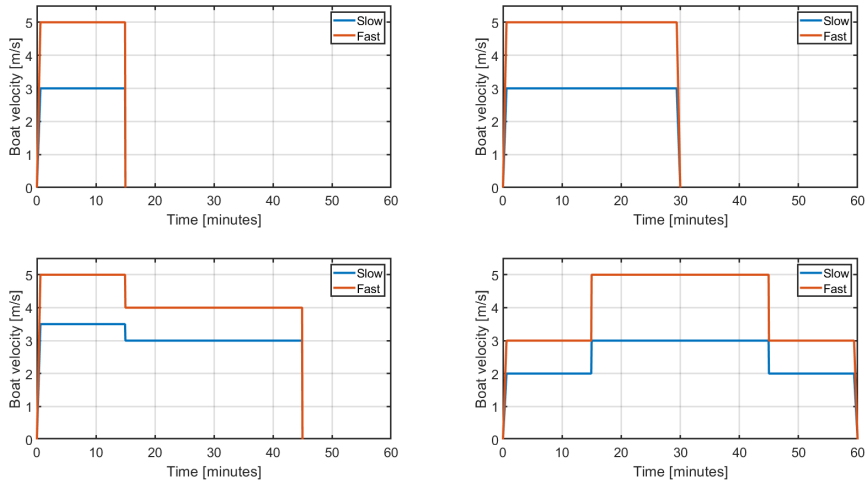


Figure 6.1. Load profiles

Different shapes were assigned to the 45 and 60 minutes travels to make them easier recognizable in a plot. One may also note how velocity gradually increases or decreases when the boat starts or concludes its journey. This avoids the system to become unstable due to velocity steep changes from and to stall position. Figure 6.2 shows how a random generated curves may look like when even pause weights are considered. The higher the pause weight, the more probable to have a lighter load profile. One can visually find out that short rides of 15 or 30 minutes have been considered more probable than longer ones of 45 or 60 minutes.

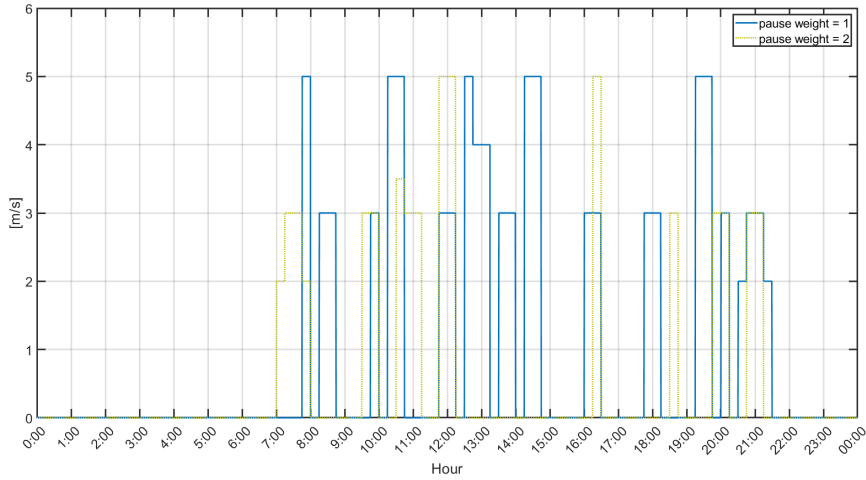


Figure 6.2. Example of random load generation

As already mentioned in section 3.3, the maximum velocity allowed in the lagoon is 20[km/h], which explains why the maximum speed attainable from the boat is set to 5 [m/s].

## 6.2 Data to export

Figure 6.3 depicts the model subsystem containing the calculations needed to extract quantities to be plotted or further analysed in the present chapter. One may note the large use of *Goto* tags to offer a clear visualization.

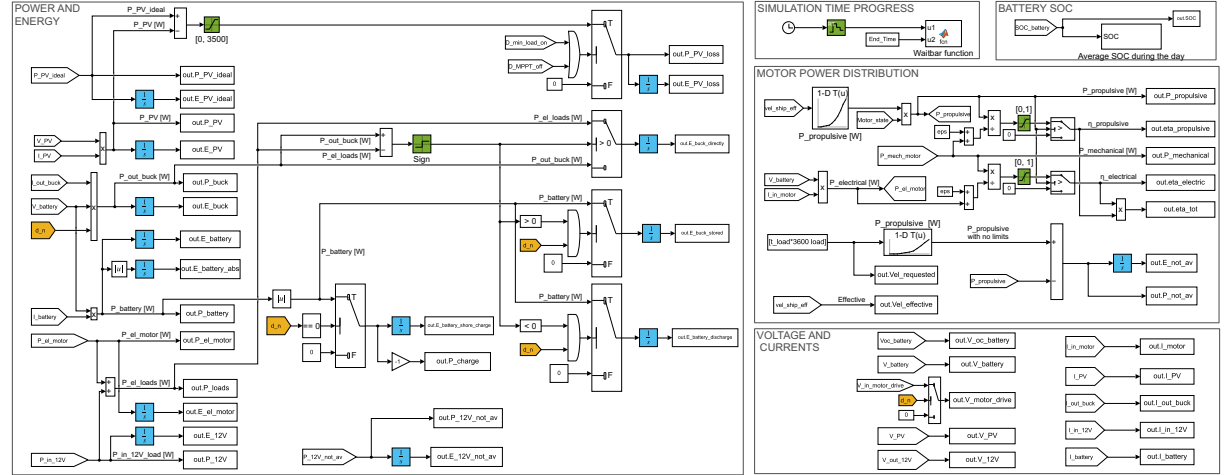


Figure 6.3. Calculation and data to export subsystem

Five sections are shown:

- **Power and energy.** It contains the calculations needed to obtain the most relevant power signals. Energy vectors are then obtained by integration in time. After possible algebraical and logical recombination aimed at extrapolating meaningful signals, they are stored as *time series objects* and fed to MATLAB<sup>®</sup> workspace.
- **Simulation time progress.** It creates a superimposed *waitbar* box that gives information on the simulation state when the model is launched from the MATLAB<sup>®</sup> script. A ZOH block with a large sample time is utilized to avoid slowing down the simulation.
- **Battery SOC.** Besides saving the actual state of charge value at every time step, it calculates its average value for every hour of the day. The latter subsystem is not further expanded. It contains an integrator block which is reset every 3600 seconds, a gain of 1/3600 to obtain the average value per hour and a ZOH block to limit the added computational cost.
- **Motor power distribution.** The most significant quantities regarding the motor subsystem are here reported. It can be noted how some numerical artifices are implemented to obtain meaningful values for efficiencies calculation.
- **Voltage and currents.** Electrical conditions of relevant system components are fed to MATLAB<sup>®</sup> workspace.

### 6.3 Dynamic plots and performance weighting parameters

In order to show how the control logic of the charge controller regulates the power distribution of the whole system, some specific load and irradiance conditions have been artificially generated with the intention to condense in a single day some of the most relevant situations that may occur when the boat is operating. The following plots contain the dynamic evolution of the main system quantities during this *ad hoc* reference day, so that their mutual dependency can be clearly understood. The input velocity load is shown in Figure 6.4, while the irradiance and ambient temperature conditions are reported in Figure 6.5. In addition to the propulsion power it is assumed a constant auxiliary loads current draw of 20[A], from 7:00 to 22:00.

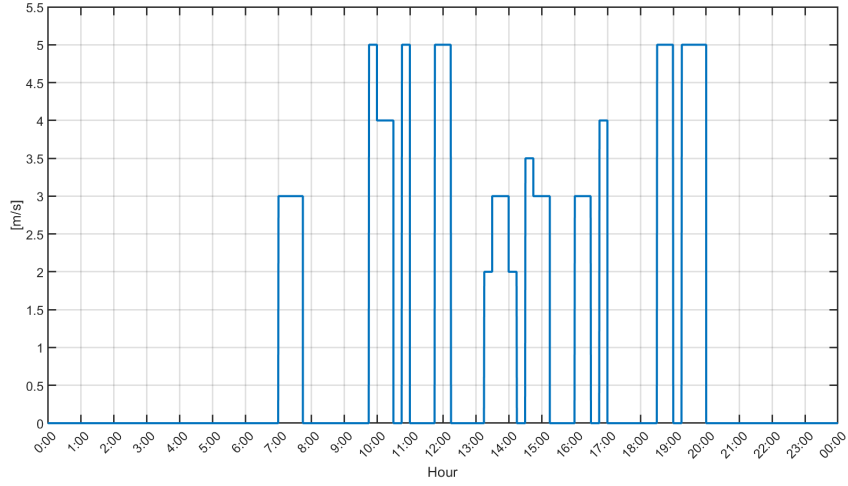


Figure 6.4. *Ad hoc day*. Velocity request

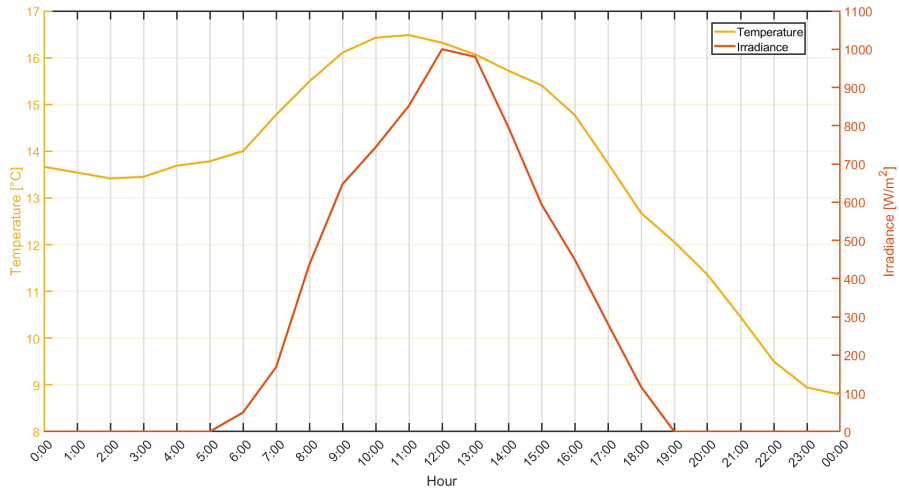
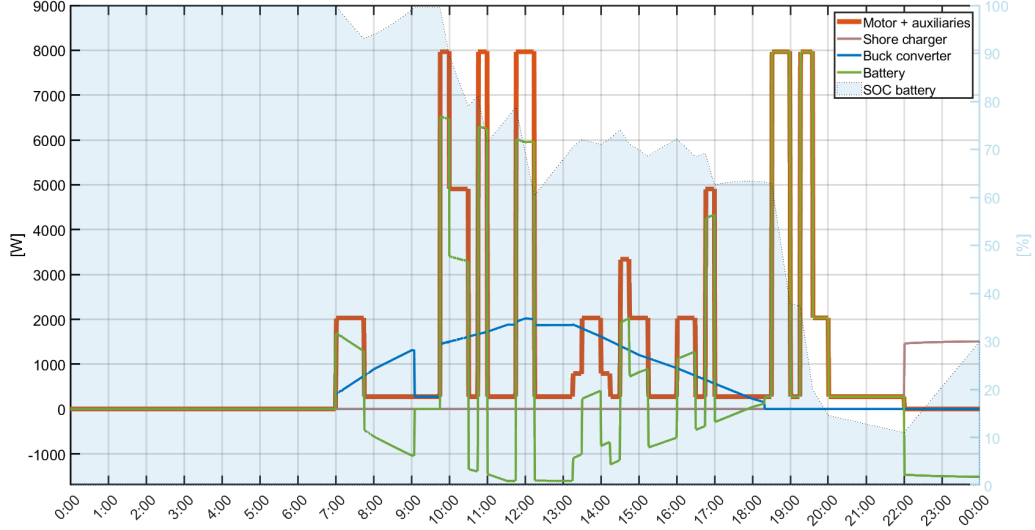


Figure 6.5. *Ad hoc day*. Ambient conditions


 Figure 6.6. *Ad hoc day.* Power distribution

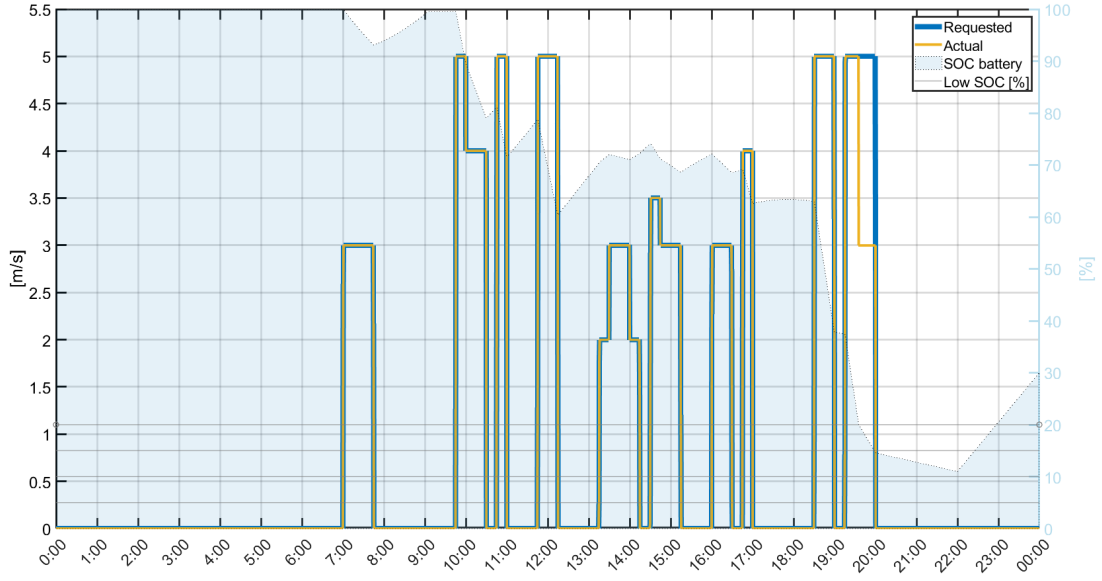
The most important dynamic plot is depicted in Figure 6.6. It summarizes the main power flows occurring during the day. The orange curve combines the electrical power input requested from the motor and the auxiliary loads, while the blue and green solid lines represents, respectively, the output power of the buck converter and the power entering (-) or exiting (+) the battery bank. The light blue area shows the evolution of battery SOC and pertains to the right y-axis. Finally, the light brown curve represents shore power charging power, which coherently starts after 10 pm. The auxiliary power request is assumed constant and equal to 275.9[W] throughout the whole day:

$$P_{aux} = \frac{V_{out} \cdot I_{out}}{\eta_{buck}} = \frac{12 \cdot 20}{0.87} = 275.86[W] \quad (6.1)$$

Despite it may not be so realistic since most of the devices are consuming power only when the boat is navigating, it still represents a good method to take into account a daily expected energy consumption of around 4[kWh]. One may note the great difference in power when the boat is travelling at 3, 4 or 5[m/s], which translates into large current draws from the DC motor, as it can be seen in Figure 6.10.

Starting from 7:00, battery contribution adds up to PV generated power to fulfill the electrical load request. At 07:45 the boat terminates its first trip and the PV production is large enough to feed the auxiliary loads while also charging the battery bank, as deducible from the negative power entering the battery, which causes its SOC to rise until a value of 100[%] is reached. At this point, to avoid power dissipation through Joule losses, the buck converter control logic forces the PV array to operate outside its maximum power point and produce the exact power needed to sustain auxiliary devices. From 09:45 onwards, it switches back to its MPP as the boat sails for another trip. Later in the day, a power curtailment occurs at 11:30 and at 12:15. Ambient conditions would in fact allow a larger power production which is instead restrained to respect the established maximum battery charging current threshold of 30[A]. The latter condition is better recognizable by looking at the curves in Figure 6.10. The boat travels other routes propelled by a mixture of photovoltaic and battery power until 18:15, when irradiance falls below the minimum value of 80[W/m<sup>2</sup>] and the battery becomes the only power source to feed the loads. The sudden drop in power experienced at 19:30 is motivated in the following figure.

Finally, at 22:00, the boat returns to the dock and is connected to a charging station.

Figure 6.7. *Ad hoc day*. Velocity load

Similarly to what has been shown at the beginning of the section, Figure 6.7 shows the velocity load that simulates the skipper action on the motor throttle. One may note how the actual speed (curve in yellow), which instead is the result of the propulsion system operation, coincides with the requested one except for the last boat trip. In fact, according to the control logic explained in section 4.2.7, as the battery SOC reaches a value smaller than 20[%], the maximum attainable velocity is limited to 3[m/s] in order to preserve battery capacity. The latter effect can be seen by looking at the variation in slope undertaken by the SOC curve at 19:30. It is important to mention that, due to the power curtailment, advancing at a lower speed requires more time to reach the desired destination. This is not taken into account in the present graph as a better option would consist in connecting the back-up generator to provide the missing energy and charge the battery bank up to a safer value. What really matters in the design phase is to estimate the energy not available when needed to better reconsider the system design, as it will be shown in Figure 6.16.

After 20:00, only the auxiliary loads are requesting electricity, and this is the reason why the SOC curves continues to slowly fall down. According to the control logic implemented in the present simulation, if SOC crossed the 5[%] threshold, auxiliary loads would be disconnected to prioritize propulsion. In a real world scenario, such a situation would hardly occur due to the prior connection of an emergency generator able to provide the energy needed to safely terminate the trip.

Figure 6.8 and 6.9 report the evolution of the parameters defining the load and motor mechanical power. Coherently with what was mentioned in section 4.2.7, the rotational speed of load and motor are identical since they physically share the same shaft. On the other hand, the motor torque slightly differs from that requested by the load due to the need to overcome friction and inertia effects. Please note that the blue lines represents the desired load profile, which are not respected from 19:30 onwards due to the low battery SOC value.

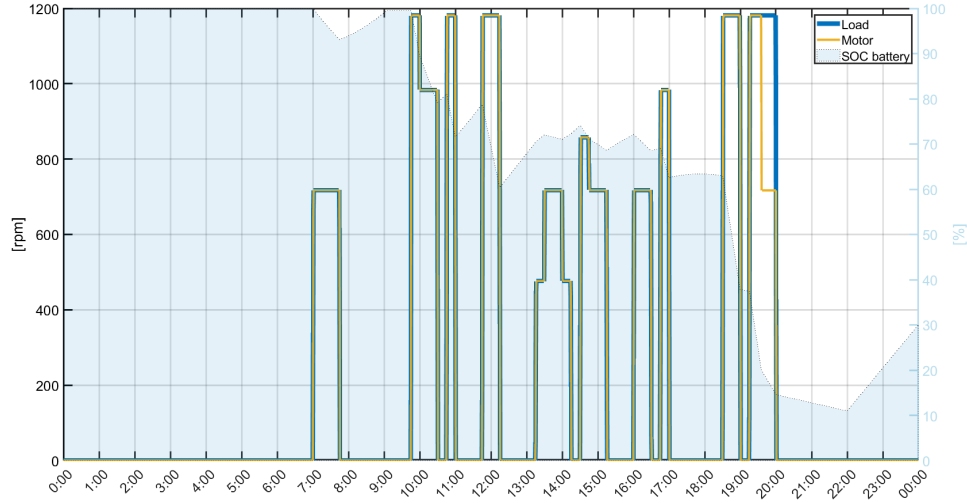


Figure 6.8. *Ad hoc day*. Load and motor rotational speed

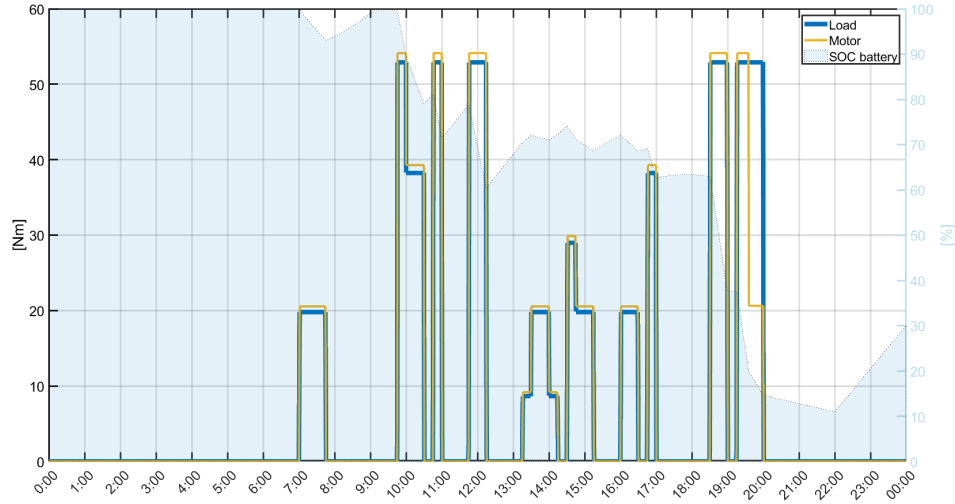


Figure 6.9. *Ad hoc day*. Load and motor torque

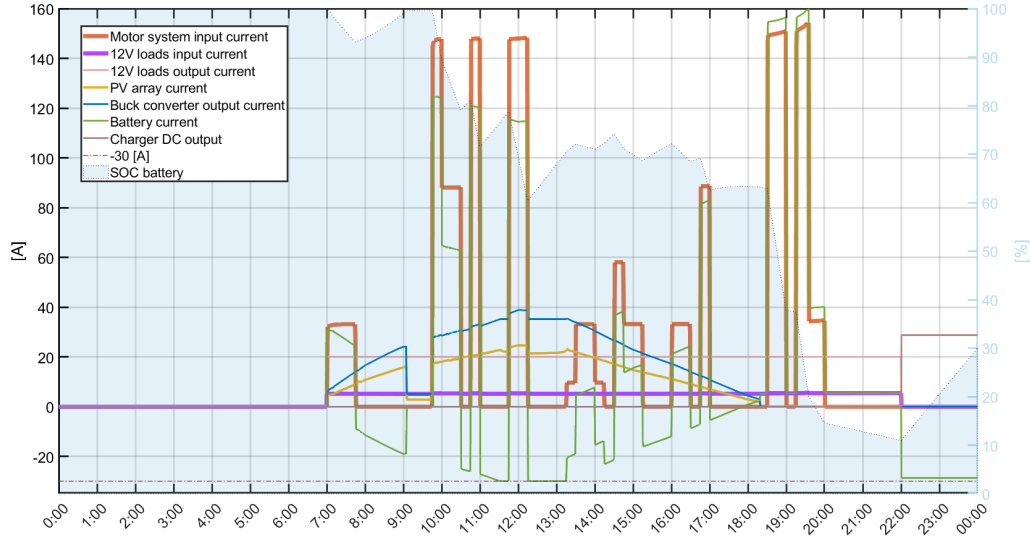

 Figure 6.10. *Ad hoc day*. Relevant currents

Figure 6.10 contains the dynamic evolutions of the most relevant current transferred across the system. Here, the load request was further broken down into motor system and auxiliary load contribution. Additionally, the actual photovoltaic current reaching the buck converter input is shown in yellow.

Recalling what was explained in the theoretical introduction, the buck converter output current is indeed bigger than the input one since the voltage chop experienced in the device cause a current rise in order to respect the energy conservation principle. The mathematical relationship is mentioned in eq. 3.24, and can be verified in the actual non-ideal case considering the assumed converter efficiency ( $\eta_{buck} = 0.9$ ) and the duty cycles reported in Figure 6.13. What immediately catches the eye is the net drop of photovoltaic current at 9 am. Since the battery is fully charged, the photovoltaic operating point moves away from MPP so that the buck converter output current exactly equals the one needed from the auxiliary loads. As to the latter, the purple solid line represents the input current needed from the 12V buck converter which, following the same physical principle explained above, is smaller than the actual output one of 20[A]. The 12V buck converter controller duty cycles are not shown in the chapter, but may be find by running the MATLAB<sup>®</sup> script in Appendix.

The aforementioned power limitations imposed to photovoltaic panels at 11:30 and 12:15 are here clarified when considering that at those times the battery charging current reaches the threshold value of 30[A]. As to the small steps experienced from the buck converter output current in between 10:30 and 11:00, those are instead caused from the relatively big drop in battery voltage occurring when a large current is drawn from it, as it can be seen in figure 6.14.

To conclude, it is to note that the orange curve refers to the current input of the whole motor system, considering engine, motor drive and buck-boost converter.



The blue line in Figure 6.11 refers to the MPP curve for PV panels, which is the objective of the buck converter controller. However, as it was already seen, at around 9:00, being the battery fully charged, the charge controller forces the panels to operate away from their maximum power point and produce only the power needed to feed the load. In particular, when the latter is represented by only the auxiliary devices, PV panels produce 306.5[W], which, net of buck converter efficiency ( $\eta_{buck} = 0.9$ ), becomes equal to the 275.9[W], i.e. the auxiliary load request. Differently, at 11:30 and 12:15, PV production is limited to avoid charging the battery with a current magnitude bigger than the desired one. The latter is set to 30[A].

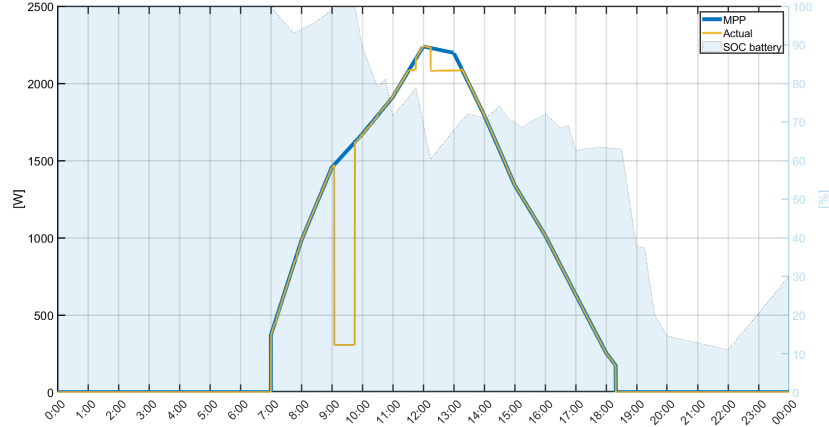
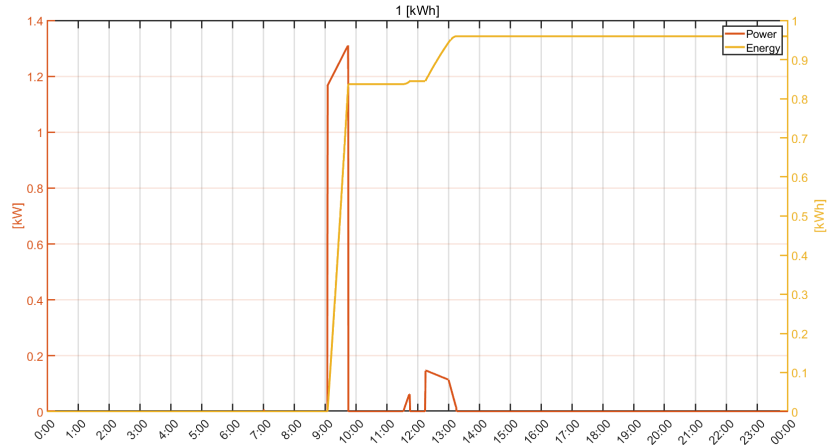
Figure 6.11. *Ad hoc day.* PV power

Figure 6.12, stores data for both the power that could have been stored in the battery bank if it was not completely charged and the one that cannot be exploited as it would overcome the charging current limitation. The integration of such resulting power over time allows to calculate the wasted potential PV energy. Both dynamic and total results can be useful in a designing phase to find the optimum sizing and specifications for both PV panels and lithium batteries.

Figure 6.12. *Ad hoc day.* Wasted power and potential PV energy loss

The duty cycle values that, through buck converter conditioning, determines PV panels operating points are reported in Figure 6.13. Recalling the control logic configuration shown in Figure 4.13, it is now clear how the buck converter operation is selected between three cases: maintaining MPP, following load request when batteries are fully charged or limiting PV production when battery charging current limits would be trespassed. The dotted line (D) coincides with one of the aforementioned option in agreement with the load profile shown so far.

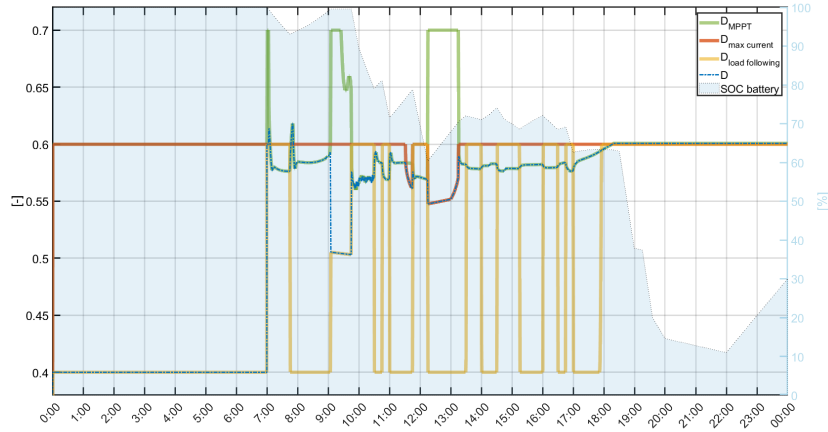


Figure 6.13. *Ad hoc day*. Relevant duty cycles

The effect on PV working voltages is depicted in Figure 6.14. One may note how, according to eq. 3.24, decreasing the duty cycle causes an increase of PV voltage, and vice versa. The latter is clearly exploited at 9:00, 11:30 and 12:15 when the selected duty cycle shifts PV operating voltages at the right of MPP, in the same fashion it was anticipated in Figure 4.10. Finally, the constant voltage input of the motor drive is here verifiable. The same can be done for the voltage provided to the 12V loads. As to the battery, one may note how, during the fastest travels, the open and close voltage differs significantly to allow a higher current draw.

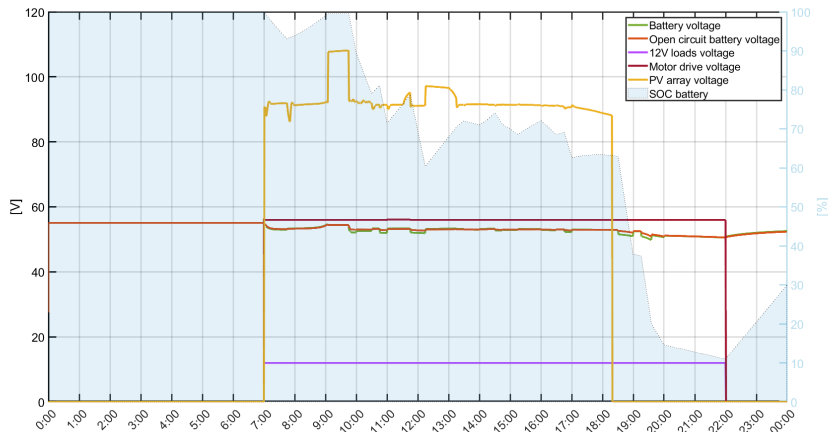


Figure 6.14. *Ad hoc day*. Relevant voltages

The most relevant powers and efficiencies of the propulsion chain are shown in Figure 6.15. The effective thrust power necessary to overcome boat resistance is shown in a solid green curve<sup>2</sup>. Moving up in the propulsion chain, the mechanical power required from the propeller during every boat trip is depicted with a blue solid line. The propulsive efficiency links the above powers, as already seen in Figure 3.7. Similarly, considering an electrical efficiency embracing the power transfer from the buck-boost converter input to the mechanical output of the motor, one can trace back to the actual electrical energy input needed upstream of the propulsion chain. Efficiency values are reported on the right y-axis of the graph. Considering that the majority of efficiencies in the propulsion chain are assumed to be constant, the slight differences are attributable to the resistance curve shape, the varying open water propeller efficiency and the friction losses at different shaft velocities. A crucial parameter validating the propeller-motor matching consists in the magnitude of the overall efficiency  $\eta_{tot}$ , which results in a value close to one shown in the reference data sheet of Table 3.5.

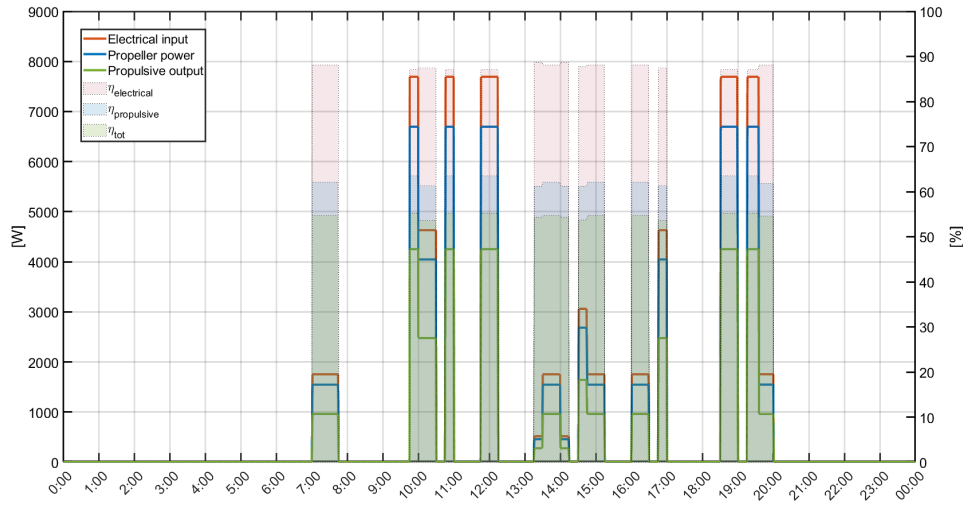


Figure 6.15. *Ad hoc day*. Motor power distribution

Whenever it is not possible to exploit the desired propulsion power, as it happens around 19:30, data on missing propulsive power are stored and simultaneously integrated to obtain a final value representing the energy shortcomings of the propulsion system<sup>3</sup>. A similar approach is followed to calculate the electrical energy shortcomings regarding the auxiliary load request<sup>4</sup>. A report on the energy that was not fed to the system due its unavailability or control logic settings helps evaluating the system performances and thus recalibrating any erroneous design choice.

<sup>2</sup>It corresponds to what is shown in Figure 3.6.

<sup>3</sup>Please note that, to ease calculations, the amount of missing propulsive power is computed and then divided by the design overall efficiency to obtain a value for the electrical energy that would have been needed from the system but was not provided to it.

<sup>4</sup>According to the system control logic, whenever the battery SOC falls below 5[%], loads are disconnected to prioritize propulsion.

The calculated electric energy not transferred to the system is reported in Figure 6.16.

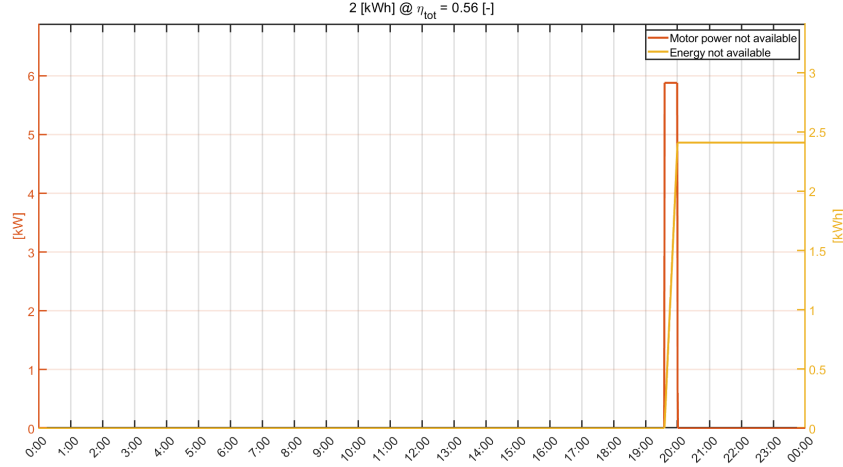


Figure 6.16. *Ad hoc day*. DC motor shortcomings

Finally, the dynamic plot in Figure 6.17 tracks the energy flow in and out of the battery. Besides monitoring the width of every charging or discharging process it is useful to divide the cumulated energy by the rated battery bank one to obtain a rough estimation of the total charge cycles that are carried out. In the absence of any aging effect implementation, the above calculation, coupled with info on SOC and current evolutions, could produce useful insights on the battery expected life<sup>5</sup>.

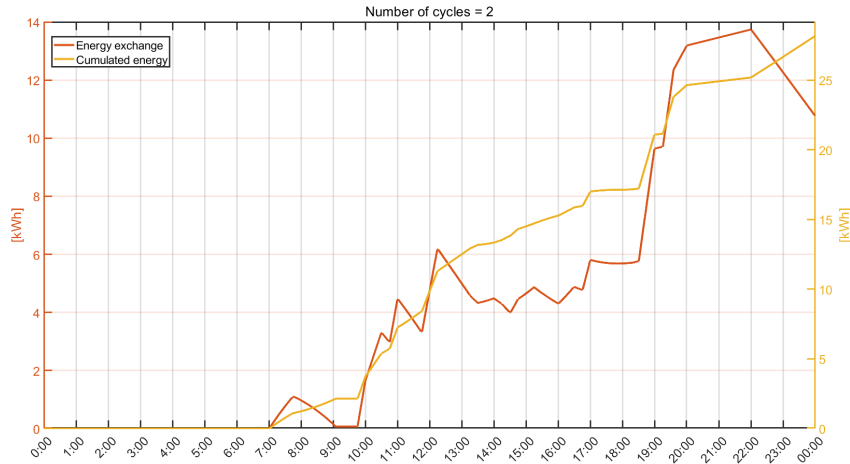


Figure 6.17. *Ad hoc day*. Estimated battery cycles

<sup>5</sup>For instance, those data could be fed to a post-processing tool that better estimates the remaining battery life.

One of the most important result summarizing model performances is represented by the energy balance reported in Figure 6.18. It is the result of a dynamic simulation already able to determine when and how power was transferred in the system,

Looking at the stacked histogram on its left, it is noticeable how part of the harvestable photovoltaic production is virtually lost when panels operate outside their maximum operating point, as it was shown in the previous plots. The energy produced, after some unavoidable conversion losses in the buck converter, is finally fed to the system. Here, according to the operation of the charge controller, it may be used to directly feed the load or to charge the battery bank. Obviously, the shore charger provides the additional energy which is stored in batteries during the overnight charge. Please note that, as the reported values refer to the integration of power during operation, the missing source contribution is nothing but the energy already contained in the battery bank before the simulation started. This graphical inconsistencies flatten out when longer time intervals are considered.

Finally, one may note how the energy shortcomings which made it impossible to power the loads have been coloured in black. It is indeed a parameter to be minimized as much as possible, since it is directly dependent from the boat capability to fulfill the assigned mission. As already stated, in a real life application, the missing energy would nonetheless be provided by a back up generator to ensure a safe travel.

To conclude, a similar plot is of great use in sizing the system components, from auxiliary generator to battery bank and PV array parallel connections. Key parameters could be utilized as performance related indicators and combined with cost functions to guide the design towards a techno-economic optimum.

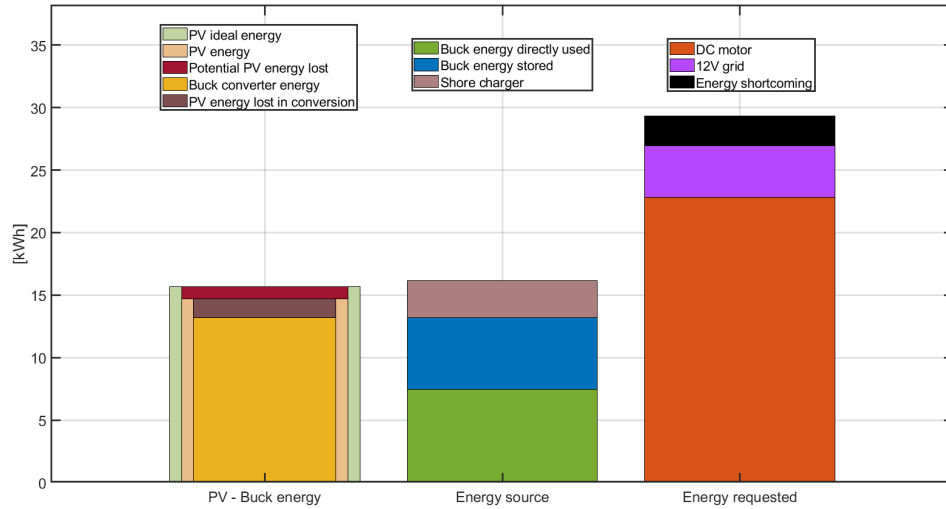


Figure 6.18. *Ad hoc day.* Energy balance

### 6.3.1 Example of energy balance

A month of taxi boat operation was simulated as reference example, providing a more relevant time span with respect to the single *ad hoc* day shown so far. Figures 6.20 and 6.19 contains, respectively, the boat performances under the same random load profile during 30 days in January or June. Certainly, the accuracy of input load profiles is of paramount importance to correctly assess the system behaviour. If this holds, then several design improvements can be adopted to improve performances. It is noticeable how the greater PV array production in June has a substantially positive impact on the capability to cope with load request. The same is not true in January, where a typical summer load profile would force the skipper to cancel many service calls. What catches the eye is the absence of wasted PV energy during January which means that the percentage of exploited PV power was the maximum possible. In June instead, the mismatch between load request and solar power availability forces the controller to reject potential power production. The difference in operating conditions between the two months is also detectable by calculating the average battery state of charge during operation, which amounts to 36[%] in January, in contrast to the way higher 63[%] in June. This parameter, combined with current draws magnitude and info on the amount of time the battery spends above or below certain SOC values, could be used to determine batteries expected lifetime.

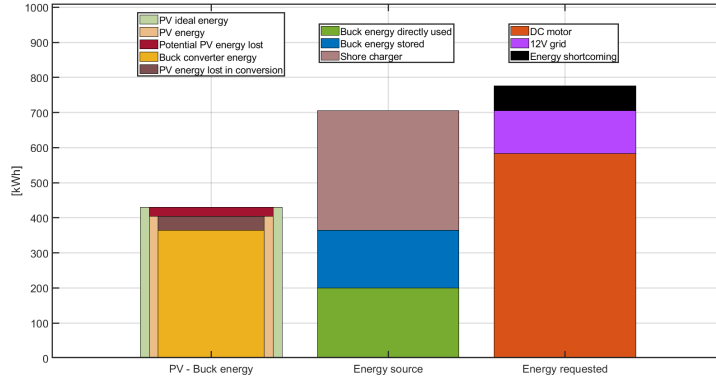


Figure 6.19. Energy balance in June

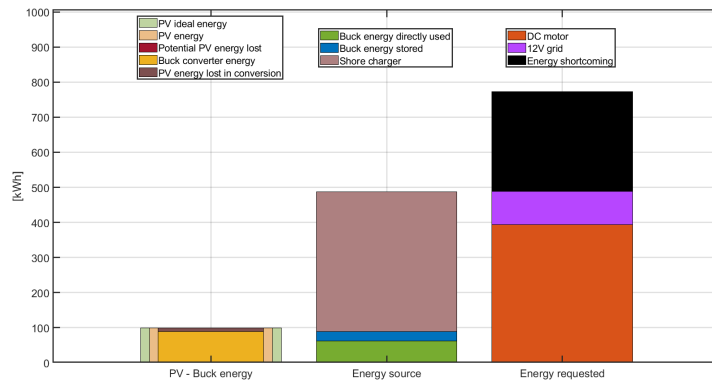


Figure 6.20. Energy balance in January

## Chapter 7

# Conclusion

A mathematical model was developed in Simulink® to mimic and evaluate the performance of a customisable propulsion system for an electric motorboat. In agreement with current market developments, photovoltaic panels are included as energy source in addition to a lithium battery bank, providing energy to a direct drive inboard motor and other auxiliary loads. Specifically, weather conditions for the boat's operating site are taken into account to accurately calculate the amount of photovoltaic energy that can be produced on board. The model description was accompanied by a case study that served the purpose to provide an example of model application. Although some results are shown, they are to be intended as mere representations of the model capability in a plausible operating condition. The aim was not to optimise the specific case study application, but to show how the mathematical model can take part in a more relevant optimisation procedure.

After a theoretical introduction on the components' working principles, where the whole propulsion chain is analysed from boat resistance to electrical input, every Simulink® subsystem was thoroughly described. Particular attention has been given to the control logic which determines the functioning of the whole system. Power electronics of voltage converters has been modelled employing averaged differential equations which are still able to capture the main system evolutions without requiring an excessive computational effort. Dynamic modelling is indeed what allows to reach a satisfying degree of fidelity, as it does not solely rely on energy balances but also considers the variation of mechanical and electrical quantities over time. As stated, the propulsion chain can be optimised by varying propeller, battery, PV array, and DC motor characteristics. Operating voltages can also be modified as long as care is given in maintaining a stable control of the voltage converter devices, whose parameters are to be tuned according to the system layout. The model is capable to simulate even months of operation in a relatively short time span, with an accuracy dependent on the chosen time step, the data sheets' exhaustiveness, and the consequent number of assumptions to compensate for missing information. Besides showing relevant dynamic plots, useful key results regarding energy management suggest further modifications to improve the initial system design and better suit the desired boat mission. For the purpose of understanding benefits and drawbacks while offering a clear view on the limits beyond which the model loses its relevance, a chapter was dedicated to the main model assumptions.

To conclude, it was described a tool that helps obtaining the best components' power sizing, which however pertain to just an energy optimisation procedure. Going a step further in the design phases requires space, weight and price considerations that, flanked by an efficient control logic and charge routine, would effectively lead to the best overall design. Consequently, once boat mission has been defined, the here developed model could be incorporated within an optimisation algorithm which, condensing information on hull geometry, boat resistance, energy and economics, would allow to reach a techno-economical optimum for the propulsion system design.





# Bibliography

- [1] Mohamad Issa, Adrian Ilinca, and Fahed Martini. «Ship Energy Efficiency and Maritime Sector Initiatives to Reduce Carbon Emissions». In: *Energies* 15.21 (2022), p. 7910.
- [2] European Environmental Agency. *European Maritime Transport Environmental Report 2021*. Sept. 1, 2021. URL: <https://www.eea.europa.eu/publications/maritime-transport/>.
- [3] Eurostat. *Maritime passenger statistics*. URL: [https://ec.europa.eu/eurostat/statistics-explained/index.php?title=Maritime\\_passenger\\_statistics#Messina\\_remained\\_the\\_largest\\_EU\\_passenger\\_port\\_in\\_2021](https://ec.europa.eu/eurostat/statistics-explained/index.php?title=Maritime_passenger_statistics#Messina_remained_the_largest_EU_passenger_port_in_2021) (visited on 11/03/2023).
- [4] European Environmental Agency. *EU maritime transport: first environmental impact report acknowledges good progress towards sustainability and confirms that more effort is needed to prepare for rising demand*. URL: <https://www.eea.europa.eu/highlights/eu-maritime-transport-first-environmental> (visited on 11/03/2023).
- [5] International Maritime Organisation. *Initial IMO GHG Strategy*. URL: <https://www.imo.org/en/MediaCentre/HotTopics/Pages/Reducing-greenhouse-gas-emissions-from-ships.aspx> (visited on 11/03/2023).
- [6] Andrea Farkas et al. «Is slow steaming a viable option to meet the novel energy efficiency requirements for containerships?» In: *Journal of Cleaner Production* 374 (2022), p. 133915.
- [7] Wartsila. *Complying with EEXI – how to speed up decarbonisation without slowing down vessels*. URL: <https://www.wartsila.com/insights/article/complying-with-eexi-how-to-speed-up-decarbonisation-without-slowing-down-vessels> (visited on 11/03/2023).
- [8] Elizabeth Lindstad and Torstein Ingebrigtsen Bo. «Potential power setups, fuels and hull designs capable of satisfying future EEDI requirements». In: *Transportation Research Part D: Transport and Environment* 63 (2018), pp. 276–290.
- [9] Mario Porru et al. «Electrification of Leisure Boats: a commercial State-of-the-Art». In: *2020 IEEE Vehicle Power and Propulsion Conference (VPPC)*. IEEE. 2020, pp. 1–6.
- [10] Cicero S Postiglione et al. «Propulsion system for an all electric passenger boat employing permanent magnet synchronous motors and modern power electronics». In: *2012 Electrical Systems for Aircraft, Railway and Ship Propulsion*. IEEE. 2012, pp. 1–6.
- [11] Giuseppe Schirripa Spagnolo et al. «Solar-electric boat». In: *Journal of Transportation Technologies* 2.2 (2012), pp. 144–149.
- [12] Al Mehedi and Mohammad Abu Abdullah. «Design and dynamic modeling of a solar electric boat power system». PhD thesis. Memorial University of Newfoundland, 2021.
- [13] Mohammad Abu Abdullah Al Mehedi and M Tariq Iqbal. «Optimal Sizing of a Hybrid Power System for Driving a Passenger Boat in Bangladesh». In: *2020 IEEE Electric Power and Energy Conference (EPEC)*. IEEE. 2020, pp. 1–6.

- [14] Waleed Obaid, Abdul Kadir Hamid, and Chaouki Ghenai. «Hybrid PEM fuel-cell-solar power system Design for Electric Boat with MPPT system and fuzzy energy management». In: *2019 International Conference on Communications, Signal Processing, and their Applications (ICCSPA)*. IEEE. 2019, pp. 1–7.
- [15] Wunna Swe. «Design Optimization and Energy Management of Photovoltaic powered Electric Boat». In: *International Journal of Scientific and Research Publications* (2019), pp. 2250–3153.
- [16] Eduard Marti Bigorra. «Design of a boat electric propulsion system based on solar energy». B.S. thesis. Universitat Politècnica de Catalunya, 2018.
- [17] Ru-Min Chao, Hung-Ku Lin, and Chih-Hsuan Wu. «Solar-powered boat design using standalone distributed PV system». In: *2018 IEEE International Conference on Applied System Invention (ICASI)*. IEEE. 2018, pp. 31–34.
- [18] G Schirripa Spagnolo, D Papalilo, and A Martocchia. «Eco friendly electric propulsion boat». In: *2011 10th International Conference on Environment and Electrical Engineering*. IEEE. 2011, pp. 1–4.
- [19] Ayu Aaron Alexander. «Modeling power distribution system of an electric ship for design and control». PhD thesis. 2015.
- [20] Ye-Rin Kim et al. «Comprehensive Design of DC Shipboard Power Systems for Pure Electric Propulsion Ship Based on Battery Energy Storage System». In: *Energies* 14.17 (2021), p. 5264.
- [21] Anders Breines. «All electric battery service vessel-Dynamic modeling of a battery fed IPMSM propulsion plant as a tool for energy estimates and functional description for an energy management system». MA thesis. UiT Norges arktiske universitet, 2017.
- [22] Tiago Freire, Duarte M Sousa, and Paulo J Costa Branco. «Aspects of modeling an electric boat propulsion system». In: *2010 IEEE Region 8 International Conference on Computational Technologies in Electrical and Electronics Engineering (SIBIRCON)*. IEEE. 2010, pp. 812–817.
- [23] Ameen Bassam et al. «Design, modelling and simulation of a hybrid fuel cell propulsion system for a domestic ferry». In: (2016).
- [24] Muhamad Zalani Daud et al. «An optimal electric machine control system design used in plug-in hybrid electric boat». In: *ARPN Journal of Engineering and Applied Sciences* 10.22 (2015), pp. 10703–10708.
- [25] A Narendra et al. «A comprehensive review of PV driven electrical motors». In: *Solar Energy* 195 (2020), pp. 278–303.
- [26] Wikipedia. *Photovoltaic effect*. URL: [https://en.wikipedia.org/wiki/Photovoltaic\\_effect](https://en.wikipedia.org/wiki/Photovoltaic_effect) (visited on 11/03/2023).
- [27] Arno Smets et al. *The physics and engineering of photovoltaic conversion, technologies and systems*. UIT Cambridge Ltd Cambridge, 2016.
- [28] Efstratios I Batzelis. «Simple PV performance equations theoretically well founded on the single-diode model». In: *IEEE Journal of Photovoltaics* 7.5 (2017), pp. 1400–1409.
- [29] Ali M Humada et al. «Solar cell parameters extraction based on single and double-diode models: A review». In: *Renewable and Sustainable Energy Reviews* 56 (2016), pp. 494–509.
- [30] Zachary P Cano et al. «Batteries and fuel cells for emerging electric vehicle markets». In: *Nature Energy* 3.4 (2018), pp. 279–289.

- [31] Lithion. *U-CHARGE XP SERIES*. URL: <https://www.lithionbattery.com/products/modules/u-charge-xp/> (visited on 11/03/2023).
- [32] MathWorks. *Generic battery model*. URL: <https://it.mathworks.com/help/sps/powersys/ref/battery.html> (visited on 11/03/2023).
- [33] J Klein Woud and Douwe Stapersma. *Design of propulsion and electric power generation systems*. IMarEST, 2002.
- [34] Torqueedo. *Spare propeller v22/p10k for Cruise 10.0/12.0*. URL: <https://www.torqueedo.com/en/products/accessories/propellers-and-fins/spare-propeller-v22-p10k-for-cruise-10.0-12.0/1961-00.html> (visited on 11/03/2023).
- [35] John Carlton. *Marine propellers and propulsion*. Butterworth-Heinemann, 2018.
- [36] Embitel. *Brushless DC Motor vs PMSM: Find Out How These Motors and Their Motor Control Solutions Work*. URL: <https://www.embitel.com/blog/embedded-blog/brushless-dc-motor-vs-pmsm-how-these-motors-and-motor-control-solutions-work> (visited on 11/03/2023).
- [37] Tutorialspoint. *Difference between BLDC Motor and PMSM Motor*. URL: <https://www.tutorialspoint.com/difference-between-bldc-motor-and-pmsm-motor> (visited on 11/03/2023).
- [38] Sang-Hoon Kim. *Electric motor control: DC, AC, and BLDC motors*. Elsevier, 2017.
- [39] Ali Bekir Yildiz. «Electrical equivalent circuit based modeling and analysis of direct current motors». In: *International Journal of Electrical Power & Energy Systems* 43.1 (2012), pp. 1043–1047.
- [40] Torqueedo. *Cruise 12.0 RS TorqLink*. URL: <https://www.torqueedo.com/en/products/outboards/cruise/cruise-12.0-r-torqlink/M-1280-00.html> (visited on 11/03/2023).
- [41] Nikolay Hinov. «Generalized models of basic DC-DC converters». In: *AIP Conference Proceedings*. Vol. 2048. 1. AIP Publishing LLC. 2018, p. 060021.
- [42] Omid Naghash Almasi et al. «Analysis, control and design of a non-inverting buck-boost converter: A bump-less two-level T–S fuzzy PI control». In: *ISA transactions* 67 (2017), pp. 515–527.
- [43] Hamed Mashinchi Mahery and Ebrahim Babaei. «Mathematical modeling of buck–boost dc–dc converter and investigation of converter elements on transient and steady state responses». In: *International Journal of Electrical Power & Energy Systems* 44.1 (2013), pp. 949–963.
- [44] Weixiang Shen, Thanh Tu Vo, and Ajay Kapoor. «Charging algorithms of lithium-ion batteries: An overview». In: *2012 7th IEEE conference on industrial electronics and applications (ICIEA)*. IEEE. 2012, pp. 1567–1572.
- [45] Edison Banguero et al. «A review on battery charging and discharging control strategies: Application to renewable energy systems». In: *Energies* 11.4 (2018), p. 1021.
- [46] Qian Lin et al. «Towards a smarter battery management system: A critical review on optimal charging methods of lithium ion batteries». In: *Energy* 183 (2019), pp. 220–234.
- [47] MathWorks. *Choose an ODE Solver*. URL: <https://it.mathworks.com/help/matlab/math/choose-an-ode-solver.html> (visited on 11/03/2023).
- [48] Thomas Huld, Richard Muller, and Attilio Gambardella. «A new solar radiation database for estimating PV performance in Europe and Africa». In: *Solar Energy* 86.6 (2012), pp. 1803–1815.

- [49] European Commission. *PHOTOVOLTAIC GEOGRAPHICAL INFORMATION SYSTEM*. URL: [https://re.jrc.ec.europa.eu/pvg\\_tools/it/#TMY](https://re.jrc.ec.europa.eu/pvg_tools/it/#TMY) (visited on 11/03/2023).
- [50] Xuan Hieu Nguyen and Minh Phuong Nguyen. «Mathematical modeling of photovoltaic cell/module/arrays with tags in Matlab/Simulink». In: *Environmental Systems Research* 4 (2015), pp. 1–13.
- [51] *Algebraic Loop Concepts*. URL: <https://it.mathworks.com/help/simulink/ug/algebraic-loops.html> (visited on 11/03/2023).
- [52] *Why you should never break a continuous algebraic loop with a Memory block*. URL: <https://blogs.mathworks.com/simulink/2015/07/18/why-you-should-never-break-an-algebraic-loop-with-with-a-memory-block/> (visited on 11/03/2023).
- [53] Nahla E Zakzouk et al. «Improved performance low-cost incremental conductance PV MPPT technique». In: *IET Renewable Power Generation* 10.4 (2016), pp. 561–574.
- [54] Ahsan Mehmood. *How to design buck converter for photovoltaic system? Buck converter design for PV module and array*. Youtube. URL: <https://www.youtube.com/watch?v=sswI6h0NdqI&t=519s> (visited on 11/03/2023).
- [55] Hanane Yatimi and Elhassan Aroudam. «Standalone Photovoltaic System with Maximum Power Point Tracking: Modeling and Simulation». In: *International Journal of System Dynamics Applications (IJSDA)* 7.3 (2018), pp. 94–111.
- [56] Wenlu Zhou et al. «Review on the battery model and SOC estimation method». In: *Processes* 9.9 (2021), p. 1685.
- [57] LH Saw et al. «Electro-thermal analysis of Lithium Iron Phosphate battery for electric vehicles». In: *Journal of Power Sources* 249 (2014), pp. 231–238.
- [58] Datong Song et al. «A generic battery model and its parameter identification». In: *Energy and Power Engineering* 10.1 (2018), pp. 10–27.
- [59] Brigitte Hauke. *Basic Calculation of a Buck Converter's Power Stage*. Application Report. Texas Instruments, 2015.
- [60] I Weiss. «Basic Calculation of an Inverting Buck-Boost Power Stage». In: *Texas Instrument* (2017).
- [61] Sarita Samal et al. «Simulation and Experimental Investigation of a Smart MPPT based Solar Charge Controller». In: *Energy Sources, Part A: Recovery, Utilization, and Environmental Effects* 44.3 (2022), pp. 7748–7763.
- [62] AG Giyantara, David Christover, and Yun Tonce Kusuma Priyanto. «Design and Implementation Buck-boost Converter using Arduino Mega 2560». In: *Proceedings of the 1st International Conference on Industrial Technology*. 2019.
- [63] Homer Energy. *How HOMER calculates the PV cell temperature*. URL: [https://www.homerenergy.com/products/pro/docs/3.11/how\\_homer\\_calculates\\_the\\_pv\\_cell\\_temperature.html](https://www.homerenergy.com/products/pro/docs/3.11/how_homer_calculates_the_pv_cell_temperature.html) (visited on 11/03/2023).

# Appendix: MATLAB<sup>®</sup> scripts

## Contents

- IMPORTANT MODEL SETTINGS
- GRAPHICAL SETTINGS
- BATTERY PARAMETERS
- MOTOR PARAMETERS
- BOAT RESISTANCE AND PROPELLER PARAMETERS
- MOTOR CONTROL PARAMETERS
- PV PARAMETERS
- MAIN BUCK CONVERTER
- 12V BUCK CONVERTER
- AUXILIARY LOADS
- BUCK-BOOST CONVERTER
- WEATHER AND LOAD, n\_days, End\_Time
- RUN
- WEATHER AND LOAD PLOTS
- RESISTANCE AND PROPULSIVE POWER PLOTS
- MOTOR - PROPELLER PLOTS
- MODEL PLOTS
- PLOTS DISTRIBUTION
- FUNCTIONS

```
clear
close all
clc
```

## IMPORTANT MODEL SETTINGS

```
REMEMBER to add a spreadsheet file to the folder. Its name in the current script is "Year_data_hourly.xlsx"
%Its "Sheet1" is composed of two columns containing the Temperature[°C] and Irradiance [W/m^2] values, a row for each hour of the year

Ts = 0.05; %Time step. For better accuracy = 0.01

decimation = 60/Ts; %Inside display and scope blocks. It saves a value per minute.
% The higher the decimation the lower the number of data to be stored
SOC_initial = 100; %Battery initial state of charge

pause_weight = 1;
first_day = '03-Sep';
last_day = '03-Sep';

plot_weather = 0;
plot_propeller = 0;
plot_model = 0;
plot_vel_drag_pow = 0;

model_name = 'Musarra_Tubi.slx'; %The name of the Simulink file
save_name = ['RUN_',first_day,'_to_',last_day,'_pw_',num2str(pause_weight)];
```

## GRAPHICAL SETTINGS

```
%setDefaults -> function to set preferred graphics
```

```
%colors vectors
blue=[0 0.44706 0.74118];
orange=[0.85098 0.32549 0.098039];
ocra=[0.92941 0.69412 0.12549];
beige = [0.92157 0.74118 0.53333];
grey = [0.50196 0.50196 0.50196];
l_green = [0.74902 0.83137 0.63137];
green = [ 0.46667 0.67451 0.18824];
purple = [0.71765 0.27451 1];
red = [0.63529 0.078431 0.18431];
brown = [0.4902 0.3098 0.3098];
l_brown = [0.67843 0.50196 0.50196];
l_blue = [0.71765 0.86667 0.92941];
```

## BATTERY PARAMETERS

```
SOC_R0_V0 = [0,0.07094,23.89222; 0.01,0.06065,24.00332; 0.02,0.05035,24.11441; 0.03,0.04017,24.2255; 0.04,0.03221,24.33659;
0.05,0.02666,24.54539; 0.06,0.02392,24.79035; 0.07,0.02096,24.93639; 0.08,0.01846,25.02517; 0.09,0.01598,25.05667;
0.1,0.01413,25.08816; 0.11,0.01268,25.11424; 0.12,0.01239,25.22533; 0.13,0.01201,25.303; 0.14,0.01164,25.36637;
0.15,0.01153,25.44271; 0.16,0.01137,25.49918; 0.17,0.0112,25.54887; 0.18,0.0113,25.60892; 0.19,0.01137,25.66532;
0.2,0.01148,25.72282; 0.21,0.01163,25.78318; 0.22,0.01156,25.81534; 0.23,0.01147,25.83855; 0.24,0.01134,25.85612;
0.25,0.01136,25.88221; 0.26,0.01139,25.90831; 0.27,0.01141,25.93318; 0.28,0.01141,25.95505; 0.29,0.0114,25.97565;
0.3,0.01139,25.99591; 0.31,0.01137,26.01321; 0.32,0.01138,26.031; 0.33,0.01139,26.0449; 0.34,0.0114,26.05703;
0.35,0.01141,26.06916; 0.36,0.01144,26.08527; 0.37,0.01148,26.10159; 0.38,0.01152,26.11792; 0.39,0.01155,26.13382;
0.4,0.01158,26.14952; 0.41,0.01155,26.15691; 0.42,0.01151,26.16308; 0.43,0.01146,26.16907; 0.44,0.01142,26.17506;
0.45,0.01138,26.18105; 0.46,0.01133,26.18705; 0.47,0.0113,26.19368; 0.48,0.01126,26.19853; 0.49,0.01122,26.2032;
0.5,0.01119,26.20787; 0.51,0.01115,26.21254; 0.52,0.01111,26.21743; 0.53,0.01108,26.22242; 0.54,0.01104,26.22742;
0.55,0.01105,26.23451; 0.56,0.01108,26.24345; 0.57,0.01111,26.2524; 0.58,0.01114,26.26134; 0.59,0.01117,26.27028;
0.6,0.0112,26.27889; 0.61,0.01122,26.28657; 0.62,0.01122,26.29321; 0.63,0.01121,26.29918; 0.64,0.01121,26.30516;
0.65,0.0112,26.31114; 0.66,0.01119,26.31711; 0.67,0.01118,26.32309; 0.68,0.01117,26.32907; 0.69,0.01121,26.34002;
0.7,0.01125,26.35254; 0.71,0.0113,26.36518; 0.72,0.01135,26.37783; 0.73,0.0114,26.39048; 0.74,0.01145,26.40313;
0.75,0.01149,26.41577; 0.76,0.01154,26.42842; 0.77,0.01159,26.44114; 0.78,0.01163,26.45099; 0.79,0.01164,26.45769;
0.8,0.01166,26.46439; 0.81,0.01168,26.47108; 0.82,0.0117,26.47778; 0.83,0.01172,26.48448; 0.84,0.01175,26.49239;
0.85,0.01179,26.50087; 0.86,0.01183,26.50934; 0.87,0.01185,26.51632; 0.88,0.01184,26.52035; 0.89,0.0119,26.52826;
0.9,0.01195,26.53626; 0.91,0.01199,26.54221; 0.92,0.01203,26.54803; 0.93,0.01205,26.55381; 0.94,0.01196,26.55228;
0.95,0.01176,26.54413; 0.96,0.01159,26.54258; 0.97,0.01134,26.54197; 0.98,0.01073,26.55759; 0.99,0.01016,26.66743;
1,0.00914,27.22747]
```

```
SOC_v = SOC_R0_V0(:,1); %State of charge vector [0,1]
R_int_v = SOC_R0_V0(:,2); %Resistance vector as a function of SOC (from Simulink)
V0_v = SOC_R0_V0(:,3); %Voltage vector as a function of SOC (from Simulink)

% Datasheet parameters
N_ser_batt = 2; %Series
N_par_batt = 4; %Parallel

E_single_battery = 1.84; %[kWh]
E_total_battery = E_single_battery*N_par_batt*N_ser_batt; %[kWh]
V_full = 27.3688*N_ser_batt; %[V]
V_nom = 25.6*N_ser_batt;
V_exp = 26.4259*N_ser_batt;
V_cut_off = 20*N_ser_batt;
V_charge_max = 29.2*N_ser_batt;

Lambda = 1.038999999968; % From Matlab generic battery model
Q_rated = 71.84*N_par_batt; %[Ah]
Q_max = 1.05*Q_rated;
Q_exp = 0.0357*Q_rated;
Q_nom = 0.83*Q_rated;
Q_MAX = Q_max*Lambda;
Q = Q_MAX;
Q_v = SOC_v*Q_rated;

I_nom = 50; %[A]
I_max_charge = 30; %To preserve battery life
I_charge = -Q_rated/10; %10% of rated capacity

R_int_single = mean(R_int_v); %[Ohm]
R_int = R_int_single*N_ser_batt/N_par_batt;

T_response = 0.001; %[s] to obtain a faster simulation

% Extraction of empirical parameters
A = (V_full - V_exp)*1.005; %[V]
V0 = V_full + R_int*I_nom - A;
B_batt = 3/Q_exp; %[Ah^-1]
K = (-V_exp + V0 - R_int*I_nom + A.*exp(-3)) * (Q-Q_exp)/(Q*(Q_exp+I_nom)); %[Ohm] or [V/Ah]
it_initial = (1-SOC_initial/100)*Q/Lambda*3600; %[Ah]

%Derived
Ia_rated = P_rated/Va_rated; %[A]
Te_rated = P_rated*eta_motor/w_rated; %[Nm]
Ra = Va_rated/Ia_rated*(1-eta_motor); %[Ohm]
La = 1.7e-3; % Armature inductance [H]
J = 0.025; % System inertia[kg*m^2]
B = 0.01; % Viscous friction coefficient [Nm/(rad/s)]

Kt = Te_rated/Ia_rated; %[Nm/A]
Ke = Kt; %[V/(rad/s)]
Ks = 1/Kt; %[A/Nm]
```

## MOTOR PARAMETERS

```
%Datasheet
P_rated = 12000; %Electrical power [W]
P_propulsive = 6720; %Propulsive power [W]
eta_total = 0.56; %From electrical input to propulsive power
Va_rated = 48; %[V]
eta_motor = 0.96; %Assumed from website
w_rated = 1400*pi/30; %[rad/s]

%Derived
Ia_rated = P_rated/Va_rated; %[A]
Te_rated = P_rated*eta_motor/w_rated; %[Nm]
Ra = Va_rated/Ia_rated*(1-eta_motor); %[Ohm]
La = 1.7e-3; % Armature inductance [H]
J = 0.025; % System inertia[kg*m^2]
B = 0.01; % Viscous friction coefficient [Nm/(rad/s)]

Kt = Te_rated/Ia_rated; %[Nm/A]
Ke = Kt; %[V/(rad/s)]
Ks = 1/Kt; %[A/Nm]
```

## BOAT RESISTANCE AND PROPELLER PARAMETERS

```
vel_drag_pow = [0,0,0;0.5,30,15;1,50,50;1.5,85,127.5;2,140,280;2.5,220,550; 3,320,960;3.5,470,1645;4,620,2480;4.5,750,3375;5,850,4250]

L_boat = 9; %[m] overall boat length

c1_v = vel_drag_pow(:,2)./(vel_drag_pow(:,1).^2); %Coefficient

%Data propeller
D = 0.32; %[m] Diameter
```

```

Pitch = 0.330; %[m]
Z = 5; %Number of blades (2 - 7)
w_max_prop = 1400; %[rpm]
np_max = w_max_prop/60; %[rev/s]
PD = Pitch/D; %Pitch/diameter ratio (0.6 - 1.4)
kp = 1; %Number of propellers

%Assumed
t = 0.15; % [-] Thrust deduction factor
w = 0.2; %[-] Wake factor
AeA0 = 0.75; %Blade area ratio (0.30 - 1.05)
eta_r = 0.99; %relative rotative efficiency
eta_hull = (1-t)/(1-w); %Hull efficiency
v_s_v = vel_drag_pow(:,1); % m/s Boat velocity vector
v_a_v = v_s_v*(1-w); % m/s Velocity of advance vector

rho = 1025; %[kg/m^3] water density
mu = 1e-3; %[Pa*s] water dynamic viscosity
Re_v = rho.*(v_s_v).*L_boat/mu; %[-] Max Reynolds number vector (2e6 - 2e9)

% N.B. There is basically no difference apported by the Re number at these speeds, so it could not be taken into account

J_min_v = v_a_v./(np_max*D); %Advance ratio based on max propeller speed

R_v = vel_drag_pow(:,2); % [N] Boat resistance vector = f(v_s)

T_v = R_v./(kp*(1-t)); % [N] Required thrust vector

c8_v = c1_v./(kp*(1-t)*(1-w)^2); %Coefficient
c7_v = c8_v./(rho*D^2); %Coefficient

J_v = (0:0.001:1.16)'; %Advance ratio vector

%Calculations
%Obtaining open water diagram curves thanks to propcalc
[Kt_v, Kq_v, eta0_v] = propcalc(Z, AeA0, PD, J_v, mean(Re_v(2:end))); %Obtain

Kt_ship_mat = zeros(length(J_v),length(v_s_v));
np_int_v = zeros(length(v_s_v),1);

J_int_v = np_int_v;
Kt_int_v = np_int_v;
Kq_int_v = np_int_v;
eta0_int_v = np_int_v;
T_prop_v = np_int_v;
Q_prop_v = np_int_v;
P_prop_v = np_int_v;
np_rpm_v = np_int_v;

for ii=2:length(v_s_v)

Kt_ship_mat(:,ii) = c7_v(ii).*J_v.^2;

int=find((Kt_v-Kt_ship_mat(:,ii))<=0 ,1,'first');

J_int_v(ii) = J_v(int);
np_int_v(ii)=v_a_v(ii)/J_int_v(ii)/D;

Kt_int_v(ii) = Kt_v(int);
Kq_int_v(ii) = Kq_v(int);
eta0_int_v(ii) = eta0_v(int);
T_prop_v(ii) = (Kt_v(int)*rho*np_int_v(ii)^2*D^4); %Propeller Thrust [N]
Q_prop_v(ii) = (Kq_v(int)*rho*(np_int_v(ii))^2*D^5)/eta_r; %Propeller Torque [Nm]
P_prop_v(ii) = 2*pi*Q_prop_v(ii)*np_int_v(ii); %Propeller load [W]
np_rpm_v(ii) = np_int_v(ii)*60; %Propeller speed [W]

end

%To be fed to Simulink lookup table
v_s_and_Q_prop = [v_s_v Q_prop_v];
v_s_and_np_rpm = [v_s_v np_rpm_v];
v_s_and_P_prop = [v_s_v P_prop_v];
v_s_and_eta0 = [v_s_v eta0_int_v];
v_s_and_T_prop = [v_s_v T_prop_v];

```

## MOTOR CONTROL PARAMETERS

```

w_ref_3 = 75.088; %rad/s at 3 m/s (717.039 rpm)
w_ref_2 = 49.867; %rad/s at 2 m/s (476.1905 rpm)

Q_ref_3 = 19.855; %Torque load at 3 m/s
Q_ref_2 = 8.6966; %Torque load at 2 m/s

% s = speed c = current

fs_chopper = 1e3; % 1 [kHz]
w_c = fs_chopper/20; %Frequency inner control loop
w_s = w_c/5; %Frequency outer control loop

Kpc = La*w_c; %Proportional gain coefficient of inner loop
Kic = Ra*w_c; %Integral gain coefficient of inner loop
Kac = 1/Kpc; %Anti wind-up coefficient

Kps = J*5; %Proportional gain coefficient of outer loop
Kis = J*w_s; %Integral gain coefficient of outer loop
Kas = 1/Kps; %Anti wind-up coefficient

```

## PV PARAMETERS

```

Ns_module = 3; %Number of series connected PV modules on a single column
Np_strings = 3; %Number of parallel connected PV modules on a single row

Irr_min = 80; %W/m^2 needed to activate the panels
% 1000 W/m^2 Reference Irradiance
T_0 = 298.15; %K -> 25degC

%Fixed
Kb = 1.3805e-23; %J/K Boltzmann constant
q = 1.6022e-19; %C electron charge
Eg0 = 1.1; %[eV] Band gap energy for silicon
dEgdT = -0.0002678; %Temperature coefficient of band gap energy

% Datasheet
Vmp_0 = 30.88; % [V] Module maximum power point voltage at 25degC and 1000 W/m^2
Imp_0 = 8.29; % [A] Module maximum power point current at 25degC and 1000 W/m^2
Voc_0 = 38; % [V] Module open circuit voltage at 25degC and 1000 W/m^2
Isc_0 = 8.85; % [A] Module short circuit current at 25degC and 1000 W/m^2
beta_Voc = -0.36/100; %[K^-1] Temperature coefficient of open circuit voltage
alpha_Isc = 0.05/100; %[K^-1] Current coefficient of open circuit voltage
Ns = 60; %Number of cells
n_d = 1.26; %Ideality factor diode

% Parameter derivation according to reference paper
delta_0 = (1-beta_Voc*T_0)/(50.1-alpha_Isc*T_0);
w_0 = lambertw(exp(1/delta_0+1));
a_0 = delta_0*Voc_0;
Rs_0 = (a_0*(w_0-1)-Vmp_0)/Imp_0;
Rsh_0 = a_0*(w_0-1)/(Isc_0*(1-1/w_0)-Imp_0);
Iph_0 = (1+Rs_0/Rsh_0)*Isc_0;
Is_0 = Iph_0*exp(-1/delta_0);
alpha_Imp = alpha_Isc + (beta_Voc - 1/T_0)/(w_0 - 1);
beta_Vmp = Voc_0/Vmp_0 * ( beta_Voc/(1+delta_0) + (delta_0*(w_0-1)-1/(1+delta_0))/T_0);
epsilon_0 = delta_0/(1+delta_0)*Voc_0/Vmp_0;
epsilon_1 = delta_0*(w_0-1)*Voc_0/Vmp_0 - 1;

```

## MAIN BUCK CONVERTER

```

fs = 25000; % Switching frequency [Hz]
eta_buck = 0.9; % Efficiency

% L and C derivation:
P_mps = Vmp_0*Imp_0*9;
V_mps = Vmp_0*3;
I_mps = Imp_0*3;

P_mpw = 0.05*P_mps;
V_mpw = 0.9*V_mps;
I_mpw = P_mpw/V_mpw;

R_mps = V_mps/I_mps;
R_mpw = V_mpw/I_mpw;

Ro = R_mps/2.5;

D_mps = sqrt(Ro/R_mps);
D_mpw = sqrt(Ro/R_mpw);

V_os = D_mps*V_mps;
I_os = V_os/Ro;

V_ow = D_mpw*V_mpw;
I_ow = V_ow/Ro;

d_V_is = 0.002*V_mps;
d_V_os = 0.002*V_os;
d_I_is = 0.2*I_mps;
d_I_os = 0.4*I_os;

d_V_iw = 0.002*V_mpw;
d_V_ow = 0.002*V_ow;
d_I_iw = 0.2*I_mpw;
d_I_ow = 0.4*I_ow;

L_buck = round((2*V_mps*D_mps*(1-D_mpw))/(d_I_ow*fs),3,"significant");
Ci_buck = round(d_I_is/(d_I_iw*fs),3,"significant");
Co_buck = round(d_I_os/(32*d_V_ow*fs),3,"significant");

```

## 12V BUCK CONVERTER

```

fs_buck_small = fs; %Switching frequency
eta_buck_small = 0.87; %Efficiency
I_max_small = 40; %[A] %40 -> According to datasheet of selected converter

%Input
V_in_buck_small = 53; % [V] Usual
V_out_ref_buck_small = 12; % [V] Desired

Dref = V_out_ref_buck_small/V_in_buck_small;

V_ripple_buck_small = 0.002;
I_ripple_buck_small = 0.2;
%-----
Delta_i_L_small = I_ripple_buck_small*I_max_small;

```



```
D_buck_small = V_out_ref_buck_small/(56*eta_buck_small);
L_buck_small = round(V_out_ref_buck_small*(V_in_buck_small-V_out_ref_buck_small)/(Delta_i_L_small*fs_buck_small*52),1,"significant");
C_buck_small = round(Delta_i_L_small/(8*fs_buck_small*V_ripple_buck_small*V_out_ref_buck_small),1,"significant");

% Buck converter controller parameters
Ki_buck_small = 0.25; %After tuning
Kp_buck_small = 0.15; %After tuning
```

## AUXILIARY LOADS

```
%Current intended as the sum of all the current request.
% It may also be a time series object if data on load usage are provided

I_load_12V = 20; %[A]
```

## BUCK-BOOST CONVERTER

```
eta_bb = 0.9; %Efficiency

Vin_bb = 53; % Usual value [V]
fsw = fs; % Switching frequency [Hz]

Vout_ref_bb = 56; % Desired [V]
D_bb = Vout_ref_bb/(Vout_ref_bb+Vin_bb);

Io_bb = 160; %[A] max
i_L_bb = Io_bb/(1-D_bb);

Delta_i_L_bb = 0.2*i_L_bb;
Delta_v_bb = 0.002*Vout_ref_bb;

L_bb = round(Vin_bb*D_bb/(Delta_i_L_bb*fsw),1,"significant");
C_bb = round(Io_bb*D_bb/(Delta_v_bb*fsw),1,"significant");
```

## WEATHER AND LOAD, n\_days, End\_Time

```
% Obtain data on ambient conditions for the selected time interval
% and create a random load request through load_and_weather function
[t_load,load,time_weather,irr_v,temp_v,n_days] = load_and_weather(first_day,last_day,pause_weight);

End_Time = 24*3600*n_days; %Fed to the simulink model call function

%Useful plot calculations
t_max = max(time_weather*3600);
t_plot = strcat(int2str(( repmat((0:23),1,n_days))'),{:':00'}));
t_plot(1,n_days*24+1)={':00:00'};
```

## RUN

```
h = waitbar(0,'Please wait...'); %To visualize simulation time advance
myoptions = simset('SrcWorkspace','current','DstWorkspace','current','Solver','ode23t'); %Selection of solver

tic
out=sim(model_name,End_Time,myoptions); %Simulation run
time_elapsed = toc; %[s]

close(h)
save(save_name) %The current workspace values are stored to a .mat file
```

## WEATHER AND LOAD PLOTS

```
if plot_weather == 1
figure(45)
plot(t_load,load)
xlabel('Hour')
ylabel(' [m/s]')
title('Velocity load')
ylim([0 5.5])
xlim([0 t_max/3600])
xticks((0:1:t_max/3600));
xticklabels(t_plot)

figure(46)
yyaxis left
plot(time_weather,temp_v,'Color',ocra)
ylabel('Temperature [degC]')
set(gca,'ycolor',ocra)

yyaxis right
plot(time_weather,irr_v,'Color',orange)
ylabel('Irradiance [W/m^2]')
ylim([0 1100])
set(gca,'ycolor',orange)
legend('Temperature','Irradiance')
xlabel('Hour')
xlim([0 t_max/3600])
xticks((0:1:t_max/3600));
xticklabels(t_plot)
end
```

## RESISTANCE AND PROPULSIVE POWER PLOTS

```
if plot_vel_drag_pow == 1

figure(51)

yyaxis left
plot(vel_drag_pow(:,1),vel_drag_pow(:,2),'Color',blue,'LineStyle','-')
hold on
xlabel('Boat velocity [m/s]')
ylabel(' [N]')
set(gca,'ycolor',blue)

yyaxis right
plot(vel_drag_pow(:,1),vel_drag_pow(:,3),'Color',red,'LineStyle','-')
ylabel(' [W]')
set(gca,'ycolor',red)

legend('Resistance','Propulsive power')
end
```

## MOTOR - PROPELLER PLOTS

```
if plot_propeller == 1

figure(24)
subplot(2,2,1)
plot(v_s_and_Q_prop(:,1),v_s_and_Q_prop(:,2))
xlabel('Boat velocity [m/s]')
ylabel(' [Nm]')
title('Propeller torque')

figure(24)
subplot(2,2,2)
plot(v_s_and_np_rpm(:,1),v_s_and_np_rpm(:,2))
xlabel('Boat velocity [m/s]')
ylabel(' [rpm]')
title('Propeller angular speed')

figure(24)
subplot(2,2,3)
plot(v_s_and_P_prop(:,1),v_s_and_P_prop(:,2)/1000)
xlabel('Boat velocity [m/s]')
ylabel(' [kW]')
title('Propeller load')

figure(24)
subplot(2,2,4)
plot(v_s_and_eta0(:,1),v_s_and_eta0(:,2))
xlabel('Boat velocity [m/s]')
ylabel(' [-]')
title('Propeller open water efficiency')

v_s_plot = 5; %Design speed

ii = round(v_s_plot*2)+1;

J_int_str = num2str(J_int_v(ii),3);
np_rpm_str = num2str(np_rpm_v(ii),4);
Q_prop_str = num2str(Q_prop_v(ii),3);
P_prop_str = num2str(P_prop_v(ii)/1000,3);
v_s_str = num2str(v_s_plot,2);
title_1 = ['Open water propeller diagram',' ',' v_{ship} = ',v_s_str,' [m/s]'];
subtitle=['J_{match} = ',J_int_str,' ', 'n_{prop} = ',np_rpm_str,' [rpm]', ', ', 'Q_{prop} = ',Q_prop_str,' [Nm]', ', ', 'P_{prop} = ',P_prop_str,' [kW]'];

figure(28)
H(4)=plot(J_v,Kt_ship_mat(:,ii),'k');
hold on
H(1)=plot(J_v,Kt_v,'Color',blue);
H(2)=plot(J_v,10*Kq_v,'Color',orange);
H(3)=plot(J_v,eta0_v,'Color',ocra);
H(5)=plot([J_min_v(ii) J_min_v(ii)], [0 0.9],'Color',grey,'LineStyle','-','LineWidth',1);
H(6)=plot([J_int_v(ii) J_int_v(ii)], [0 0.9],'Color',green,'LineStyle','-','LineWidth',1);
plot(J_int_v(ii),Kt_int_v(ii),'Color',green,'MarkerSize',30,'Marker','s')

ylim([0 0.8])
title(title_1,subtitle)
xlabel('Advance ratio J')
legend(H,'K_t','10K_q','\eta_0','Kt_{ship}','J_{min}','J_{match}','location','westoutside')

v_s_plot = 2; %Any other value in between [0:0.5:5] can be chosen

ii = round(v_s_plot*2);

J_int_str = num2str(J_int_v(ii),3);
np_rpm_str = num2str(np_rpm_v(ii),3);
Q_prop_str = num2str(Q_prop_v(ii),3);
P_prop_str = num2str(P_prop_v(ii)/1000,3);
v_s_str = num2str(v_s_plot,2);
title_1 = ['Open water propeller diagram',' ',' v_{ship} = ',v_s_str,' [m/s]'];
subtitle=['J_{match} = ',J_int_str,' ', 'n_{prop} = ',np_rpm_str,' [rpm]', ', ', 'Q_{prop} = ',Q_prop_str,' [Nm]', ', ', 'P_{prop} = ',P_prop_str,' [kW]'];

figure(29)
H(4)=plot(J_v,Kt_ship_mat(:,ii),'k');
hold on
H(1)=plot(J_v,Kt_v,'Color',blue);
H(2)=plot(J_v,10*Kq_v,'Color',orange);
H(3)=plot(J_v,eta0_v,'Color',ocra);
H(5)=plot([J_min_v(ii) J_min_v(ii)], [0 0.9],'Color',grey,'LineStyle','-','LineWidth',1);
```

```
H(6)=plot([J_int_v(ii) J_int_v(ii)],[0 0.9],'Color',green,'LineStyle','-','LineWidth',1);
plot(J_int_v(ii),Kt_int_v(ii),'Color',green,'MarkerSize',30,'Marker','.')
ylim([0 0.8])
title(title_1,subtitle)
xlabel('Advance ratio J')
legend(H,'K_t','10K_q','\eta_0','K_t_{ship}','J_{min}','J_{match}','location','westoutside')

end
```

## MODEL PLOTS

```
if plot_model == 1

% Comparison between ideal and actual pv power
figure(1)

yyaxis left
plot(out.P_PV_ideal.Time,out.P_PV_ideal.Data,'LineWidth',6,'Color',blue)
hold on
plot(out.P_PV.Time,out.P_PV.Data,'Color',ocra,'LineStyle','-')
ylabel('W')
set(gca,'ycolor','k')

yyaxis right
fill_curves(out.SOC.Time,zeros(length(out.SOC.Time),1),out.SOC.Data,blue,0.1);
ylabel('%')
ylim([0 100])
set(gca,'ycolor','l_blue')

xlabel('Time [Hour]')
title('PV Power')
legend('MPP','Actual','SOC battery')
xlim([0 t_max])
xticks((0:3600:t_max));
xticklabels(t_plot)

% Overview of main power output and input involved (PV,battery,loads)
figure(2)

yyaxis left
plot(out.P_loads.Time,medfilt1(out.P_loads.Data,6),'Color',orange,'LineStyle','-','LineWidth',6)
hold on
plot(out.P_charge.Time,-medfilt1(out.P_charge.Data,6),'Color','l_brown','LineStyle','-','LineWidth',3)
plot(out.P_buck.Time,medfilt1(out.P_buck.Data,6),'Color',blue,'LineStyle','-','LineWidth',3)

plot(out.P_battery.Time,medfilt1(out.P_battery.Data,6),'Color',green,'LineStyle','-','LineWidth',3)

xlabel('Time [Hour]')
ylabel('W')
ylim([-1700 14000])
xlim([0 t_max])
xticks((0:3600:t_max));
xticklabels(t_plot)
set(gca,'ycolor','k')
ylim([-1700 9000])

yyaxis right
fill_curves(out.SOC.Time,zeros(length(out.SOC.Time),1),out.SOC.Data,blue,0.1);
ylabel('%')
ylim([0 100])
set(gca,'ycolor','l_blue')

title('Power distribution')
legend('Motor + auxiliaries','Shore charger','Buck converter','Battery','SOC battery')

% Effective and requested speed
figure(3)

yyaxis right
fill_curves(out.SOC.Time,zeros(length(out.SOC.Time),1),out.SOC.Data,blue,0.1);
hold on
plot([0 86400*n_days],[5 5],'LineStyle','-','Color',[grey,0.7],'LineWidth',1)
plot([0 86400*n_days],[10 10],'LineStyle','-','Color',[grey,0.7],'LineWidth',1)
plot([0 86400*n_days],[15 15],'LineStyle','-','Color',[grey,0.7],'LineWidth',1)
plot([0 86400*n_days],[20 20],'LineStyle','-','Color',[grey,0.7],'LineWidth',1)
ylabel('%')
ylim([0 100])
set(gca,'ycolor','l_blue')

yyaxis left
plot(out.Vel_requested.Time,out.Vel_requested.Data,'Color',blue,'LineStyle','-','LineWidth',6)
hold on
plot(out.Vel_effective.Time,out.Vel_effective.Data,'Color',ocra,'LineStyle','-')
ylim([0 5.5])
xlabel('Time [Hour]')
ylabel('m/s')
set(gca,'ycolor','k')

xlim([0 t_max])
xticks((0:3600:t_max));
xticklabels(t_plot)
title('Boat velocity')
legend('Requested','Actual','SOC battery','Low SOC [%]')

% Motor and load speed
figure(4)

yyaxis left
```

```

plot(out.w_load.Time,medfilt1(out.w_load.Data,6)*30/pi,'Color',blue,'LineStyle','-', 'LineWidth',6)
hold on
plot(out.w_motor.Time,medfilt1(out.w_motor.Data,6)*30/pi,'Color',ocra,'LineStyle','-', 'LineWidth',6)
xlabel('Time [Hour]')
ylabel('rpm')
set(gca,'ycolor','k')

yyaxis right
fill_curves(out.SOC.Time,zeros(length(out.SOC.Time),1),out.SOC.Data,blue,0.1);
ylabel('X')
ylim([0 100])
set(gca,'ycolor','l_blue')
xlim([0 t_max])
xticks((0:3600:t_max));
xticklabels(t_plot)
title('Load and motor rotational speed')
legend('Load','Motor','SOC battery')

% Motor and load torque
figure(5)

yyaxis left
plot(out.Q_load.Time,medfilt1(out.Q_load.Data,6),'Color',blue,'LineStyle','-', 'LineWidth',6)
hold on
plot(out.Q_motor.Time,medfilt1(out.Q_motor.Data,6),'Color',ocra,'LineStyle','-', 'LineWidth',6)
xlabel('Time [Hour]')
ylabel('Nm')
set(gca,'ycolor','k')

yyaxis right
fill_curves(out.SOC.Time,zeros(length(out.SOC.Time),1),out.SOC.Data,blue,0.1);
ylabel('X')
ylim([0 100])
set(gca,'ycolor','l_blue')
xlim([0 t_max])
xticks((0:3600:t_max));
xticklabels(t_plot)

title('Load and motor torque')
legend('Load','Motor','SOC battery')

% Relevant voltages
figure(6)

yyaxis left
plot(out.V_battery.Time,medfilt1(out.V_battery.Data,6),'Color',green,'LineStyle','-', 'LineWidth',6)
hold on
plot(out.V_oc_battery.Time,medfilt1(out.V_oc_battery.Data,6),'Color',orange,'LineStyle','-', 'LineWidth',6)
plot(out.V_12V.Time,medfilt1(out.V_12V.Data,6),'Color',purple,'LineStyle','-', 'LineWidth',6)
plot(out.V_motor_drive.Time,medfilt1(out.V_motor_drive.Data,6),'Color',red,'LineStyle','-', 'LineWidth',6)
plot(out.V_PV.Time,medfilt1(out.V_PV.Data,6),'Color',ocra,'LineStyle','-', 'Marker','none')
set(gca,'ycolor','k')
ylabel('V')

yyaxis right
fill_curves(out.SOC.Time,zeros(length(out.SOC.Time),1),out.SOC.Data,blue,0.1);
ylabel('X')
ylim([0 100])
set(gca,'ycolor','l_blue')
xlim([0 t_max])
xticks((0:3600:t_max));
xticklabels(t_plot)
xlabel('Time [Hour]')
title('Relevant Voltages')
legend('Battery voltage','Open circuit battery voltage','12V loads voltage','Motor drive voltage','PV array voltage','SOC battery')

% Relevant currents
figure(7)

yyaxis left
plot(out.I_motor.Time,medfilt1(out.I_motor.Data,6),'Color',[orange,0.8],'LineStyle','-', 'LineWidth',5)
hold on
plot(out.I_in_12V.Time,medfilt1(out.I_in_12V.Data,6),'Color',purple,'LineStyle','-', 'LineWidth',5)
plot(out.I_PV.Time,medfilt1(out.I_PV.Data,6),'Color',ocra,'LineStyle','-', 'LineWidth',5)
plot(out.I_out_buck.Time,medfilt1(out.I_out_buck.Data,6),'Color',blue,'LineStyle','-', 'LineWidth',2,'Marker','none')
plot(out.I_battery.Time,medfilt1(out.I_battery.Data,6),'Color',green,'LineStyle','-', 'Marker','none', 'LineWidth',2)
plot([0 max(out.I_battery.Time)],[-30 -30],'Color',red,'LineStyle','-', 'LineWidth',1,'Marker','none')
set(gca,'ycolor','k')
ylabel('A')
ylim([-35 160])

yyaxis right
fill_curves(out.SOC.Time,zeros(length(out.SOC.Time),1),out.SOC.Data,blue,0.1);
ylabel('X')
ylim([0 100])
set(gca,'ycolor','l_blue')

xlabel('Time [Hour]')
xlim([0 t_max])
xticks((0:3600:t_max));
xticklabels(t_plot)
title('Relevant Currents')
legend('Motor system input current','12V loads input current','PV array current','Buck converter output current','Battery current','SOC battery')

% Motor power distribution
figure(8)
yyaxis left
plot(out.P_el_motor.Time,medfilt1(out.P_el_motor.Data,6),'Color',orange,'LineStyle','-', 'LineWidth',6)
hold on
plot(out.P_mechanical.Time,medfilt1(out.P_mechanical.Data,6),'Color',blue,'LineStyle','-', 'LineWidth',6)

```

```

plot(out.P_propulsive.Time,medfilt1(out.P_propulsive.Data,6),'Color',green,'LineStyle','--')
xlabel('Time [Hour]')
ylabel(' [W]')
ylim([0 9000])
set(gca,'ycolor','k')

yyaxis right
fill_curves(out.eta_electric.Time,zeros(length(out.SOC.Time),1),medfilt1(out.eta_electric.Data,6)*100,red,0.1);
hold on
fill_curves(out.eta_propulsive.Time,zeros(length(out.SOC.Time),1),medfilt1(out.eta_propulsive.Data,6)*100,blue,0.15);
fill_curves(out.eta_tot.Time,zeros(length(out.SOC.Time),1),medfilt1(out.eta_tot.Data,6)*100,green,0.2);
ylabel(' [%]')
xlabel('Time [Hour]')
ylim([0 100])
set(gca,'ycolor','k')
xlim([0 t_max])
xticks((0:3600:t_max));
xticklabels(t_plot)
title('Motor power distribution')
legend('Electrical input','Mechanical output','Propulsive output','\eta_{electrical}','\eta_{propulsive}','\eta_{tot}')

% Relevan duty cycles
figure(9)

yyaxis left
plot(out.D_MPPT.Time,medfilt1(out.D_MPPT.Data,6),'Color',[green,0.6],'LineStyle','--','LineWidth',5)
hold on
plot(out.D_max_current.Time,medfilt1(out.D_max_current.Data,6),'Color',[orange,0.8],'LineStyle','--','LineWidth',5)
plot(out.D_to_follow_load.Time,medfilt1(out.D_to_follow_load.Data,6),'Color',[ocra,0.6],'LineStyle','--','LineWidth',5)
plot(out.D.Time,medfilt1(out.D.Data,6),'Color',blue,'LineStyle','--','LineWidth',2)
ylim([0.38 0.72])
ylabel(' [-]')
set(gca,'ycolor','k')

yyaxis right
fill_curves(out.SOC.Time,zeros(length(out.SOC.Time),1),out.SOC.Data,blue,0.1);
ylabel(' [%]')
ylim([0 100])
set(gca,'ycolor',l_blue)

xlim([0 t_max])
xticks((0:3600:t_max));
xticklabels(t_plot)
xlabel('Time [Hour]')
title('Relevant Duty Cycles')
legend('D_{MPPT}','D_{max current}','D_{load following}','D','SOC battery')

% Energy shortcomings: DC MOTOR
eta_total_str = num2str(eta_total);
figure(10)
yyaxis left
plot(out.P_not_av.Time,medfilt1(out.P_not_av.Data/1000/eta_total,6),'Color',orange,'LineStyle','--')
xlabel('Time [Hour]')
ylabel(' [kW]')
set(gca,'ycolor',orange)
ylim([ 0 max(out.P_not_av.Data/1000/eta_total)+1])

yyaxis right
plot(out.E_not_av.Time,medfilt1(out.E_not_av.Data/1000/3600/eta_total,6),'Color',ocra,'LineStyle','--')

ylabel(' [kWh]')
set(gca,'ycolor',ocra)
ylim([0 max(out.E_not_av.Data/1000/3600/eta_total)+1])
xlim([0 t_max])
xticks((0:3600:t_max));
xticklabels(t_plot)

subtitle = [num2str(max(out.E_not_av.Data/1000/3600/eta_total),'%.0f'),' [kWh]', ' @ \eta_{tot} = ',eta_total_str,' [-]'];
title('DC motor: Energy shortcomings',subtitle)
legend('Motor power not available','Energy not available')

% Battery energy and cycles
figure(11)

n_cycles = max(out.E_battery_abs.Data/1000/3600)/E_total_battery;
n_cycles_str = num2str(round(n_cycles));
str_title = ['Number of cycles = ',n_cycles_str];

yyaxis left
plot(out.E_battery.Time,medfilt1(out.E_battery.Data/1000/3600,6),'Color',orange,'LineStyle','--')
xlabel('Time [Hour]')
ylabel(' [kWh]')
set(gca,'ycolor',orange)

yyaxis right
plot(out.E_battery_abs.Time,medfilt1(out.E_battery_abs.Data/1000/3600,6),'Color',ocra,'LineStyle','--')

ylabel(' [kWh]')
set(gca,'ycolor',ocra)
xlim([0 t_max])
xticks((0:3600:t_max));
xticklabels(t_plot)

ylim([ 0 max(out.E_battery_abs.Data/1000/3600)+1])

title('Battery energy and cycles',str_title)
legend('Energy exchange','Cumulated energy')

```

```
% Potential PV energy lost
figure(12)
yyaxis left
plot(out.P_PV_loss.Time,medfilt1(out.P_PV_loss.Data/1000,6),'Color',orange,'LineStyle','-')
xlabel('Time [Hour]')
ylabel('kW')
set(gca,'ycolor',orange)

yyaxis right
plot(out.E_PV_loss.Time,medfilt1(out.E_PV_loss.Data/1000/3600,6),'Color',ocra,'LineStyle','-')

ylabel('kWh')
set(gca,'ycolor',ocra)
xlim([0 t_max])
xticks((0:3600:t_max));
xticklabels(t_plot)
subtitle = [num2str(max(out.E_PV_loss.Data/1000/3600),'%.0f'),' [kWh]'];
title('Potential PV energy lost',subtitle)
legend('Power','Energy')

% Energy shortcomings: 12V grid
figure(13)
yyaxis left
plot(out.P_12V_not_av.Time,medfilt1(out.P_12V_not_av.Data/1000,6),'Color',purple,'LineStyle','-')
xlabel('Time [Hour]')
ylabel('kW')
set(gca,'ycolor',purple)
ylim([0 max(out.P_not_av.Data/1000/eta_total)+1])
yyaxis right
plot(out.E_12V_not_av.Time,medfilt1(out.E_12V_not_av.Data/1000/3600,6),'Color',ocra,'LineStyle','-')

ylabel('kWh')
set(gca,'ycolor',ocra)
ylim([0 max(out.E_12V_not_av.Data/1000/3600)+1])
xlim([0 t_max])
xticks((0:3600:t_max));
xticklabels(t_plot)
subtitle = [num2str(max(out.E_12V_not_av.Data/1000/3600),'%.0f'),' [kWh]'];

title('Energy shortcomings - 12V grid',subtitle)
legend('12V power not available','Energy not available')

% Energy balance

E_PV_ideal = max(out.E_PV_ideal.Data)/1000/3600;
E_PV = max(out.E_PV.Data)/1000/3600;
E_buck = max(out.E_buck.Data)/1000/3600;
E_PV_loss = max(out.E_PV_loss.Data)/1000/3600;
E_12V = max(out.E_12V.Data)/1000/3600;
E_el_motor = max(out.E_el_motor.Data)/1000/3600;
E_buck_directly = max(out.E_buck_directly.Data)/1000/3600;
E_buck_stored = max(out.E_buck_stored.Data)/1000/3600;
E_battery_discharge = max(out.E_battery_discharge.Data)/1000/3600;
E_battery_shore_charge = max(out.E_battery_shore_charge.Data)/1000/3600;
E_not_av_motor = max(out.E_not_av.Data/1000/3600/eta_total);
E_not_av_12V = max(out.E_12V_not_av.Data/1000/3600);

figure(14)

X1 = categorical({'PV - Buck energy'});
X2 = categorical({'Energy source'});
X3 = categorical({'Energy requested'});

Y1_1 = E_PV_ideal;
Y1_2 = [E_PV E_PV_loss];
Y1_3 = [E_buck E_PV-E_buck];
Y2 = [E_buck_directly E_buck_stored E_battery_shore_charge];
Y3 = [E_el_motor E_12V E_not_av_motor+E_not_av_12V];

H1 = bar(X1,Y1_1,0.8, 'FaceColor','flat');
set(H1, 'FaceColor', 'Flat')
H1(1).CData = 1_green;
hold on

H2 = bar(X1,Y1_2,0.7,'stacked','FaceColor','flat');
H2(1).CData = beige;
H2(2).CData = red;

H3 = bar(X1,Y1_3,0.6,'stacked','FaceColor','flat');
H3(1).CData = ocra;
H3(2).CData = brown;

H4=bar(X2,Y2,'stacked', 'FaceColor','flat');
H4(1).CData = green;
H4(2).CData = blue;
H4(3).CData = 1_brown;

H5=bar(X3,Y3,'stacked', 'FaceColor','flat');
H5(1).CData = orange;
H5(2).CData = purple;
H5(3).CData = [0 0 0];

title('Energy Balance')
ylim([0 1.3*max([sum(Y1_1),sum(Y2),sum(Y3)])])
legend([H1,H2,H3],'PV ideal energy','PV energy','Potential PV energy lost','Buck converter energy','PV energy lost in conversion','Location','NorthWest')
ylabel('kWh')
axaxes('position',get(gca,'position'),'visible','off');
legend(a,H4,'Buck energy directly used','Buck energy stored','Shore charger','Location','North');
baxes('position',get(gca,'position'),'visible','off');
legend(b,H5,'DC motor','12V grid','Energy shortcoming');
```

```
% SOC average
SOC_time = out.SOC_av_h.Time(2:end)/3600;
SOC_av = out.SOC_av_h.Data(2:end);

count_on=0;
count_SOC_on =0;
count_off=0;
count_SOC_off =0;

for zz=1:n_days
for ii=1:24

if (SOC_time(ii+(zz-1)*24)>7+(zz-1)*24 && SOC_time(ii+(zz-1)*24)<=22+(zz-1)*24)
count_on = count_on+1;
count_SOC_on = count_SOC_on+SOC_av(ii+(zz-1)*24);
else
count_off = count_off+1;
count_SOC_off = count_SOC_off+SOC_av(ii+(zz-1)*24);
end
end
end

SOC_on_av = count_SOC_on/count_on;
SOC_off_av = count_SOC_off/count_off;

SOC_on_av_str = num2str(SOC_on_av,3);
SOC_off_av_str = num2str(SOC_off_av,3);

subtitle=['SOC_{mean} during the day = ',SOC_on_av_str,' [X], ',...
'SOC_{mean} during the night charge = ',SOC_off_av_str,' [X], '];

figure(15)

fill_curves(out.SOC.Time,zeros(length(out.SOC.Time),1),out.SOC.Data,blue,0.3);
xlim([0 t_max])
xticks((0:3600:t_max));
xticklabels(t_plot)
hold on
H1 = bar(out.SOC_av_h.Time-3600/2,out.SOC_av_h.Data,0.5, 'FaceColor','ocra');
plot([0 t_max],[SOC_on_av SOC_on_av],'Color',orange,'LineStyle','--','LineWidth',2)
plot([0 t_max],[SOC_off_av SOC_off_av],'Color',l_brown,'LineStyle','-','LineWidth',2)
ylabel(' [X]')
ylim([0 100])
xlabel('Time [Hour]')
title('Battery State of Charge [SOC]',subtitle)
legend('SOC battery','Hourly average','SOC_{mean} day','SOC_{mean} charge')

end
```

## PLOTS DISTRIBUTION

```
% 1 Comparison between ideal and actual PV power
% 2 Overview of main power output and input involved (PV,battery,loads,shore charger)
% 3 Effective and requested boat velocity
% 4 Load and motor rotational speed
% 5 Load and motor torque
% 6 Relevant voltages
% 7 Relevant currents
% 8 Motor power distribution
% 9 Relevant duty cycles
% 10 Energy shortcomings DC motor
% 11 Battery energy and cycles
% 12 Potential PV energy lost
% 13 Energy shortcomings 12V grid
% 14 Energy balance
% 15 SOC and SOC average

% 24 Propeller torque load
% 24 Propeller angular speed
% 24 Propeller load
% 24 Propeller open water efficiency
% 28 Open water diagram v = 2 [m/s]
% 29 Open water diagram v = 5 [m/s]
% 45 Weather
% 46 Load
% 51 Velocity Drag and Power

% In case distFig function is present in the directory
%distFig('Only',24)
%distFig('Position','E','Only',[28 29])
%distFig('Position','E','Only',[25 27])
%distFig('Position','SW','Only',3)
%distFig('Position','W','Only',[1 2])
%distFig('Position','E','Only',[6 7])
%distFig('Position','SE','Only',9)
%distFig('Position','E','Only',[3 8])
%distFig('Position','E','Only',[7 9])
%distFig('Position','W','Only',[10,11])
%distFig('Position','E','Only',[12,13])
%distFig('Position','E','Only',[45 46])
%distFig('Position','E','Only',[4 5])
%distFig('Only',14)
%distFig('Only',15)
```

## FUNCTIONS

```
function [t_load,load,time_weather,irr_v,temp_v,n_days] = load_and_weather(first_day,last_day,pause_weight)

first_day = day( datetime(first_day, 'InputFormat', 'dd-MMM' ), 'dayofyear' );
last_day = day( datetime(last_day, 'InputFormat', 'dd-MMM' ), 'dayofyear' );

n_days = last_day-first_day + 1;

Table = readtable('Year_data_hourly.xlsx','Sheet','Sheet1','VariableNamingRule','preserve');

%% TIME AND WEATHER
time_weather = (0:1:n_days*24)';
irr_v = Table((first_day-1)*24+1:last_day*24+1,"Irradiance [W/m^2]");
temp_v = Table((first_day-1)*24+1:last_day*24+1,"Temperature [°C]");

%% TIME AND LOADS
t_ultra_short = [0 0.01 0.02 0.03 0.04 0.05 0.06 0.07 0.249 0.25]';
ultra_short_slow = [0 3 3 3 3 3 3 3 0]';
ultra_short_fast = [0 5 5 5 5 5 5 5 0]';

t_short = [0 0.01 0.02 0.03 0.04 0.05 0.06 0.07 0.49 0.5]';
short_slow = [0 3 3 3 3 3 3 3 0]';
short_fast = [0 5 5 5 5 5 5 5 0]';

t_medium = [0 0.01 0.02 0.03 0.04 0.05 0.249 0.25 0.749 0.75]';
medium_slow = [0 3.5 3.5 3.5 3.5 3.5 3.5 3.5 0]';
medium_fast = [0 5 5 5 5 5 5 4 0]';

t_long = [0 0.01 0.249 0.25 0.49 0.5 0.749 0.75 0.99 1]';
long_slow = [0 2 2 3 3 3 3 2 0]';
long_fast = [0 3 3 5 5 5 5 3 0]';

A_load_time = [t_ultra_short t_ultra_short t_short t_short t_medium t_medium t_long t_long];

A_load = [ultra_short_slow ultra_short_fast short_slow short_fast...
medium_slow medium_fast long_slow long_fast];

%% BUILD
pd_load = makedist('Multinomial','Probabilities',[0.175 0.175 0.175 0.175 0.1 0.1 0.05 0.05] );
pd_pause = makedist('Multinomial','Probabilities',[0.3 0.3 0.2 0.2]);

%Build load vector

t_load = zeros(1000*n_days,1);
load = zeros(1000*n_days,1);
t_load(1) = 0;
t_load(2) = 7;

ii = 2;

for zz =1:n_days
while t_load(ii) < 24*zz
flag_pause = randi([0, 1], [1, 1]);

if (t_load(ii)>=7+(zz-1)*24 && t_load(ii)<=21+(zz-1)*24 && flag_pause==0)

r=random(pd_pause,1,1);
t_load(ii+1) = t_load(ii)+0.25*r*pause_weight;
ii = ii+1;

elseif (t_load(ii)>=7+(zz-1)*24 && t_load(ii)<=21+(zz-1)*24 && flag_pause==1)

r_l=random(pd_load,1,1);
t_moment = t_load(ii);

for jj=1:10

t_load(ii) = t_moment + A_load_time(jj,r_l);
load(ii) = A_load(jj,r_l);

if jj < 10
ii = ii+1;
end

end

t_load(iii+1) = t_load(ii)+0.25*pause_weight;
ii = ii+1;

else

t_load(ii+1) = 7+24*zz;
ii = ii+1;

if t_load(ii) > n_days*24
t_load(ii)=n_days*24;
end
end
end
end

t_load = t_load(1:ii);
load = load(1:ii);

end
```



```

function [Kt, Kq, eta0] = propcalc(Z, AeA0, PD, J, Rn)
%PROPCALC Calculates the Wageningen B-Series polynomials from the polynomial fits from Carlton J. - Marine Propellers and Propulsion created by ir. EAE Duchateau
% (version 08-04-2013)
%
%
% Input Parameters:
% Z      = Number of blades (2 - 7)
% AeA0   = Blade area ratio (0.30 - 1.05)
% PD     = Pitch/diameter ratio (0.6 - 1.4)
% J      = Advance (J = Va/(n*D))
% (Rn)   = Reynolds number (2e6 - 2e9)

if nargin <5
    Rn = [];
end

% Z=4
% AeA0=0.85
% PD=1.2
% J=[0:0.2:1.2]
% Rn=[]

J = reshape(J,[],1);

CKt = [ 0.00880496 0 0 0 0; -0.204554 1 0 0 0; 0.166351 0 1 0 0; 0.158114 0 2 0 0; -0.147581 2 0 1 0;
-0.481497 1 1 1 0; 0.415437 0 2 1 0; 0.0144043 0 0 0 1; -0.0530054 2 0 0 1; 0.0143481 0 1 0 1;
0.0606826 1 1 0 1; -0.0125894 0 0 1 1; 0.0109689 1 0 1 1; -0.133698 0 3 0 0; 0.00638407 0 6 0 0;
-0.00132718 2 6 0 0; 0.16849 3 0 1 0; -0.0507214 0 0 2 0; 0.0854559 2 0 2 0; -0.0504475 3 0 2 0;
0.010465 1 6 2 0; -0.00648272 2 6 2 0; -0.00841728 0 3 0 1; 0.0168424 1 3 0 1; -0.00102296 3 3 0 1;
-0.0317791 0 3 1 1; -0.018604 1 0 2 1; -0.00410798 0 2 2 1; -0.000606848 0 0 0 2; -0.0049819 1 0 0 2;
0.0025983 2 0 0 2; -0.000560528 3 0 0 2; -0.00163652 1 2 0 2; -0.000328787 1 6 0 2; 0.000116502 2 6 0 2;
0.000690904 0 0 1 2; 0.00421749 0 3 1 2; 0.0000565229 3 6 1 2; -0.00146564 0 3 2 2];

CKq = [ 0.00379368 0 0 0 0; 0.00886523 2 0 0 0; -0.032241 1 1 0 0; 0.00344778 0 2 0 0; -0.0408811 0 1 1 0; -0.108009 1 1 1 0;
-0.0885381 2 1 1 0; 0.188561 0 2 1 0; -0.00370871 1 0 0 1; 0.00513696 0 1 0 1; 0.0209449 1 1 0 1;
0.00474319 2 1 0 1; -0.00723408 2 0 1 1; 0.00438388 1 1 1 1; -0.0269403 0 2 1 1; 0.0558082 3 0 1 0; 0.0161886 0 3 1 0;
0.00318086 1 3 1 0; 0.015896 0 0 2 0; 0.0471729 1 0 2 0; 0.0196283 3 0 2 0; -0.0502782 0 1 2 0;
-0.030055 3 1 2 0; 0.0417122 2 2 2 0; -0.0397722 0 3 2 0; -0.00350024 0 6 2 0; -0.0106854 3 0 0 1;
0.00110903 3 3 0 1; -0.000313912 0 6 0 1; 0.0035985 3 0 1 1; -0.00142121 0 6 1 1; -0.00383637 1 0 2 1;
0.0126803 0 2 2 1; -0.00318278 2 3 2 1; 0.00334268 0 6 2 1; -0.00183491 1 1 0 2; 0.000112451 3 2 0 2;
-0.0000297228 3 6 0 2; 0.000269551 1 0 1 2; 0.00083265 2 0 1 2; 0.00155334 0 2 1 2; 0.000302683 0 6 1 2;
-0.0001843 0 0 2 2; -0.000425399 0 3 2 2; 0.0000869243 3 3 2 2; -0.0004659 0 6 2 2; 0.0000554194 1 6 2 2];

% Kt calculation
temp = zeros(39,length(J));

for i = 1:39
    temp(i,:) = CKt(i,1).*J.^CKt(i,2).*PD.^CKt(i,3).*AeA0.^CKt(i,4).*Z.^CKt(i,5);
end

Kt = sum(temp);
Kt = Kt';

if ~isempty(Rn)
    dKt = 0.000353485 ...
    - 0.00333758.*AeA0.*J.^2 ...
    - 0.00478125.*AeA0.*PD.*J ...
    + 0.000257792*(log10(Rn)-0.301)^2.*AeA0.*J.^2 ...
    + 0.0000643192*(log10(Rn)-0.301)*PD.^6.*J.^2 ...
    - 0.0000110636*(log10(Rn)-0.301)^2.*PD.^6.*J.^2 ...
    - 0.0000276305*(log10(Rn)-0.301)^2.*Z.*AeA0.*J.^2 ...
    + 0.0000954*(log10(Rn)-0.301)*Z.*AeA0.*PD.*J ...
    + 0.0000032049*(log10(Rn)-0.301)*Z.^2.*AeA0.*PD.^3.*J;
    Kt = Kt + dKt;
end

% Kq calculation
temp = zeros(47,length(J));

for i = 1:47
    temp(i,:) = CKq(i,1).*J.^CKq(i,2).*PD.^CKq(i,3).*AeA0.^CKq(i,4).*Z.^CKq(i,5);
end

Kq = sum(temp);
Kq = Kq';

if ~isempty(Rn)
    dKq = - 0.000591412 ...
    + 0.00696898*PD ...
    - 0.0000666654.*Z.*PD.^6 ...
    + 0.0160818.*AeA0.^2 ...
    - 0.000938091*(log10(Rn)-0.301)*PD ...
    - 0.00059593*(log10(Rn)-0.301)*PD.^2 ...
    + 0.0000782099*(log10(Rn)-0.301)^2.*PD.^2 ...
    + 0.0000052199*(log10(Rn)-0.301)*Z.*AeA0.*J.^2 ...
    - 0.0000088528*(log10(Rn)-0.301)^2.*Z.*AeA0.*PD.*J ...
    + 0.0000230171*(log10(Rn)-0.301)*Z.*PD.^6 ...
    - 0.0000018434*(log10(Rn)-0.301)^2.*Z.*PD.^6 ...
    - 0.00400252*(log10(Rn)-0.301)*AeA0.^2 ...
    + 0.000220915*(log10(Rn)-0.301)^2.*AeA0.^2;
    Kq = Kq + dKq;
end

% Etha 0
eta0 = (Kt./Kq).*(J./(2*pi));
eta0((find(eta0<0,1)+1):end) = NaN;
end

```

```
function [h]=fill_curves(x,y1,y2,color,opaque)

if iscolumn(x)
    x=x';
end

if iscolumn(y1)
    y1=y1';
end

if iscolumn(y2)
    y2=y2';
end

hold on

% plot(x,y1,'k', 'LineWidth', 1);
% plot(x,y2, 'k', 'LineWidth', 1);
x2 = [x, fliplr(x)];
inBetween = [y2,fliplr(y1)];
h=fill(x2, inBetween,color);
% Choose a number between 0 (invisible) and 1 (opaque) for facealpha.
set(h,'facealpha',opaque)
end
```

# List of Acronyms

<b>AC</b> Alternate Current . . . . .	21, 35, 42, 76
<b>BLDC</b> Brushless Direct Current Motor . . . . .	35, 76
<b>BOS</b> Balance Of System . . . . .	21
<b>CII</b> Carbon Intensity Index . . . . .	15
<b>DC</b> Direct Current . . . . .	17, 21, 24, 25, 35, 36, 38–40, 42, 50, 56–58, 61, 62, 66, 67, 70, 72, 75–77
<b>EEDI</b> Energy Efficiency Design Index . . . . .	15
<b>EEXI</b> Energy Efficiency Existing Ship Index . . . . .	15
<b>EMF</b> Electro-Motive Force . . . . .	36
<b>GHG</b> Greenhouse Gases . . . . .	15
<b>IGBT</b> Insulated Gate Bipolar Transistor . . . . .	39
<b>IMO</b> International Maritime Organisation . . . . .	15
<b>MOSFET</b> Metal Oxide Semiconductor Field Effect Transistor . . . . .	39
<b>MPP</b> Maximum Power Point . . . . .	42, 45, 48, 50, 53, 54, 56, 83, 86–88
<b>MPPT</b> Maximum Power Point Tracking . . . . .	45, 47, 50, 52–54
<b>PDU</b> Power Distribution Unit . . . . .	58
<b>PI</b> Proportional Integral . . . . .	35, 38, 55, 61, 62, 65, 69, 71, 75
<b>PMDC</b> Permanent Magnet Direct Current . . . . .	35, 67, 76
<b>PMSM</b> Permanent Magnet Synchronous Motor . . . . .	35, 76
<b>PV</b> Photovoltaic . . . . .	16, 17, 21, 24, 25, 39, 42, 44, 45, 47–50, 53–58, 62, 75, 77, 79, 83, 87, 92
<b>PVGIS</b> european commission PhotoVoltaic Geographical Information System . . . . .	46, 79
<b>PWM</b> Pulse Width Modulation . . . . .	21, 39, 42, 54, 68, 71, 75
<b>SEPIC</b> Single Ended Primary Inductor Converter . . . . .	75
<b>SOC</b> State of Charge . . . . .	42, 50, 54, 62, 67, 68, 81, 83–85, 89, 92
<b>STC</b> Standard Testing Conditions . . . . .	13, 22, 56
<b>TF</b> Transfer Functions . . . . .	49
<b>V-I</b> Voltage-Current . . . . .	24, 49
<b>ZOH</b> Zero Order Hold . . . . .	45, 81